THE INFLUENCE OF RESIDUAL STRESS DUE TO COLD BENDING ON THIN-WALLED OPEN SECTIONS

THE INFLUENCE OF RESIDUAL STRESS
DUE TO COLD BENDING
ON THIN-WALLED OPEN SECTIONS

by

LESLIE R. DANIELS, B.ENG. (HONS.)

A Thesis

Submitted to the Faculty of Graduate Studies

in Partial Fulfilment of the Requirements

for the Degree

Master of Engineering

McMaster University

May 1969

MASTER OF ENGINEERING
(Civil Engineering)

McMASTER UNIVERSITY
Hamilton, Ontario.

TITLE: The Influence of Residual Stress Due to Cold Bending on Thin-walled Open Sections

AUTHOR: Leslie R. Daniels, B.Eng. (Hons.) (Sheffield University)

SUPERVISOR: Dr. R. M. Korol

NUMBER OF PAGES: *xii*, 152

SCOPE AND CONTENTS:

This thesis deals with the analytical and experimental study of the influence of residual stress due to cold bending on the behaviour of thin-walled open sections. The residual stress distribution caused by cold forming the sections is predicted theoretically. The influence of this residual stress on the load-displacement characteristic, and load carrying capacity of similarly curved tension and compression specimens is then analyzed. A local buckling analysis based on the virtual work and incremental theories is performed to predict the collapse load of compression specimens containing residual stresses.

The experimental work consisted of tests to confirm theoretical elastic springback strains due to cold bending of steel sheet to various radii. Tension and compression tests were then performed on various cold formed sections

to observe the effects of residual stress and to confirm analytical predictions.

Conclusions have been deduced from the theory and from these tests, and suggestions made for further research.

ACKNOWLEDGEMENTS

The author wishes to express his sincere appreciation to Dr. R. M. Korol for his guidance and encouragement throughout the research program.

Acknowledgement is also made to McMaster University for providing sufficient financial support for the completion of this thesis.

The author is grateful for the invaluable assistance of John Myers and his technical staff, and Dofasco, Dominion Foundries and Steel Ltd., who provided the steel sheeting.

TABLE OF CONTENTS

CHAPTER		PAGE
I	INTRODUCTION	1
II	ANALYTICAL DETERMINATION OF RESIDUAL STRESS IN A COLD FORMING PROCESS	7
III	THEORETICAL PREDICTIONS OF THE BEHAVIOUR OF COLD FORMED SECTIONS UNDER LOAD	37
	Section 1. Influence of Residual Stress on the Characteristics of Tensile Specimens	38
	Section 2. Influence of Residual Stress on the Characteristics of Compression Specimens (Local Buckling Theory)	48
IV	EXPERIMENTAL WORK AND RELATED DISCUSSIONS	86
V	COMPARISON OF EXPERIMENTAL RESULTS WITH THEORY	128
VI	CONCLUSIONS AND SUGGESTIONS FOR FURTHER RESEARCH	135
APPENDIX		
1	Calculation of Dimensions of Compression Specimens after Elastic Springback	139
2	Numerical Prediction of Load vs. Displacement Characteristic for Specimens Containing Residual Stress	141
3	Computer Programs	146
REFERENCES		150

LIST OF FIGURES

		PAGE
Fig. 2.1	Metal Sheet During Bending	8
Fig. 2.2	Stresses and Strains Through Cross Section	8
Fig. 2.3	Von Mises' Yield Criterion	9
Fig. 2.4	Tresca's Yield Criterion	10
Fig. 2.5	Representation of Axes	11
Fig. 2.6	Theoretical Stress-Strain Curves for Sheet Bending (Von Mises)	19
Fig. 2.7	Theoretical Stress-Strain Curves for Sheet Bending (Tresca)	20
Fig. 2.8	Elastic Recovery of Outside Fibres	22
Fig. 2.9	Circumferential Stress Distributions During Elastic Springback	23
Fig. 2.10	Stress Analysis in Circumferential Direction (Von Mises)	26
Fig. 2.11	Stress Analysis in Circumferential Direction (Tresca)	27
Fig. 2.12	Variation of Elastic Springback Strain with Ratio a/c	32
Fig. 2.13	Stress Analysis in Longitudinal Direction (Von Mises)	33
Fig. 2.14	Stress Analysis in Longitudinal Direction (Tresca)	34
Fig. 3.1	Fibre Stresses During Loading (Von Mises)	39
Fig. 3.2	Applied Axial Stress at Initial Yield vs. a/c (Von Mises)	43
Fig. 3.3	Applied Axial Stresses Necessary for Yield of Various Fibres (Von Mises)	43

LIST OF FIGURES (cont'd)

		PAGE
Fig. 3.4	Fibre Stresses During Loading (Tresca)	44
Fig. 3.5	Applied Axial Stress at Initial Yield vs. a/c (Tresca)	45
Fig. 3.6	Applied Axial Stresses Necessary for Yield of Various Fibres (Tresca)	45
Fig. 3.7	Theoretical Load vs. Displacement Characteristics for Tensile Specimens	47
Fig. 3.8	Compression Specimen Showing Assumed Mode of Failure	52
Fig. 3.9	Intersection of Post-Buckling Equilibrium Paths and Apparent Theoretical Stress-Strain Curve	75
Fig. 3.10	Intersection of Post-Buckling Equilibrium Paths and Experimental Stress-Strain Curve	77
Fig. 3.11	Detail of Intersection of Post-Buckling Paths and Experimental Stress-Strain Curve	78
Fig. 3.12	Variation of Tangent Modulus for Experimental Stress-Strain Curve	81
Fig. 3.13	Tangent Modulus vs. Stress for Experimental Curve Showing Post-Buckling Equilibrium Paths for Various R/T Values	82
Fig. 3.14	Critical Buckling Stress for Local Buckling Failure	83
Fig. 4.1	Tensile Test No. 3	88
Table 4.2	Tensile Test Results	89
Table 4.3	Poisson's Ratio Test Results	90
Fig. 4.4	Sheet Bending Operation Showing Positions and Orientation of Strain Gauges	93

LIST OF FIGURES (cont'd)

		PAGE
Fig. 4.5	Circumferential Strain of Outer Fibres During Bending	94
Fig. 4.6	Dimensions of Tensile Specimens	99
Fig. 4.7	Tensile Tests - 1" ϕ Bend	102
Fig. 4.8	Tensile Tests - 2 5/16" ϕ Bend	103
Fig. 4.9	Tensile Tests - 3" ϕ Bend	104
Fig. 4.10	Stages During Fabrication of Compression Specimens	107
Table 4.11	Dimensions of Compression Specimens	113
Fig. 4.12	Compression Specimens Showing Strain Gauges	110
Fig. 4.13	Compression Specimen Type C Showing Strain Gauges	111
Fig. 4.14	Typical Characteristics for Compression Specimens - Type A	117
Fig. 4.15	Compression Specimen Type B - Containing Residual Stress	118
Fig. 4.16	Compression Specimen Type B - Stress Relieved	119
Fig. 4.17	Compression Specimen Type C - Containing Residual Stress	120
Fig. 4.18	Compression Specimen Type C - Stress Relieved	121

LIST OF PHOTOGRAPHS

		PAGE
Photograph 4.1	Pyramid Roller Used in Fabrication	92
Photograph 4.2	Grooves in Roll for Strain Gauge Clearance	92
Photograph 4.3	Layout of Testing Apparatus	97
Photograph 4.4	Tensile Specimen	98
Photograph 4.5	Formation of Lips in Compression Specimen	108
Photograph 4.6	Final Bending of Compression Specimen	109
Photograph 4.7	Compression Specimens	112
Photograph 4.8	Local Buckling Failure of Compression Specimen	122

NOMENCLATURE

A_1, A_2	Areas under stress-strain distributions.
A	Mathematical constant.
a	Half-thickness of sheet.
at	Amplitude of buckling wave.
C_{11}, C_{12}, C_{22}, C_3	Coefficients in the stress-strain relationships.
C	Constant of integration.
c	Half width of purely elastic region of sheet.
D_{11}, D_{12}, D_{22}, D_3	Bending moment coefficients.
D	Distance ratio of elastic and plastic areas.
E	Young's modulus of elasticity.
E^p_{TAN}	Plastic tangent modulus.
E_T	Tangent modulus.
F, G, H	Coefficients in work equations.
J_2	Von Mises' yield function.
K	Length coefficient.
K_b	Springback ratio coefficient based on dimensions before springback.
K_p	Springback ratio coefficient based on dimensions after springback.
L	Length of member.
l	Length of buckling wave.
M_x, M_s, M_{xs}	Bending and twisting moments in shell.

NOMENCLATURE (cont'd)

P, Q, R, S	Variables in post-buckling equilibrium equations.
R	Radius of bent sheet to neutral axis.
R_y	Radius of initial yielding of outside fibres.
r	Radius of gyration; variable for radius of curved section.
S_{ij}	Deviator stress.
t	Thickness of sheet.
u, v, w	Incremental displacements in axial, circumferential and radial directions.
W_i	Work done by internal forces.
W_e	Work done by external forces.
W	Total work done by internal and external forces.
x, s, z	Coordinates in axial, circumferential and radial direction.
γxs	Middle surface shear strain.
δ_{ij}	Kronecker delta.
ε_x, ε_s, ε_z	Normal strains.
ε_x^o	Value of strain when yielding commences.
ε_{s_t}	Total strain before springback.
ε_{s_s}	Springback strain.
ε_{s_r}	Residual strain.
ε^e_{ij}, ε^p_{ij}	Elastic and plastic strains in tensor notation.
λ	Scalar multiplier.
ν	Poisson's ratio.
η_1, η_2	Reduced length parameters.

NOMENCLATURE (cont'd)

$\bar{\sigma}$	Static Yield Stress in uniaxial tension.
σ_x, σ_s, σ_z	Normal stresses.
σ_c	Critical stress.
σ_{s_o}	Value of stress when yielding commences.
σ_{s_A}	Applied loading stress.
σ_{s_R}	Residual stress.
τ_{xs}	Shear stress.
θ_b, θ_p	Angle subtended by curved arc of sheet before and after springback.
ϕ	Airy stress function.
$d\varepsilon_x$, $d\varepsilon_s$	Incremental strain values.
$d\lambda$	Proportionality factor in Prandtl-Reuss equations.

CHAPTER I

INTRODUCTION

1.1 Historical Review

Extensive research has recently been carried out at Lehigh University[1,2,3], and at various other institutions to investigate the various effects of residual stresses on load carrying members. The majority of this work has been concerned with the measurement, and the study of the effects of residual stresses due to differential cooling. The most important conclusion to be derived from this research was that the presence of residual stresses results in a considerable lowering of column strength below values predicted by coupon tests. Although it was found that the ultimate strength of sections containing residual stress is not appreciably lower than those samples which are stress free, it was noticed that the load-displacement characteristic is considerably different, with a marked lowering of the limit of proportionality in the case of the residual stressed specimens.

From these results it was seen that the presence of residual stress has a definite influence upon the overall behaviour of structural steel members. An applied uniform stress below the nominal yield point causes partial yielding of a cross section, and the increased strains in the remaining elastic parts of the cross-section render the load-displacement relationship non-linear. Assuming the applicability of the tangent-modulus concept, investigations indicated a consequent influence of residual stress upon column strength.

If residual stress is present only in the longitudinal direction*, the initial non-linearity will occur when the sum of the applied longitudinal stress and the residual stress in the fibre having the highest value of residual stress equals the yield stress of the material, i.e., if the longitudinal direction is denoted by x,

$$\sigma x_A = \bar{\sigma} - \sigma x_{R\ MAX} \qquad (1,1)^2$$

where, $\bar{\sigma}$ = yield stress in uniaxial tension for material free from residual stress.

σx_R = residual stress in longitudinal direction.

σx_A = applied stress in longitudinal direction.

---

* As will be seen in Chapter II, residual stress in the longitudinal direction is unlikely to occur without being accompanied by a residual stress in a perpendicular direction. This fact was clearly overlooked in the derivation of Equation (1,1), but this equation appeared to give acceptable results because of the effects of work hardening of the material.

A correct prediction for the stress at which yielding will first occur can only be made by giving due consideration to the type of yield criterion employed.

After this point the load-displacement characteristic will be non-linear as the load is redistributed to other parts of the cross section, until all the cross section has yielded and the section becomes perfectly plastic.

Since Shanley's classic paper[14], research into the realm of inelastic buckling has been placed on a more scientific foundation, in which the assumption of simultaneous lateral deflection with load results in a continuous fibre loading process. This theory has resulted in a lowering of the critical buckling load to values which generally correspond more with experiment than did those employing the reduced modulus theory. Furthermore, the tangent modulus theory predicts a safe value of the buckling load which is essential for rational design.[23]

Changes in the load-displacement characteristic of a load carrying member can also be caused by residual stresses that have been formed in the section by a process of cold bending. Various computations have been carried out to predict theoretically the springback occurring after a cold bending operation[5], and the resulting residual stress distribution throughout the cross section.[6] These computations have been based on the classical theories of Tresca, Von Mises and Prandtl-Reuss[4], and it is also from these theories that some of the theoretical work in this thesis is derived.

1.2 Outline of Research

It is evident that there has not been a great deal of experimental work carried out to determine exactly how residual stress due to cold-bending affects thin-walled open sections subjected to compressive loads. It is therefore part of the purpose of the experimental work in this thesis to determine how this type of residual stress influences the behaviour of thin-walled open sections, and also to study its effect upon the ultimate load capacity of various compression members. Consideration is given particularly to sections which are not especially sensitive to imperfections, and will fail consistently in one particular mode. For this reason specimens were employed which contained length parameters smaller than those usually used in practice, and stiffness was provided in parts of the cross section to minimize the effect of imperfections. The specimens were fabricated from sheet steel which exhibited a stress-strain characteristic that was approximately purely elastic - perfectly plastic. This type of steel was chosen to attempt to ensure that the influence of residual stress due to cold bending was not submerged by the influence of change in strength of the material due to work hardening. It will be seen that this was not entirely possible, and the effect of work hardening and also the Bauschinger effect was quite considerable.

The first part of the experimental work performed for this thesis consisted of bending steel sheets to various radii, and then allowing elastic springback to occur. Strains were measured in the outside fibres to be compared with theoretical results. Tensile tests were next performed on curved specimens containing residual stresses, with the object of providing stress-strain characteristics to be used in theoretical predictions of collapse loads of similarly-curved compression specimens. Finally, specially designed compressive specimens were tested to destruction to obtain complete load-displacement characteristics, and experimental values determined for collapse loads of thin-walled open sections.

The theoretical analysis for local buckling failure of the compression specimens is based on the virtual work and incremental theories of plasticity using an assumed buckling wave shape. An attempt has been made to isolate the separate effects of residual stress from work hardening and Bauschinger's effect, by basing theoretical predictions on both theoretical and experimental stress-strain characteristics. The theoretical analysis performed is primarily only for the type of specimens used in the experimental work. It is hoped, however, to illustrate the way in which this type of analysis may be applied to various shapes of thin-walled sections containing various distributions of residual stress.

CHAPTER II

ANALYTICAL DETERMINATION OF RESIDUAL STRESS IN A COLD FORMING PROCESS

2.1 Sheet Bending

The analysis outlined in this chapter shows a method for predicting the elastic springback, and the resulting residual stress distribution in a wide metal sheet subjected to cold bending in one direction. Initially the classical elastic and plastic theories necessary for this analysis are used to obtain the stresses and strains in the sheet in three directions prior to springback. Subsequently, a construction is outlined which enables the residual stress distribution in a cross section which has been bent through a particular angle to be obtained in both the transverse and longitudinal directions.

The initial bending of a metal sheet is purely elastic, and if at this stage the bending force is removed, the sheet will spring back to its flat position. Further bending causes the outer fibres of the sheet to yield and become plastic and a permanent strain will result. As shown in Fig. 2.1, the condition will arise where the

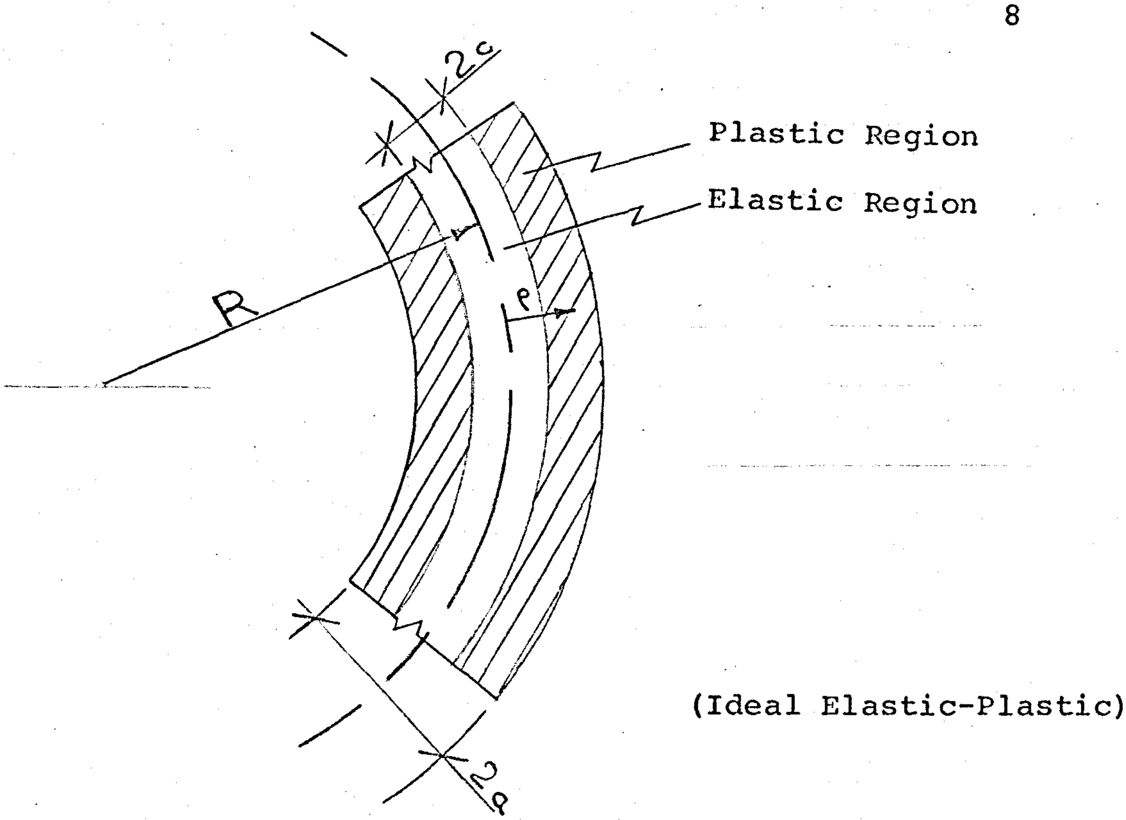

FIG.2.1 METAL SHEET DURING BENDING.

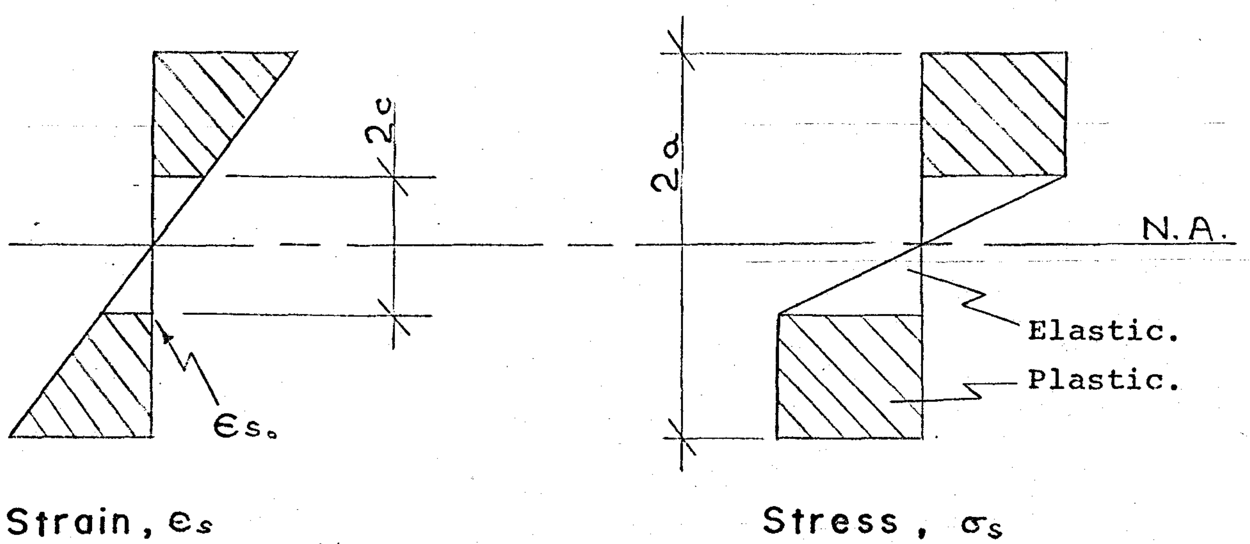

FIG.2.2 STRESSES AND STRAINS THROUGH CROSS-SECTION.

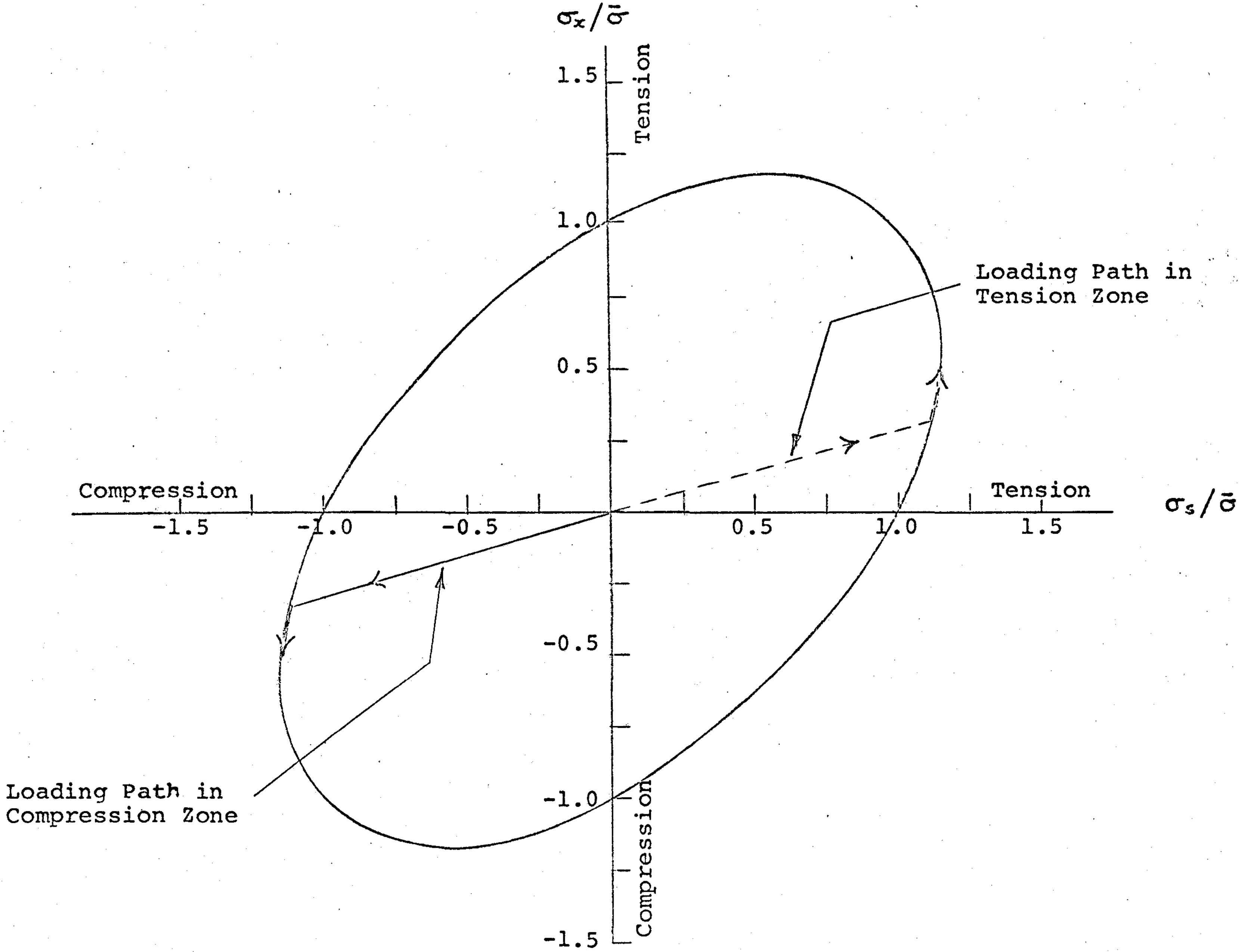

FIG. 2.3 VON MISES' YIELD CRITERION.

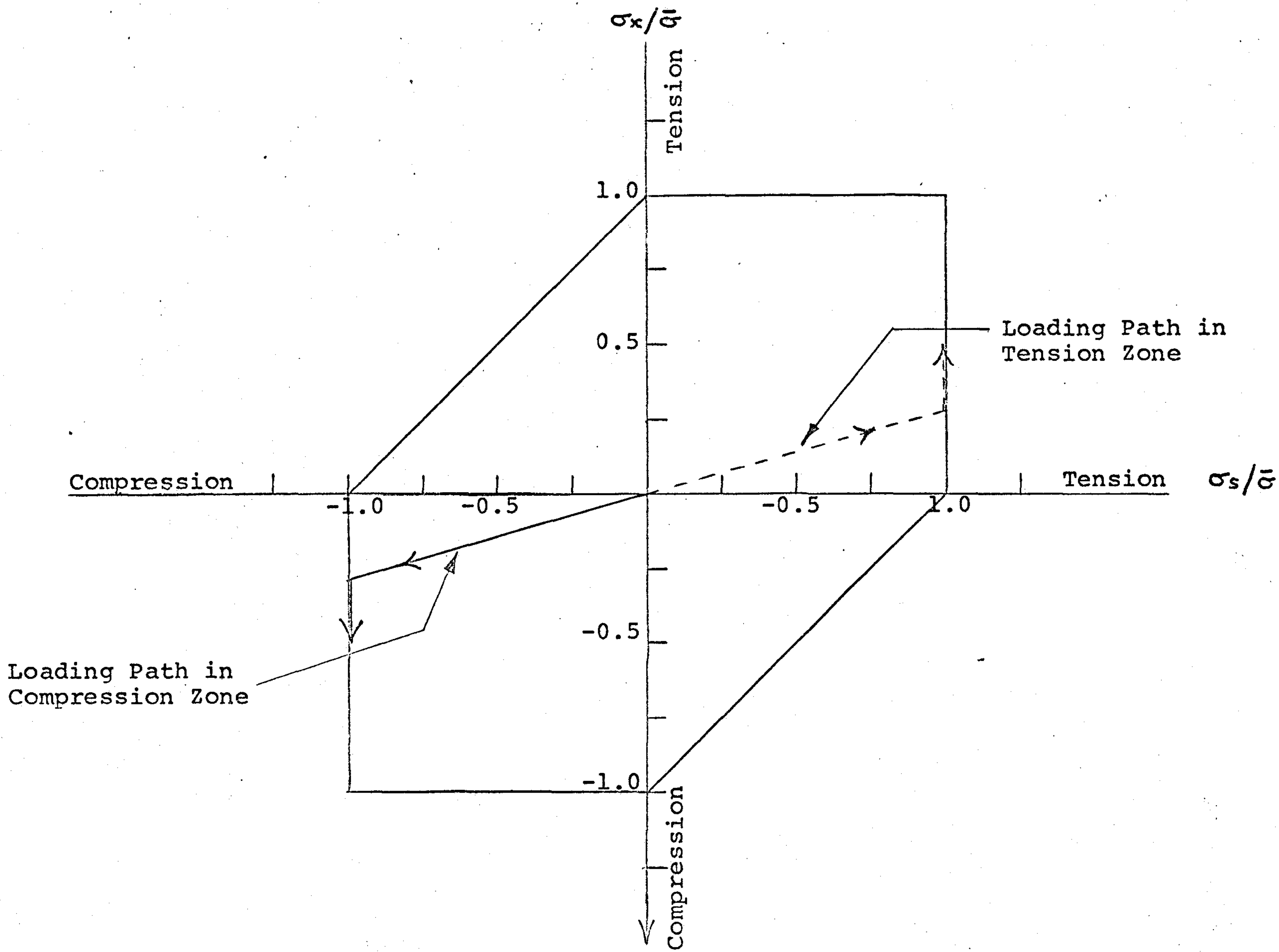

FIG. 2.4 TRESCA'S YIELD CRITERION.

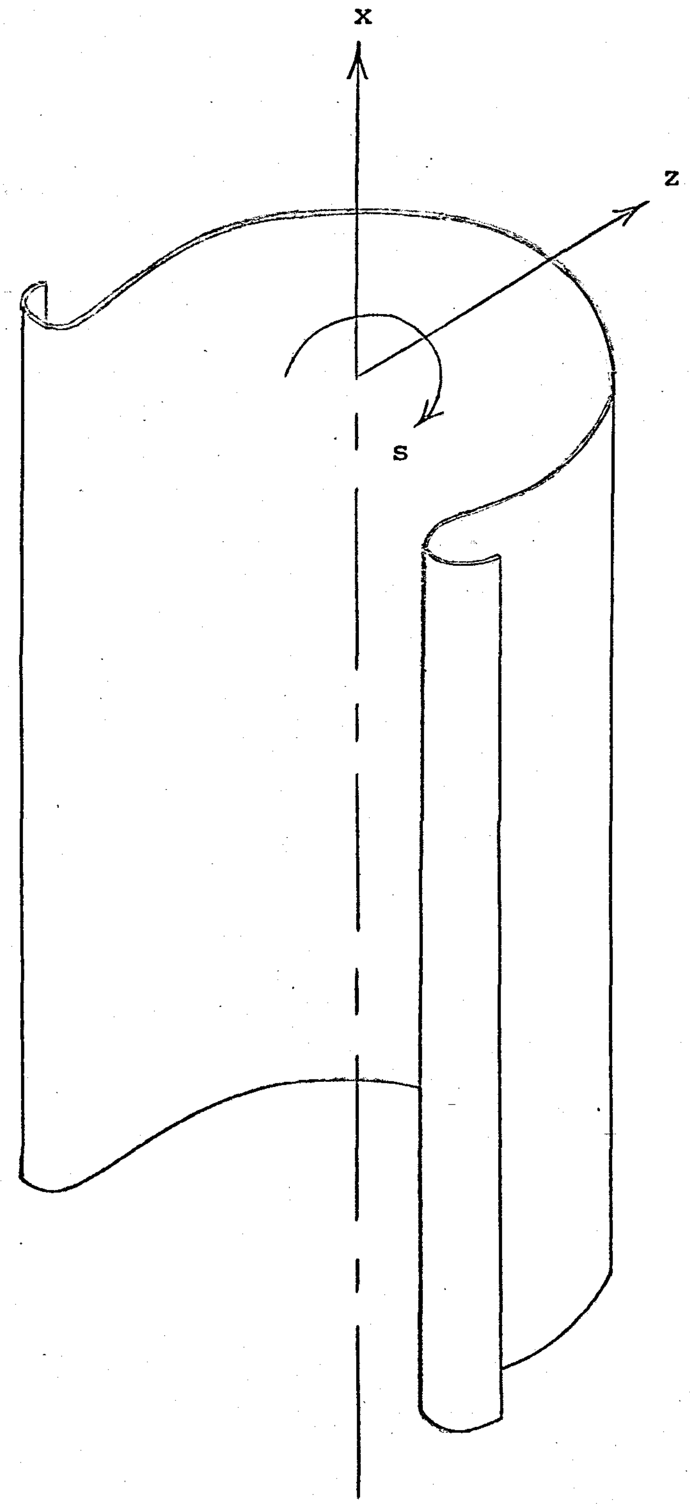

FIG.2.5 REPRESENTATION OF AXES.

centre core of the cross section is elastic, and the outer fibres are plastic. As bending continues, the thickness of this purely elastic core diminishes, and the ratio, a/c, increases. This ratio, a/c, is a useful parameter describing the elastic core of the sheet, and also the residual stress distribution. To predict the stress at which a particular fibre in the cross section ceases to be in the elastic range, a suitable yield criterion is required. The two most widely applicable criteria are those due to Von Mises and Tresca, both of which agree well with experimental values obtained. These are shown in Figs. 2.3 and 2.4 and the properties of these criteria are described fully by Hill.[4]

For the various radii of curvature attained during bending, the stresses and strains through the cross section of the sheet will be calculated. The axes used are shown in Fig. 2.5. It is assumed in the analysis that the width of the sheet is much greater than the thickness, thus the anticlastic curvature is concentrated at the ends. The material is assumed to be ideally elastic - perfectly plastic with no strain hardening. It is also assumed that transverse planes remain plane, and there is no Bauschinger effect. From these conditions it can be assumed:

$$\sigma_z = 0; \quad \sigma_x = 0 \tag{2.1}$$

Von Mises' Yield Criterion

$$\sigma_s^2 - \sigma_s\sigma_x + \sigma_x^2 = \bar{\sigma}^2 \tag{2.2}$$

by using the elastic condition:

$$\sigma_x = \nu\sigma_s \tag{2.3}$$

Circumferential stress at commencement of yield,

$$\sigma_{s_o} = \frac{\bar{\sigma}}{\sqrt{1 - \nu + \nu^2}} \tag{2.4}$$

Tresca's Yield Criterion

$$\sigma_s - \sigma_z = \bar{\sigma} \tag{2.5}$$

where, for positive stress values: $\sigma_s > \sigma_x > \sigma_z$

$$\therefore \sigma_{s_o} = \bar{\sigma} \tag{2.6}$$

From elastic conditions, circumferential strain at the instant of yielding, for either criterion is given by:

$$\varepsilon_{s_o} = \frac{\sigma_{s_o}}{E}(1-\nu^2) \tag{2.7a}$$

$$\varepsilon_{z_o} = -\frac{1}{1-\nu} \cdot \varepsilon_{s_o} \tag{2.7b}$$

Radius of bend to middle plane at initial yield in outside fibre,

$$R_y = a/\varepsilon_{s_o} \tag{2.8}$$

Ratio of actual radius to initial yield radius,

$$\varepsilon_s/\varepsilon_{s_o} = a/c \tag{2.9}$$

By evaluating equations, (2.2) and (2.5), the maximum stresses attainable may be calcuated,

$$\text{Von Mises:} \quad \sigma_{s_{max}} = \frac{2\bar{\sigma}}{\sqrt{3}}\,; \quad \sigma_{x_{max}} = \frac{\bar{\sigma}}{\sqrt{3}} \tag{2.10}$$

$$\text{Tresca:} \quad \sigma_{s_{max}} = \bar{\sigma}; \quad \sigma_{x_{max}} = \frac{\bar{\sigma}}{2} \tag{2.11}$$

If a value of 0.3 is assumed for Poisson's Ratio, the theoretical values for sheet bending behaviour can be summarized as follows:

	Von Mises	Tresca
σ_{s_o}	$1.127\ \bar{\sigma}$	$\bar{\sigma}$
σ_{x_o}	$0.338\ \bar{\sigma}$	$0.3\ \bar{\sigma}$
ε_{s_o}	$1.025\ \bar{\sigma}/E$	$0.91\ \bar{\sigma}/E$
ε_{z_o}	$-1.465\ \bar{\sigma}/E$	$-1.3\ \bar{\sigma}/E$
$\sigma_{s_{max}}$	$1.156\ \bar{\sigma}$	$\bar{\sigma}$
$\sigma_{x_{max}}$	$0.578\ \bar{\sigma}$	$0.5\ \bar{\sigma}$

The loading path during the bending operation is shown in Figs. 2.3 and 2.4 for the yield criterion assumed.

2.2 Incremental Stress-Strain Analysis

To obtain a theoretical prediction of the complete stress-strain curve for the bending of a thin sheet, the transition between the purely elastic and the perfectly plastic portions of the curve must be analysed. Suitable equations are those due to Prandtl-Reuss as given in Hill.[4] These can be expressed in incremental form as:

$$\left.\begin{aligned} d\varepsilon_s &= \frac{1}{3}(2\sigma_s - \sigma_z - \sigma_x)\,d\lambda + \frac{1}{E}(d\sigma_s - \nu d\sigma_z - \nu d\sigma_x) \\ d\varepsilon_z &= \frac{1}{3}(2\sigma_z - \sigma_x - \sigma_s)\,d\lambda + \frac{1}{E}(d\sigma_z - \nu d\sigma_x - \nu d\sigma_s) \\ d\varepsilon_x &= \frac{1}{3}(2\sigma_x - \sigma_s - \sigma_z)\,d\lambda + \frac{1}{E}(d\sigma_x - \nu d\sigma_s - \nu d\sigma_z) \end{aligned}\right\} \quad (2.12)$$

where $d\lambda$ is the proportionality factor. Substituting Equation (2.1); $\varepsilon_x = \sigma_z = 0$,

$$d\varepsilon_s = \frac{1}{3}(2\sigma_s - \sigma_x)\,d\lambda + \frac{1}{E}(d\sigma_s - \nu d\sigma_x)$$

and,

$$0 = \frac{1}{3}(2\sigma_x - \sigma_s)\,d\lambda + \frac{1}{E}(d\sigma_x - \nu d\sigma_s)$$

Eliminating the proportionality factor,

$$E\,d\varepsilon_s = \frac{2\sigma_s - \sigma_x}{2\sigma_x - \sigma_s}(\nu d\sigma_s - d\sigma_x) + (d\sigma_s - \nu d\sigma_x) \quad (2.13)$$

also,

$$E\,d\varepsilon_z = -\frac{\sigma_s + \sigma_x}{2\sigma_x - \sigma_s}(\nu d\sigma_s - d\sigma_x) - (\nu d\sigma_s + \nu d\sigma_x) \quad (2.14)$$

These differential equations for strains in the s and z directions can be integrated to obtain expressions for strains in incremental form,

Von Mises Yield Criterion

By subsitution of $\sigma_s{}^2 - \sigma_s\sigma_x + \sigma_x{}^2 = \bar{\sigma}^2$ and $\frac{d\sigma_s}{d\sigma_x} = -\frac{(2\sigma_x - \sigma_s)}{(2\sigma_s - \sigma_x)}$, Equation (2.13) becomes

$$E\ d\varepsilon_s = \left[1 - 2\nu + \frac{3\bar{\sigma}^2}{(\sigma_s - 2\sigma_x)(2\sigma_s - \sigma_x)}\right] d\sigma_x$$

$$\therefore E(\varepsilon_s - \varepsilon_{s_o}) = (1 - 2\nu)\sigma_x + \int \frac{3\bar{\sigma}^2}{(\sigma_s - 2\sigma_x)(2\sigma_s - \sigma_x)} \cdot d\sigma_x \tag{2.15}$$

now, let $I = \int \frac{3\bar{\sigma}^2}{(\sigma_s - 2\sigma_x)(2\sigma_s - \sigma_x)} \cdot d\sigma_x$

$$(2\sigma_s - \sigma_x)\,d\sigma_s = -(2\sigma_x - \sigma_s)\ d\sigma_x$$

$$\therefore I = -\int \frac{3\bar{\sigma}^2}{(\sigma_s - 2\sigma_x)(2\sigma_x - \sigma_s)} \cdot d\sigma_s$$

$\therefore$ Using Von Mises criterion, $\sigma_s\sigma_x = \sigma_s{}^2 + \sigma_x{}^2 - \bar{\sigma}^2$

$$I = -\int \frac{3\bar{\sigma}^2}{3\sigma_s{}^2 - 4\bar{\sigma}^2} \cdot d\sigma_s$$

This is a standard form, yielding

$$I = -\frac{\sqrt{3}}{4}\,\bar{\sigma}.\ \log\left|\frac{2\bar{\sigma}/\sqrt{3} - \sigma_s}{2\bar{\sigma}/\sqrt{3} + \sigma_s}\right| + C$$

$$\therefore\ E(\varepsilon_s - \varepsilon_{s_o}) = (1-2\nu)\sigma_x - \frac{\sqrt{3}\bar{\sigma}}{4}\ .\ \log\left|\frac{2\bar{\sigma}/\sqrt{3} - \sigma_s}{2\bar{\sigma}/\sqrt{3} + \sigma_s}\right| + C \qquad (2.16)$$

where C is given by the boundary conditions of zero stress at zero strain:

$$C = \frac{\sqrt{3}\bar{\sigma}}{4}\ .\ \log\left|\frac{2\sqrt{1-\nu+\nu^2} - \sqrt{3}}{2\sqrt{1-\nu+\nu^2} + \sqrt{3}}\right| - \frac{\nu\bar{\sigma}(1-2\nu)}{\sqrt{1-\nu+\nu^2}} \qquad (2.17)$$

<u>Tresca's Yield Criterion</u>

A similar solution is obtained for this criterion:

$$E(\varepsilon_s - \varepsilon_{s_o}) = (0.5 - \nu)(\sigma_x - \nu\bar{\sigma}) + \frac{3}{4}\,\bar{\sigma}.\log\left|\frac{1-2\nu}{(1-2\sigma_x/\bar{\sigma})}\right| \qquad (2.18)$$

in which the constant of integration is included.

These equations have been evaluated by means of a computer to obtain the complete stress-strain characteristic for both Von Mises' and Tresca's yield criteria. The programs used are shown in the Appendix.

2.3 <u>Elastic Springback Analysis</u>

Using a value for Poisson's ratio of 0.3, the values obtained from these equations are plotted in

Figs. 2.6 and 2.7. These curves describe the stress-strain characteristic in two directions of an element in the cross section of a thin sheet which is subjected to bending into the plastic range. These curves can also show the complete stress distribution throughout the whole cross-section of the sheet for a particular radius of bend. This is done by drawing the curves in such a way that the ratio of the elastic portion of the curve to the complete curve is the same as a particular value of the ratio, a/c. If this is achieved, the stress distribution before springback will be obtained, and the strain axis will also become equivalent to a measure of the distance of the various fibres from the neutral axis of the sheet.

Arranging the stress-strain curves in this fashion, enables them to be employed in a construction which depicts graphically the adjustment of the various stresses and strains within the sheet during elastic springback. By obeying the basic requirements of equilibrium and planes remaining plane, the stress unloading path of each fibre in the sheet can be traced during the elastic springback. This interaction enables the residual stress distribution occurring after elastic springback to be predicted throughout the thickness of the sheet. This construction also obtains the theoretical values of the elastic springback for all values of the ratio a/c.

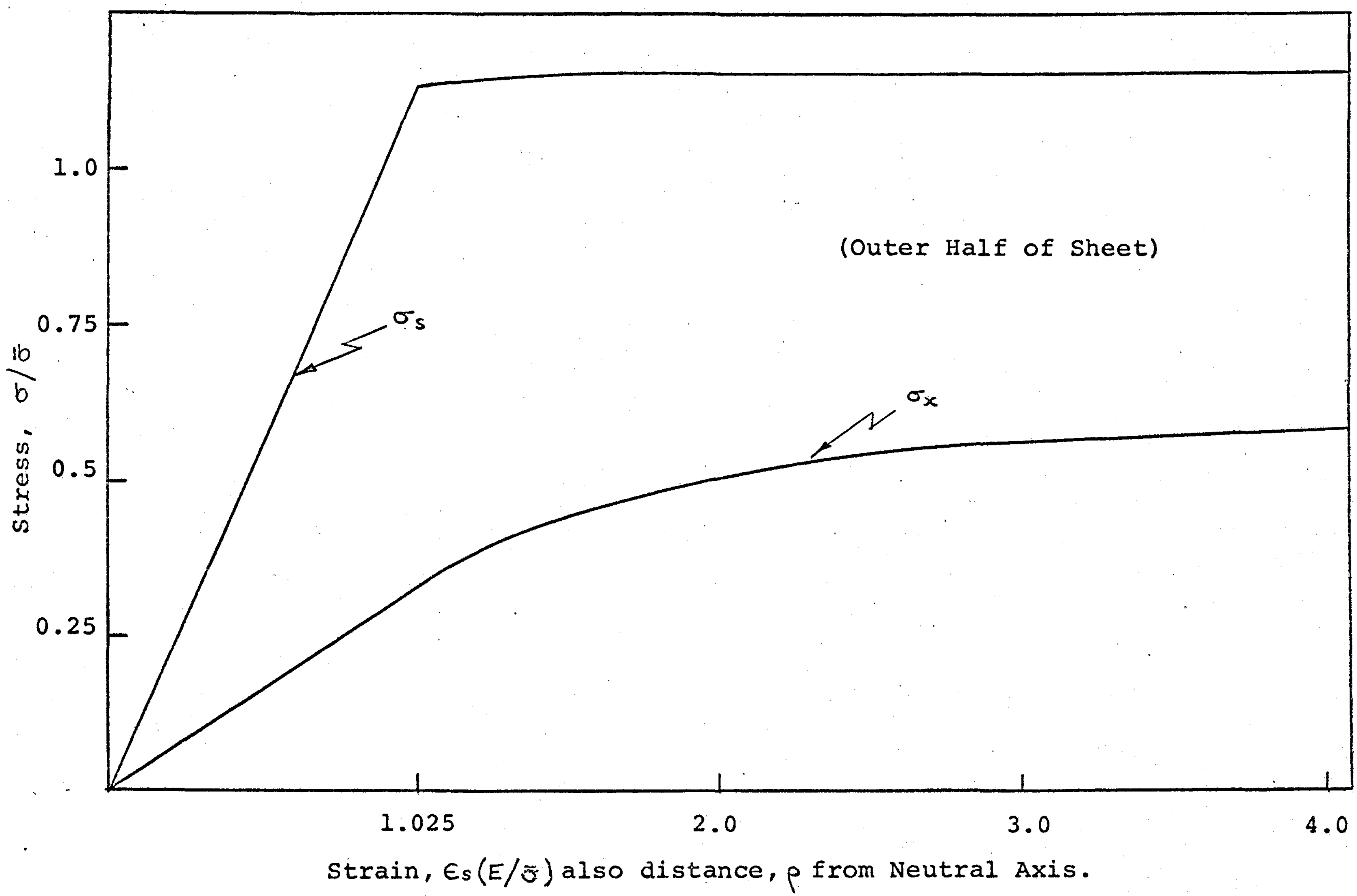

FIG. 2.6 THEORETICAL STRESS-STRAIN CURVES FOR SHEET BENDING. (Von Mises)

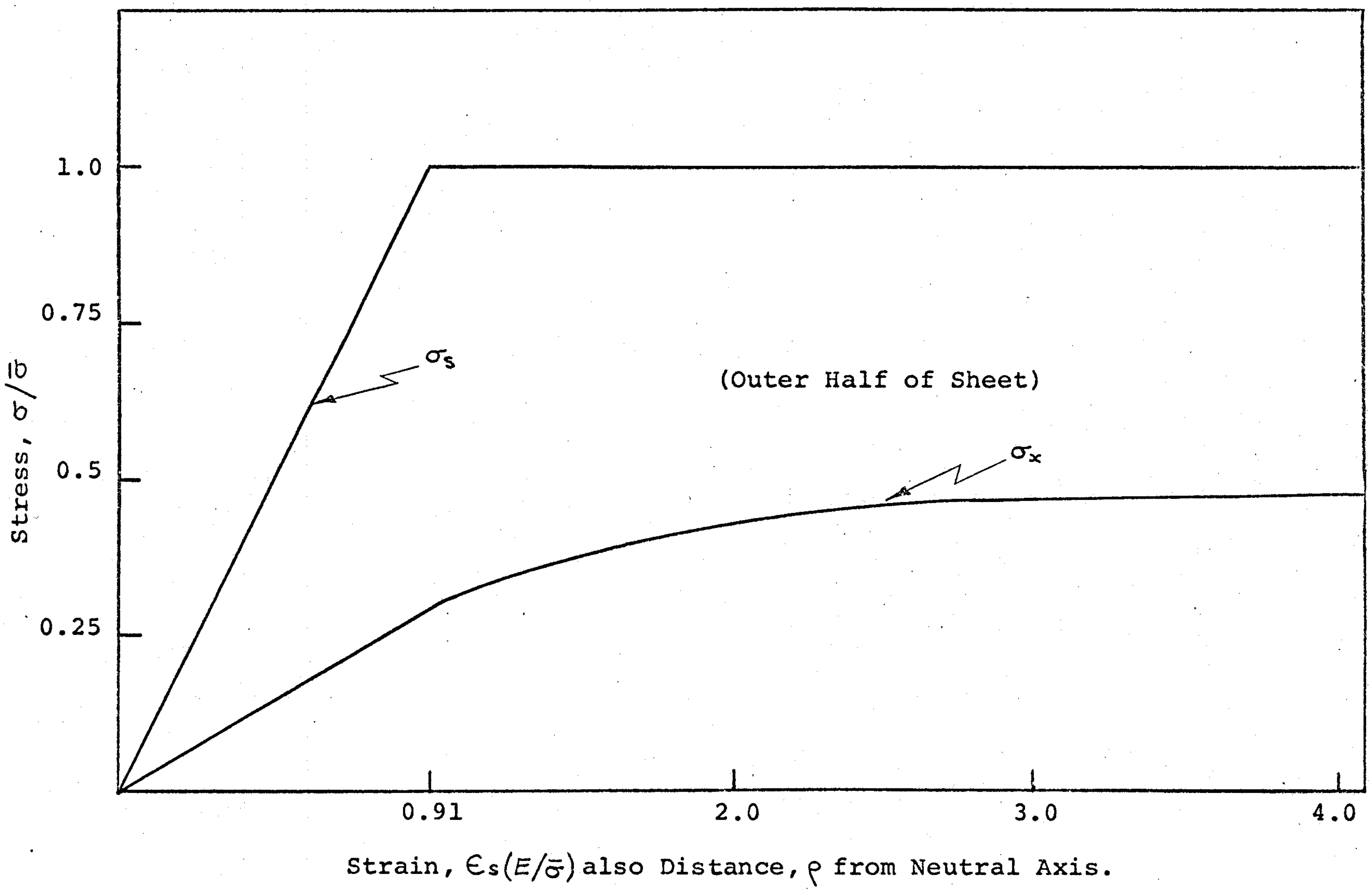

FIG. 2.7 THEORETICAL STRESS-STRAIN CURVES FOR SHEET BENDING. (Tresca)

To explain this construction, it is convenient to initially consider only the outer circumferential fibres of the sheet, and follow their stress-strain relationship during a bending operation. This approach was first performed by Schroeder[5] and is shown in Fig. 2.8. Each circumferential outer fibre during bending would follow its respective curve until it reached the point P. When the bending force is released, elastic recovery along the lines PQ would occur until all the stress is released and a permanent strain, ε_r remains.

It is obvious, however, that the other fibres in the cross section all influence the final distribution of stress throughout the sheet, and that the stress-strain characteristic for the outside fibre will not in fact be as in Fig. 2.8. The actual stress distribution that occurs in the circumferential direction is shown in Fig. 2.9.

It can be seen that the outer curve, representing the stress-strain characteristic before the bending force is removed, has five equidistant points marked out along it. Each of these points characterizes the behaviour of a fibre through the cross section of the sheet which will follow its own stress path during springback. The process of springback is purely elastic, so each of these points must follow an elastic unloading line as shown. Now, the changes in strain remain in direct proportion to the

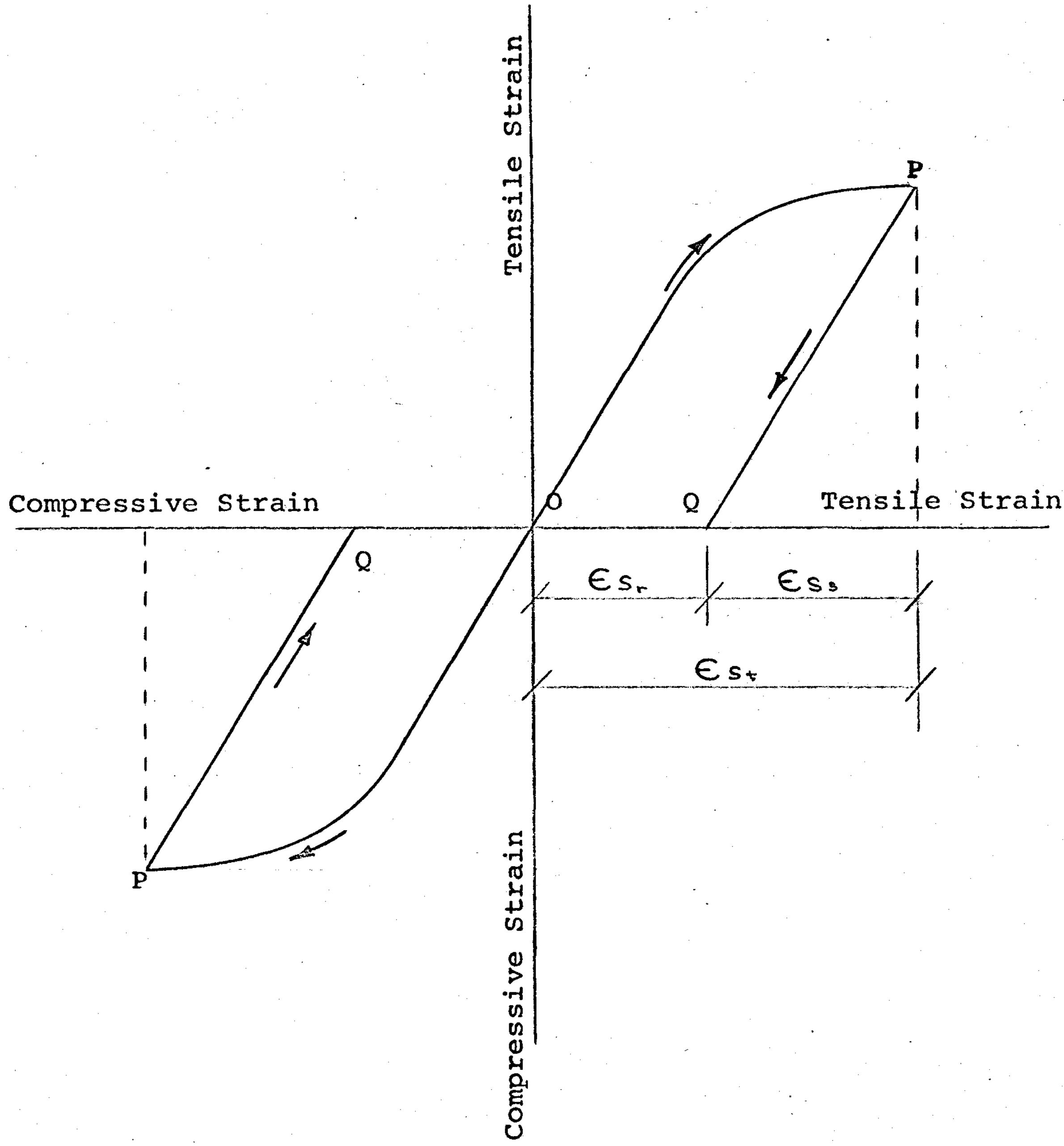

FIG.2.8 ELASTIC RECOVERY OF OUTSIDE FIBRES.
(neglecting influence of inner fibres.)

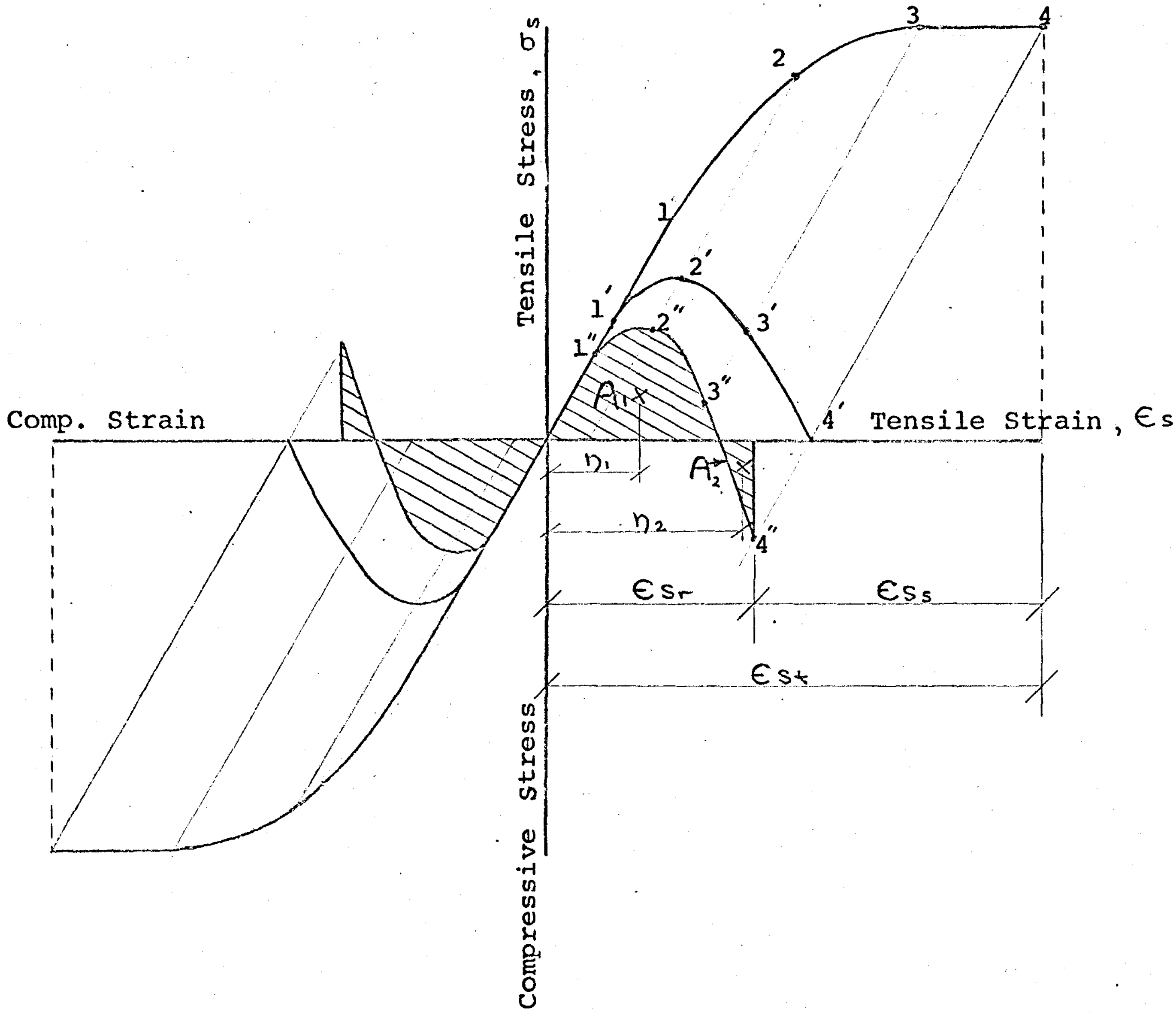

FIG. 2.9 CIRCUMFERENTIAL STRESS DISTRIBUTIONS DURING ELASTIC SPRINGBACK.

distances of the fibres from the neutral axis. The points marked must remain evenly spaced along the axis which represents strain, ε_s as shown in Fig. 2.9, and so the curve, 0-1'-2'-3'-4' can be drawn. This curve represents a residual hoop stress distribution through the sheet at some time during elastic springback. To find the final distribution of residual stress in the circumferential direction occurring on completion of elastic springback, the condition of equilibrium must be satisfied.

For equilibrium, the moments of the resulting residual stresses in the s-direction on each side of the neutral axis must be zero; so the condition must be found so that,

$$\int_0^a \sigma s_R z dz = 0$$

Let $\eta = \frac{\varepsilon s_r}{\varepsilon s_t} z$, be a reduced length parameter to facilitate solution of the residual stress, σs_R. Now,

$$d\eta = \frac{\varepsilon s_r}{\varepsilon s_t} dz$$

$$\therefore \int_0^{\frac{\varepsilon s_r}{\varepsilon s_t} a} \sigma s_R \left(\frac{\varepsilon s_t}{\varepsilon s_r}\right)^2 \eta . d\eta = 0$$

or
$$\int_0^{\frac{\varepsilon s_r}{\varepsilon s_t} a} \sigma s_R \, \eta \, d\eta = 0 \qquad (2.19)$$

where εs_t = total strain in circumferential direction.

εs_r = residual strain in circumferential direction.

In terms of a graphical representation, equation (2.19) can be replaced by

$$A_1\eta_1 = A_2\eta_2 \tag{2.19a}$$

where A_1, A_2, η_1, η_2 are as shown in Fig. 2.9. It is to be observed that equilibrium is now based on a reduced thickness to simplify the trial and error process associated with the evaluating of residual stress distributions. The trial and error process involves drawing in various trial curves, measuring the areas A_1 and A_2 and the moment arms η_1 and η_2, and substituting into Equation (2.19a). The stress distribution is subsequently adjusted until this equilibrium condition is satisfied.

Constructions of this type have been carried out for the criteria of both Von Mises and Tresca, assuming elastic-perfectly plastic material, and for various values of the ratio a/c. The detailed constructions are shown in Figs. 2.10 and 2.11 for Von Mises' and Tresca's yield criteria respectively. It will be seen that the constructions represent the stress distributions only on one side of the neutral axis, the other side being equal and of opposite sign.

In Figs. 2.10 and 2.11 the final residual stress

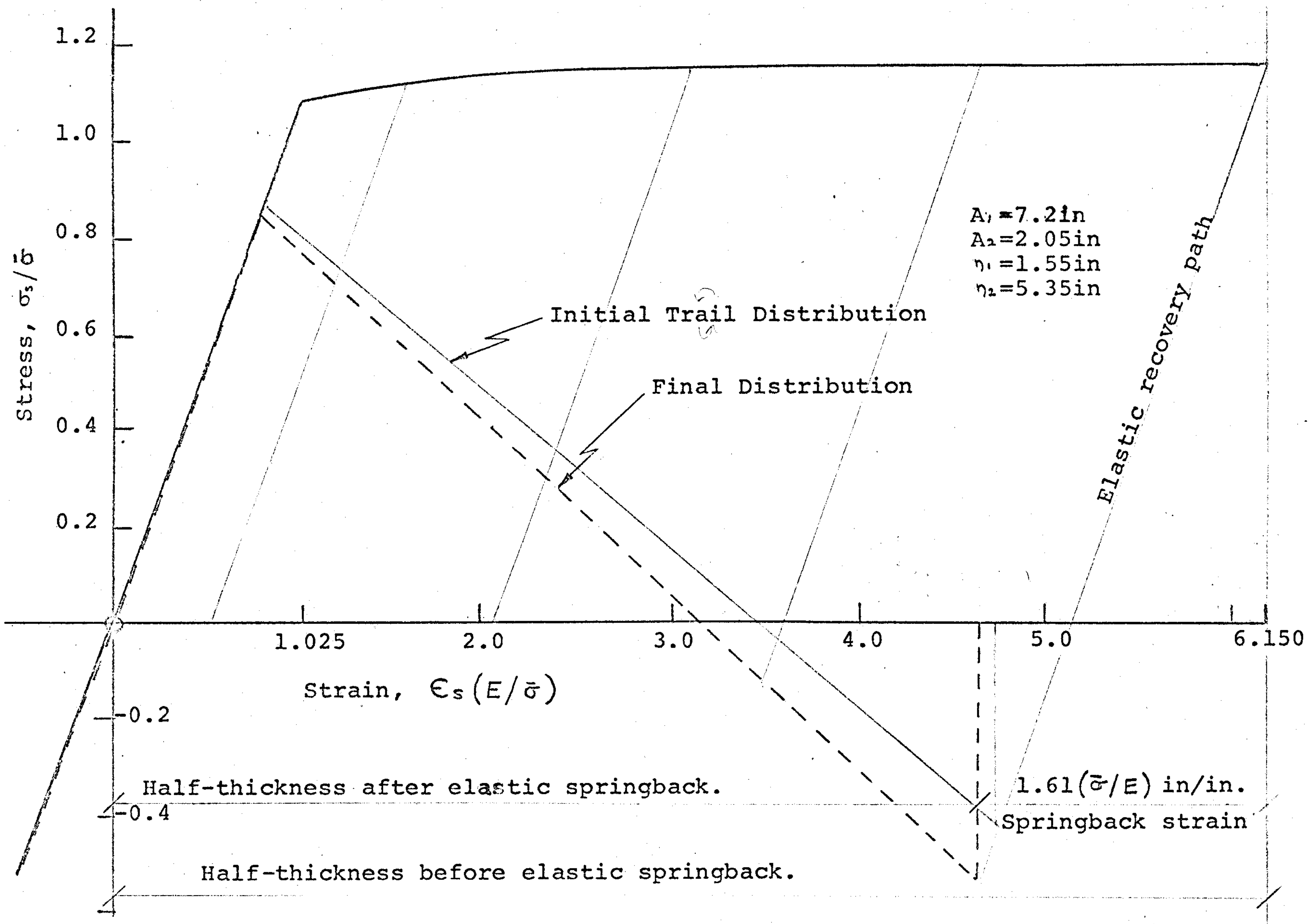

FIG.2.10 STRESS ANALYSIS IN CIRCUMFERENTIAL DIRECTION. (Von Mises)

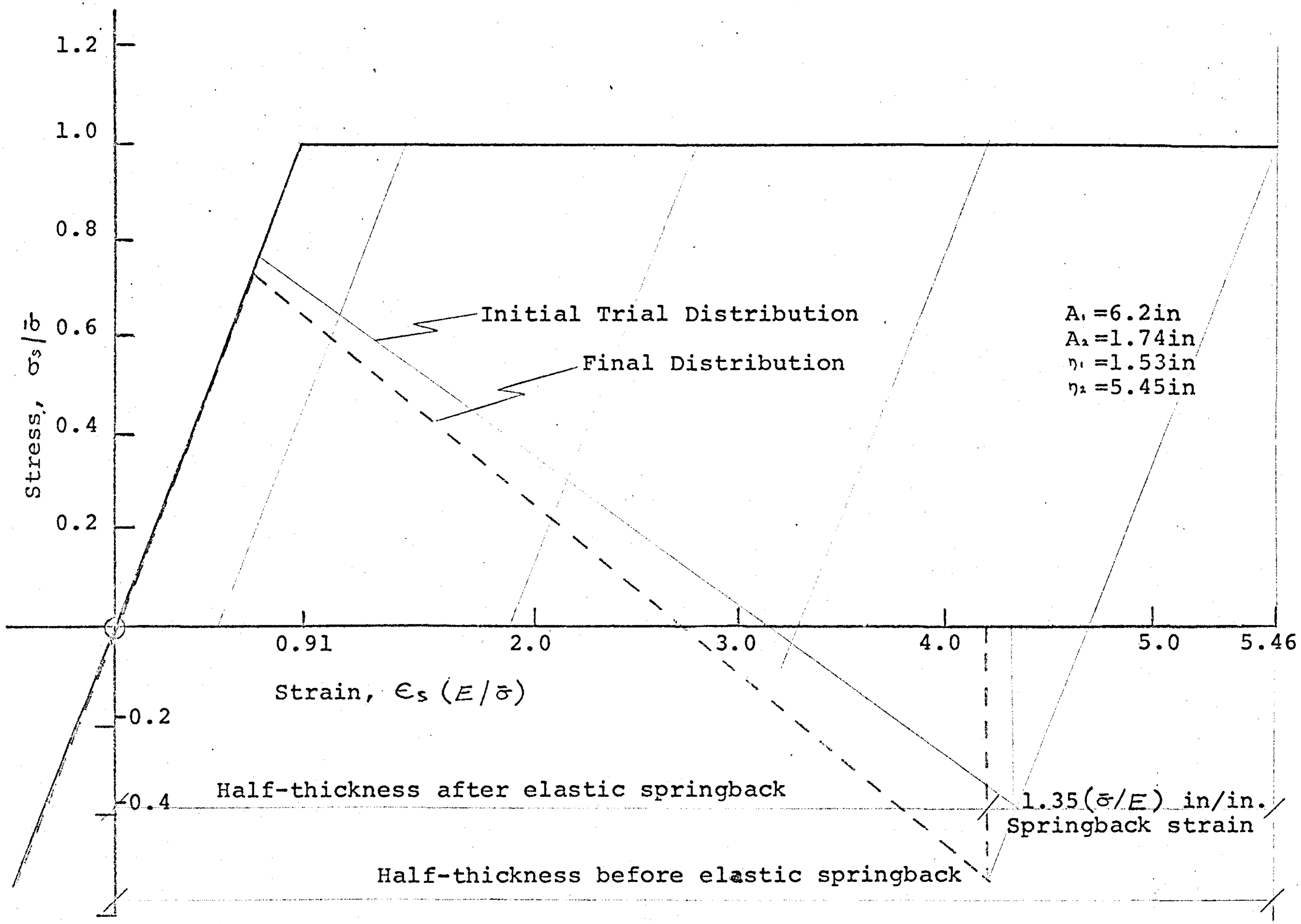

FIG. 2.11 STRESS ANALYSIS IN CIRCUMFERENTIAL DIRECTION. (Tresca)

distribution occurring after elastic springback is shown by the dotted line. The thickness of the sheet is now depicted on a smaller scale, and the stresses in the s-direction throughout the thickness of the sheet are given directly by the dotted line.

The theoretical variation of the outside fibre strain occurring during elastic springback may be read directly from the s-axis of the construction as shown in Figs. 2.10 and 2.11. Having obtained graphically the residual strain, εs_r, and the springback strain, $\varepsilon s_s = \varepsilon s_t - \varepsilon s_r$ when the initial bending strain is known, the theoretical change in radius during elastic springback may be deduced.

During the cold bending operation, the invariance of the length of the neutral axis is given by

$$R\theta = \text{const.} \tag{2.20}$$

Outer fibre strain before springback is

$$\varepsilon s_t = a/R_b$$

while outer fibre strain after springback is

$$\varepsilon s_r = a/R_p$$

where R_b = radius of bend to N.A. before springback.

R_p = radius of bend to N.A. after springback.

Also, $R_b\theta_b = R_p\theta_p$

$$\therefore \frac{\theta_p}{\theta_b} = \frac{R_b}{R_p} = \frac{\varepsilon s_r}{\varepsilon s_t} \tag{2.21}$$

Equation 2.21 may be used to obtain the angle change, and change in radius occurring during elastic springback corresponding to a particular change in outside fibre strain.

With respect to the hoop direction, Schroeder[5] developed two significant indices, K_b and K_p, for the amount of springback occurring in any given case, expressed as a fraction of either the total strain before springback or the residual strain after springback. These indices can also be expressed in terms of angle change or change in radius

$$\frac{\theta_s}{\theta_b} = \frac{R_p - R_b}{R_p} = \frac{\varepsilon_{s_s}}{\varepsilon_{s_t}} = K_b \qquad (2.22)$$

and,

$$\frac{\theta_s}{\theta_p} = \frac{R_p - R_b}{R_b} = \frac{\varepsilon_{s_s}}{\varepsilon_{s_r}} = K_p \qquad (2.23)$$

where θ_b = angle of bend per unit length before springback.

θ_p = angle of bend per unit length after springback.

From these equations two important points may be noted:

1. The hoop strain in any bend is a function only of R and a, not of the total angle.*

---

* Not strictly true in actual bends due to nonuniformity of strain distribution around the bend and effect of flow from adjacent straight sections.

2. The springback ratio, θ_s/θ_b, being proportional to the strain is also only a function of R and a, not of the total angle of the band. Thus the springback per degree of bend is constant, regardless of the total angle of bend.

In Figs. 2.10 and 2.11 the scale of the strain axis is dependent upon the values of Young's modules and the yield stress of the material. The strains in the s-direction are expressed on the graph as a coefficient times $(\frac{\bar{\sigma}}{E})$. Substitution of values of $\bar{\sigma}$ and E for a particular material will give the actual strain values in inches per inch.

For the construction performed in Fig. 2.10 for Von Mises' yield criterion and ratio a/c = 6.0, the theoretical elastic springback strain is 1.61 $(\frac{\bar{\sigma}}{E})$ in/in. with $E = 29.5 \times 10^6$ lb/in^2, and $\bar{\sigma} = 31{,}000$ lb/in^2, this elastic springback results in a change of radius from 3.82 ins. to 5.15 ins., and an elastic springback strain in the outside fibres of 0.0017 in/in. The maximum residual stress value in the s-direction is $0.87\bar{\sigma}$ occurring at a distance a/6 from the neutral axis. The fibres on the outside surface of the bend have a residual stress of $0.55\bar{\sigma}$ in compression, and correspondingly the fibres on the inside surface are in tension at a value of $0.55\bar{\sigma}$.

The construction performed for Tresca's yield criterion under similar conditions gives a theoretical elastic springback strain of $1.35(\frac{\bar{\sigma}}{E})$ in/in. For steel sheet thickness 0.049 in, with $E = 29.5 \times 10^6 \text{lb/in}^2$ and $\bar{\sigma} = 31{,}000 \text{ lb/in}^2$, this elastic springback results in a change of radius from 4.28 in to 5.71 in, and an elastic springback strain in the outside fibres of .0015 in/in. The maximum residual stress value is $0.75\bar{\sigma}$ occurring at a distance of a/6 from the neutral axis, and the residual stress values at the outside fibres are $\pm 0.46\bar{\sigma}$.

These constructions have been performed for various values of the ratio, a/c for both Von Mises' and Tresca's yield criteria, and the variation of elastic springback strain with a/c obtained. This relation is shown in Fig. 2.12. Curves may be drawn for K_b and K_p versus a/R_b and a/R_p[5], but it was considered sufficient here to obtain theoretical values of elastic springback for various a/c to compare with the experimental results.

2.4 Analysis of Stresses in Longitudinal Direction

The residual stresses which are of primary importance when considering their effect on thin-walled fabricated sections under load, are those occurring in the longitudinal direction, (x-direction). To obtain a theoretical distribution of the residual stresses in this direction, a further construction may be performed

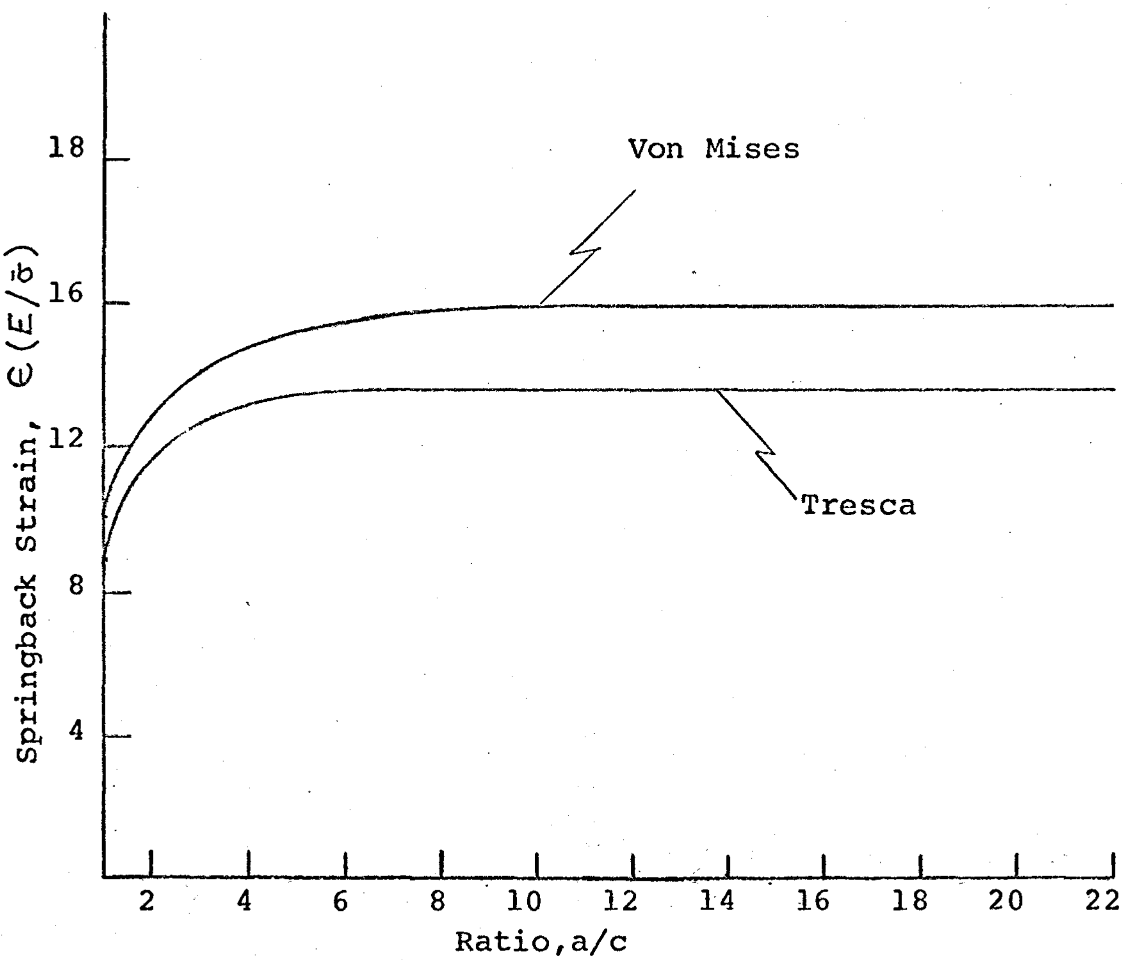

FIG. 2.12 VARIATION OF ELASTIC SPRINGBACK STRAIN WITH RATIO, a/c.

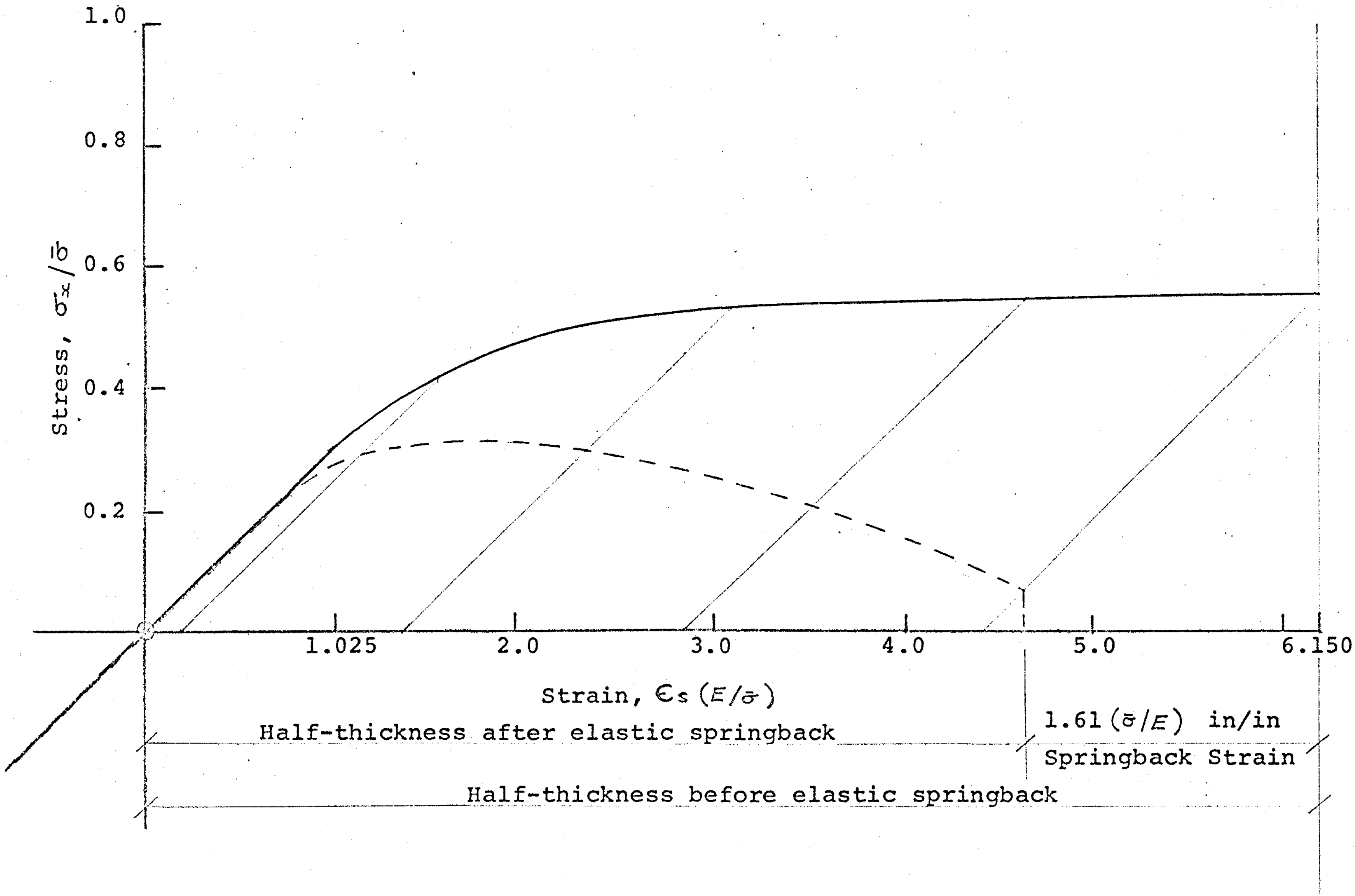

FIG. 2.13 STRESS ANALYSIS IN LONGITUDINAL DIRECTION. (Von Mises)

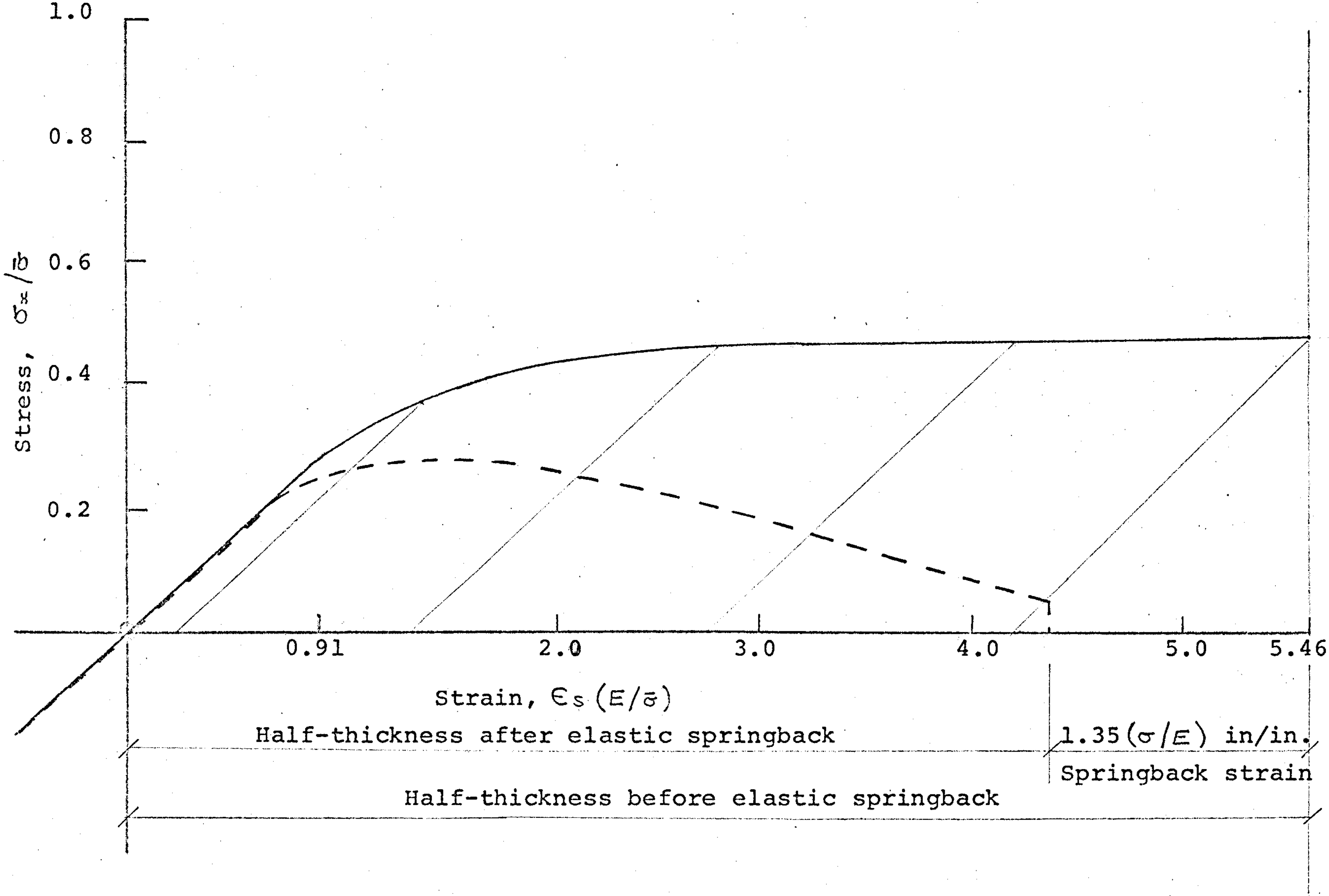

FIG. 2.14 STRESS ANALYSIS IN LONGITUDINAL DIRECTION. (Tresca)

making use of the distributions obtained for the residual stresses in the s-direction. In Fig. 2.13, the curve describing the stresses in the x-direction throughout the cross section before elastic springback is shown for Von Mises' yield criterion and the ratio $a/c = 6.0$. As before, particular fibres throughout the cross section will unload elastically during springback. Since the strains remain in direct proportion to the distances of the fibres from the neutral axis, and the ratio of the stresses, σ_x/σ_s in bending in the elastic range is 0.3, then the residual stress distribution after elastic springback may be plotted for the x-direction.

It is not necessary to have zero moments of the residual stress components in the x-direction about the neutral axis, as an out-of-balance of moments tending to cause rotation is balanced by membrane stresses at the ends of the sheet. This action produces an anticlastic curvature which is concentrated at the ends of the sheet. Fung and Wittrich[19] have shown that the total extent of this anticlastic curvature is only of the order of $3\sqrt{Rt}$ from the ends, and that the apparent out-of-balance of moments about the s-direction produces no curvature effect through the remainder of the sheet.

The complete residual stress distribution in both the longitudinal and circumferential directions for a sheet subject to cold bending in one direction, have now been obtained for both Von Mises' and Tresca's yield criteria for the ratio a/c = 6.0. Constructions for various other values of the ratio a/c have also been carried out in a similar way to obtain various predicted values for residual stress distribution and elastic springback. It has therefore been shown how to predict both the residual stress distribution, and the elastic springback likely to occur when a thin sheet of any particular thickness is bent to any known radius and then released.

Having thus obtained these residual stress distributions, it is necessary to consider their effects upon load-bearing members which have been fabricated from thin sheet by a cold bending process. These effects will be considered in detail in subsequent chapters.

CHAPTER III

THEORETICAL PREDICTIONS OF THE BEHAVIOUR OF COLD-FORMED SECTIONS UNDER LOAD

In this chapter the behaviour of cold-formed sections loaded axially in tension is predicted theoretically, and a theoretical collapse load is obtained for loading in compression.

Initially, the load vs. displacement characteristic for a curved tensile specimen is obtained, taking into account the influence of a residual stress distribution of the type obtained in Chapter II. This characteristic is then used to portray an apparent stress-strain relation for thin-walled open sections loaded axially in compression.

Various modes of failure likely to occur in thin-walled open compression members containing residual stress are outlined, and their applicability to the experimental cross-sections is discussed.

A detailed analysis is then performed for the case of local buckling failure based on the virtual work and incremental plasticity theories.

3.1 Influence of Residual Stress on the Characteristics of Tensile Specimens

3.1.1 Beginning of Non-linearity in Tension

The residual stress distributions, σ_{s_R} and σ_{x_R} across the thickness of a bent sheet which were illustrated in Figs. 2.10 and 2.13 respectively, may be usefully represented by plotting them against each other as shown in Fig. 3.1. The Von Mises' ellipse also shown, represents the stress locus of a point at which an element will deform plastically.

If the cross section of a member, containing this type of residual stress distribution, is loaded axially in tension, the axial fibre stresses will follow the paths indicated by the dotted lines in the figure. Pure tension in the x-direction produces no change in the stress in the s-direction in the elastic range, so that the stress in the x-direction increases while the stress in the s-direction remains at its original value. Similar conditions occur for purely compressive loading, and hence the fibre stresses follow the dotted lines shown in the negative direction. For this case, it is presumed that buckling does not occur for illustration purposes only.

Yielding of a particular fibre will occur when

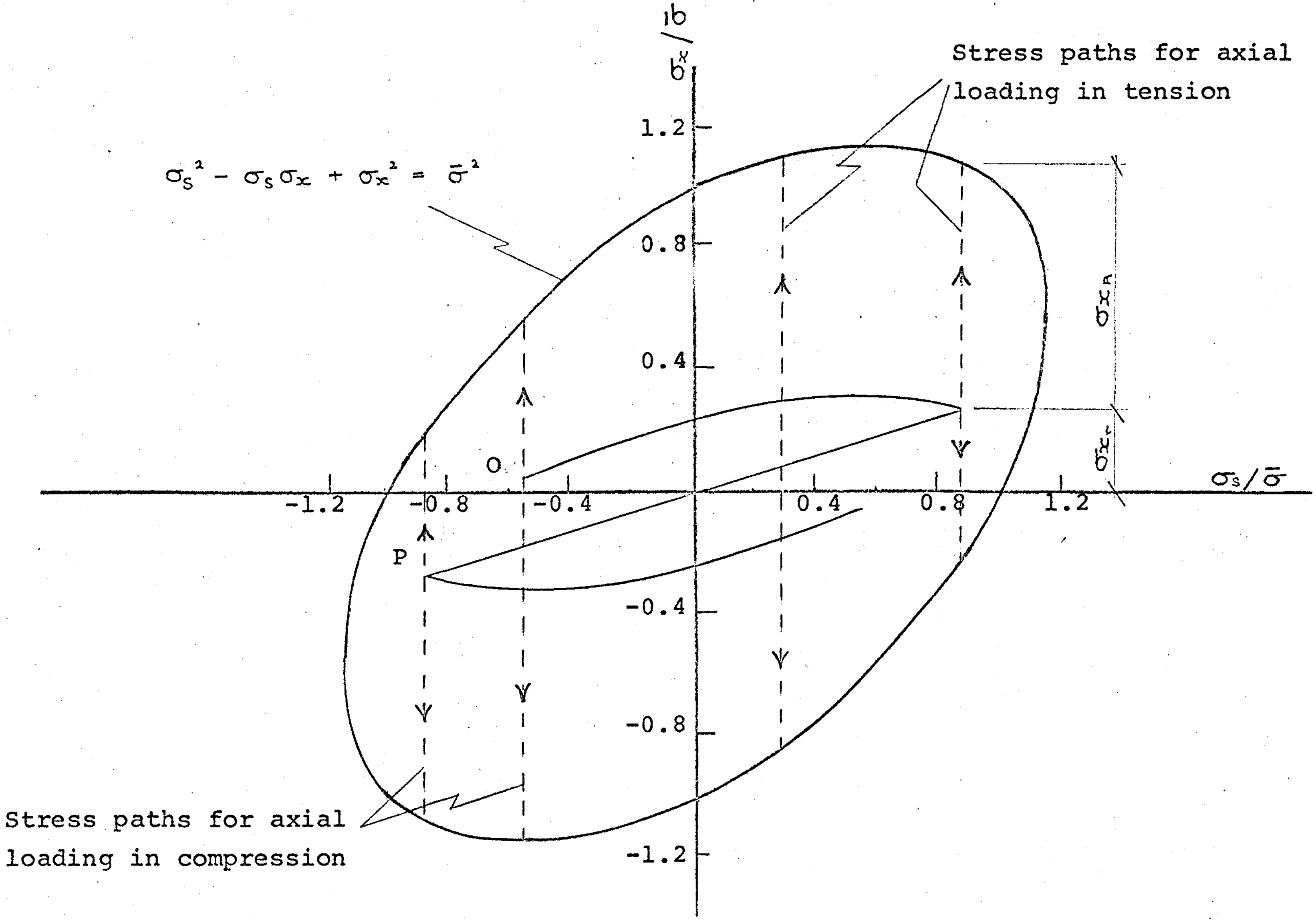

FIG. 3.1 FIBRE STRESSES DURING LOADING. (Von Mises)

its stress path reaches the Von Mises' ellipse. Each fibre will therefore yield when Equation (3.1) is satisfied.

$$\sigma_{s_R}^{2} - \sigma_{s_R}(\sigma_{x_R} + \sigma_{x_A}) + (\sigma_{x_R} + \sigma_{x_A})^{2} = \bar{\sigma}^{2} \qquad (3.1)$$

where σ_{s_R} = residual stress in s-direction.

σ_{x_R} = residual stress in x-direction.

σ_{x_A} = applied loading stress.

If Tresca's yield criterion is used, the various fibres through the thickness of the material yield as shown in Fig. 3.4. The conditions governing the yielding of a fibre are given in Equations (3.2).

$$\left.\begin{array}{ll}
\underline{\sigma_x \text{ increasing (tension)}} & \\
0 < \sigma_{s_R}/\bar{\sigma} < 1 & \sigma_{x_R} + \sigma_{x_A} = \bar{\sigma} \\
-1 < \sigma_{s_R}/\bar{\sigma} < 0 & \sigma_{x_R} + \sigma_{x_A} = (\bar{\sigma} + \sigma_{s_R}) \\
\underline{\sigma_x \text{ decreasing (compression)}} & \\
0 < \sigma_{s_R}/\bar{\sigma} < 1 & \sigma_{x_R} + \sigma_{x_A} = (\sigma_{s_R} - \bar{\sigma}) \\
-1 < \sigma_{s_R}/\bar{\sigma} < 0 & \sigma_{x_R} + \sigma_{x_A} = -\bar{\sigma}
\end{array}\right\} \qquad (3.2)$$

During loading it is assumed that all fibres are equally strained at the same rate, and so the stress rate, $\dot{\sigma}_x$ is presumed to be a constant until some fibre yields. Since $\dot{\sigma}_s = 0$ satisfies the boundary conditions at all times, it is reasonable to assume that $\dot{\sigma}_s = 0$ throughout the thickness and over the full arc length of the cross section. It follows that once the stress of a fibre meets the yield surface it remains at its point of intersection throughout the subsequent plastic loading history.

From Fig. 3.1 for the Von Mises' yield criterion it will be noticed that for tensile loading, fibres at two different regions are likely to become plastic before the rest of the cross section. These are the fibres in the regions O and P, the region O being at the outside circumference of the bend, and the region P at a distance from the neutral axis corresponding to the half-width, c/2 of the purely elastic zone.

For the ratio a/c = 6.0, the fibres at the region O first become plastic when the applied tensile axial stress reaches a value of $0.51\bar{\sigma}$. Fibres at the region P yield at a value of $0.48\bar{\sigma}$, so it is clear that the first fibre to yield in this case is in the region P. This type of construction may be performed for all values of the ratio a/c for both Von Mises' and Tresca's yield criteria. In this way the predicted value for the limit of proportionality may be obtained for members containing any residual stress distribution and subjected to tensile loading.

Fig. 3.2 illustrates the stresses at which the fibres in the regions O and P reach the limit of the elastic zone for various values of the ratio a/c. For values of $a/c < 4.0$, the outside surface fibres in the region O become plastic before any others throughout the cross section at an applied loading stress of above $0.6\bar{\sigma}$. For values of $a/c > 4.0$, the fibres in the region P become plastic first at the applied loading stress shown in the figure.

Clearly the cross section ceases to behave purely elastic at lower values of applied loading stress for larger values of a/c, indicating an apparently lower limit of proportionality for small radius bends than for large radius bends.

3.1.2 Apparent Stress-Strain Characteristics After Yielding

As the loading of a member is increased beyond the limit of proportionality, the load vs. displacement characteristic will be non-linear. The exact path of the load-displacement characteristic subsequent to this initial yielding may be obtained theoretically by considering the complete applied axial stress distribution required to produce yielding of all the fibres across the thickness of the sheet. The distribution of σ_{x_A} for Von Mises' yield

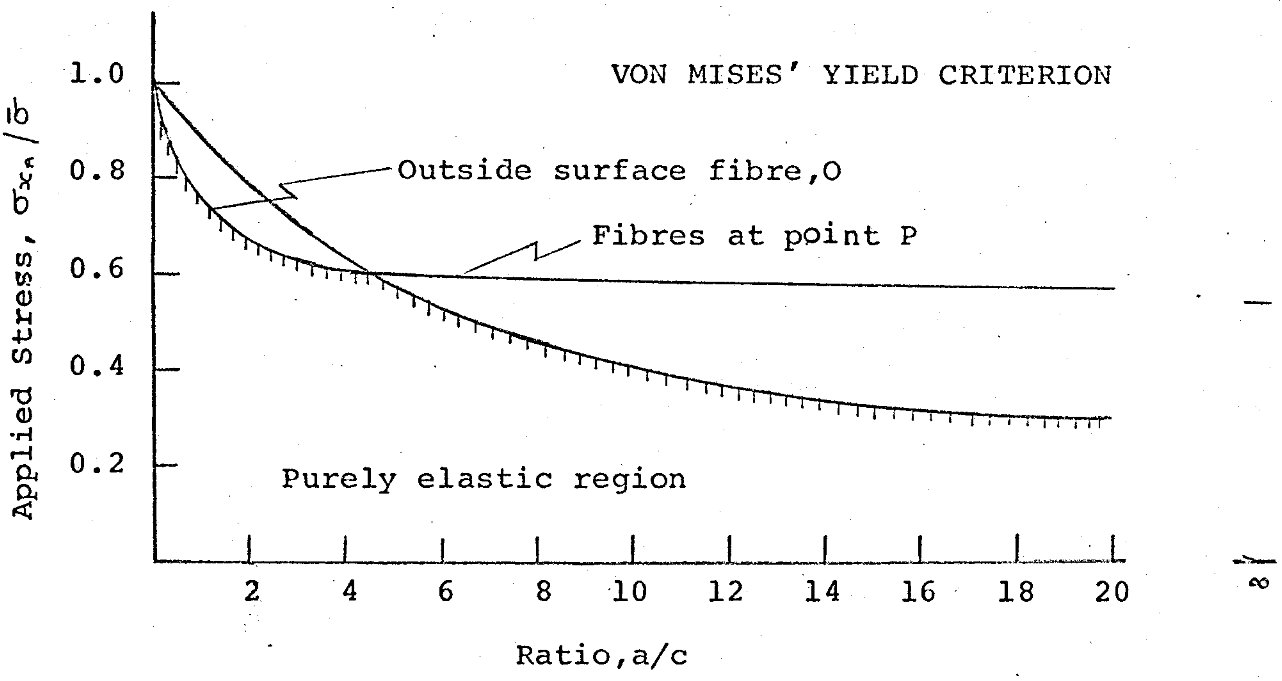

FIG. 3.2 APPLIED AXIAL STRESS AT INITIAL YIELD vs. a/c .

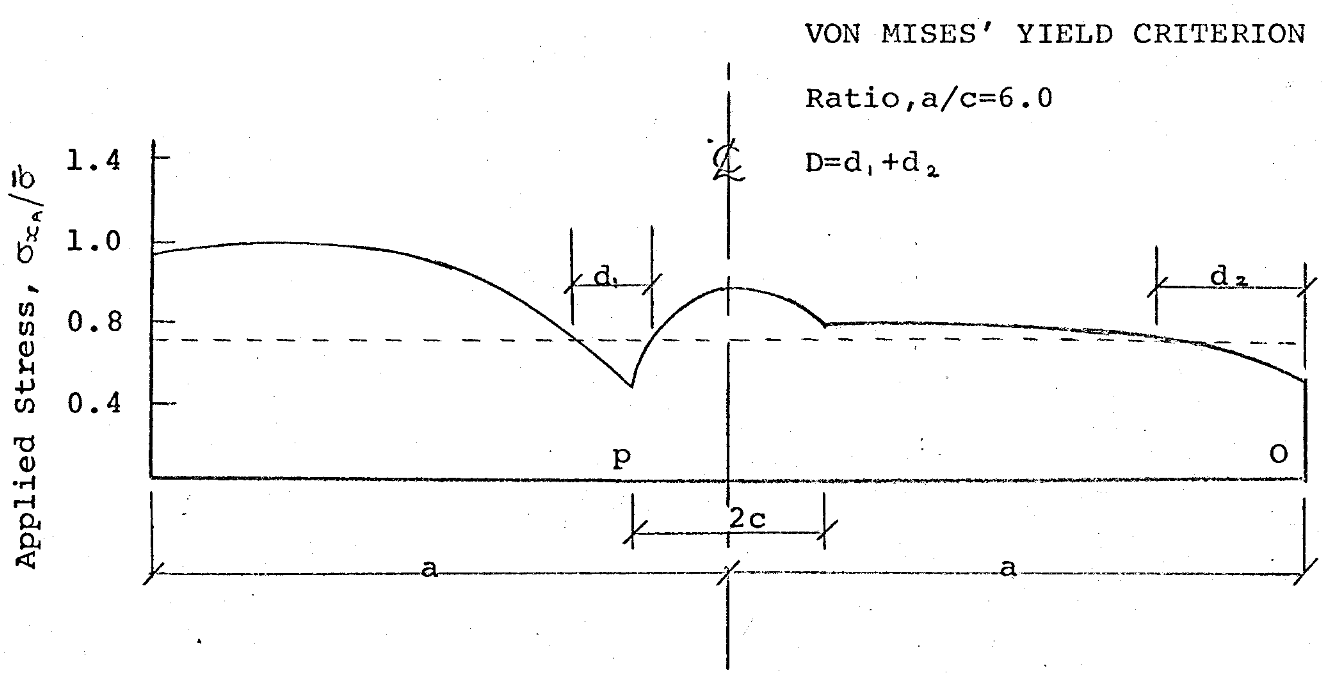

FIG.3.3 APPLIED AXIAL STRESSES NECESSARY FOR YIELD OF VARIOUS FIBRES.

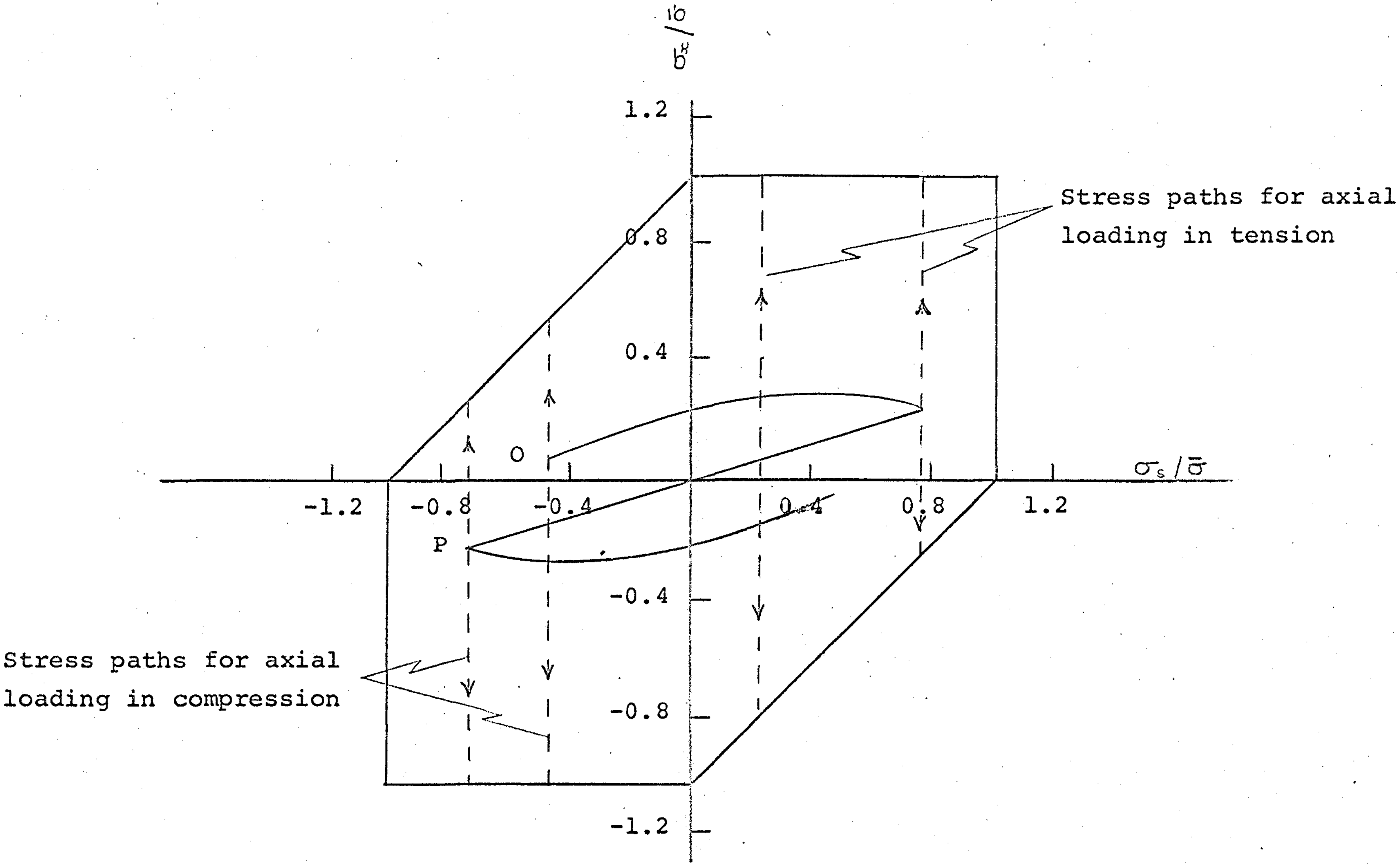

FIG. 3.4 FIBRE STRESSES DURING LOADING. (Tresca.)

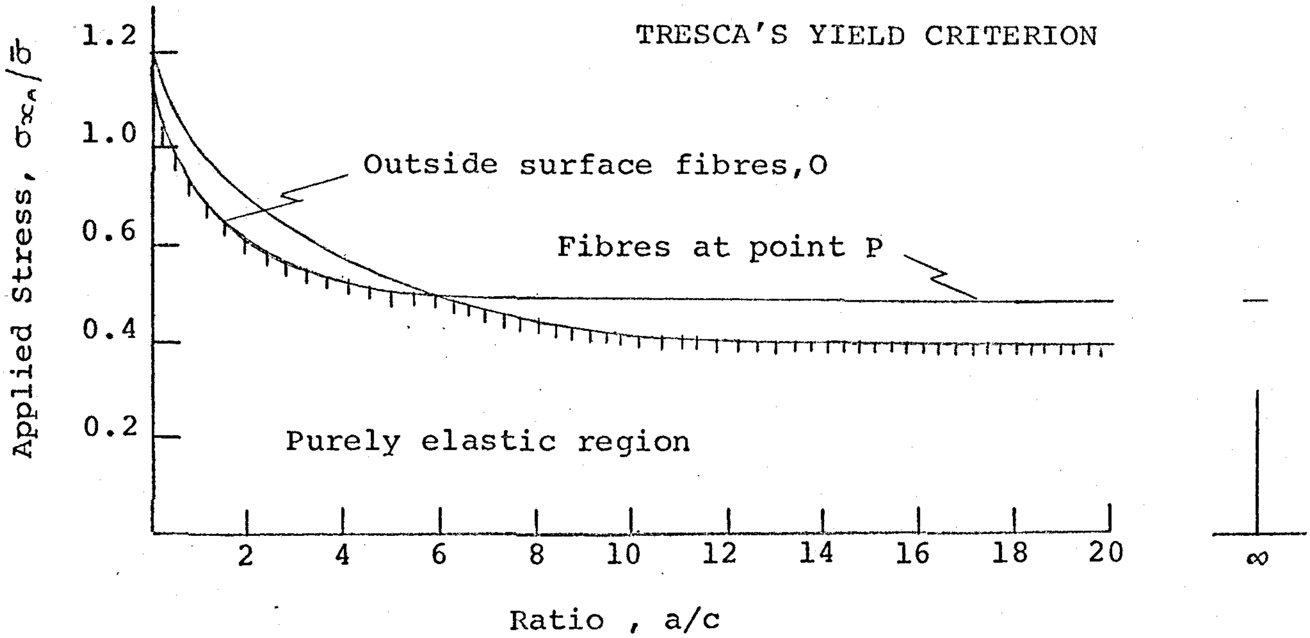

FIG.3.5 APPLIED AXIAL STRESS AT INITIAL YIELD vs. a/c.

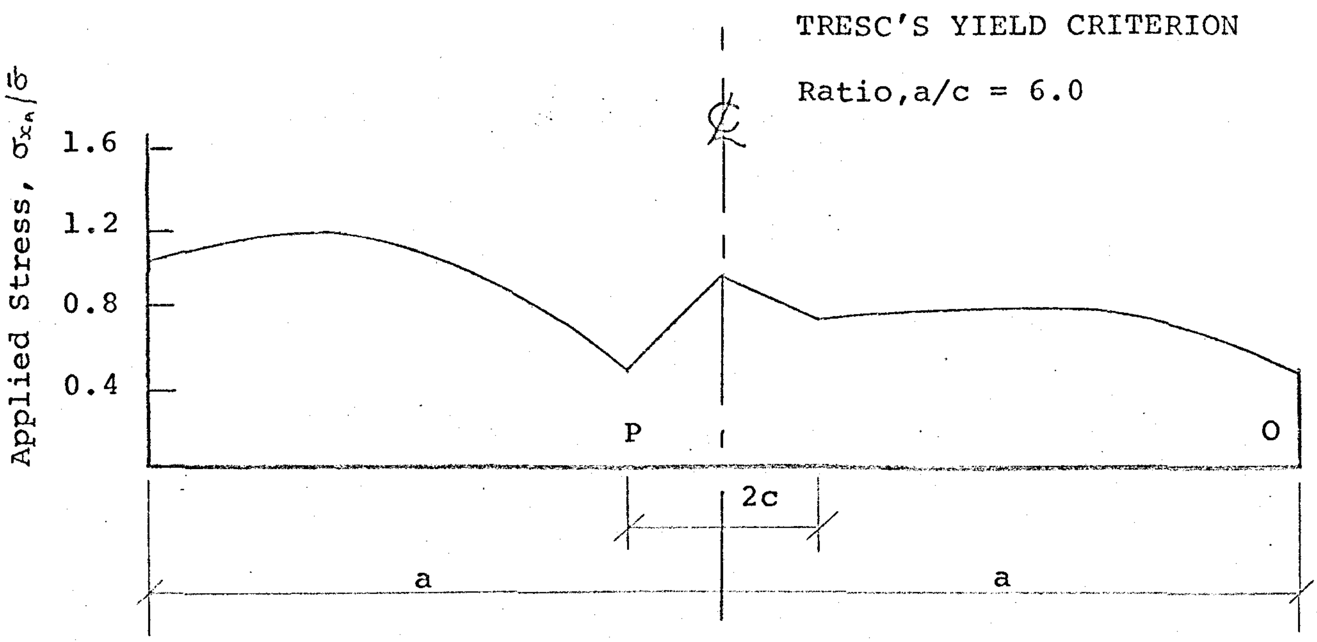

FIG.3.6 APPLIED AXIAL STRESSES NECESSARY FOR YIELD OF VARIOUS FIBRES.

criterion and an a/c ratio of 6.0 is given in Fig. 3.3.

To obtain points on the load vs. displacement curve subsequent to the initial yield, the average applied axial stress throughout the thickness of the material must be determined incrementally for stresses occurring during loading.

Consider in Fig. 3.3 the stage at which the maximum applied fibre stress in the x-direction has reached a value of $0.7\bar{\sigma}$. It can be seen that 15% of the thickness of the sheet has yielded. Once a fibre has become plastic it will not carry any further increase in load, so the value of stress in the fibre remains at the value existing when yielding occurred. It is clear, therefore, that 85% of the thickness of the material will be carrying load at an applied stress level of $0.7\bar{\sigma}$, and that the remaining 15% will be carrying load at an applied stress level between $0.48\bar{\sigma}$ and $0.7\bar{\sigma}$. The average applied stress throughout the thickness of the sheet will consequently be somewhat less than the maximum value of $0.7\bar{\sigma}$. In this manner, the values of average applied stress may be obtained for incremental values of maximum applied stress.

To enable the load-displacement curve to be plotted, it must be remembered that the displacement of a specimen depends upon the maximum applied stress on

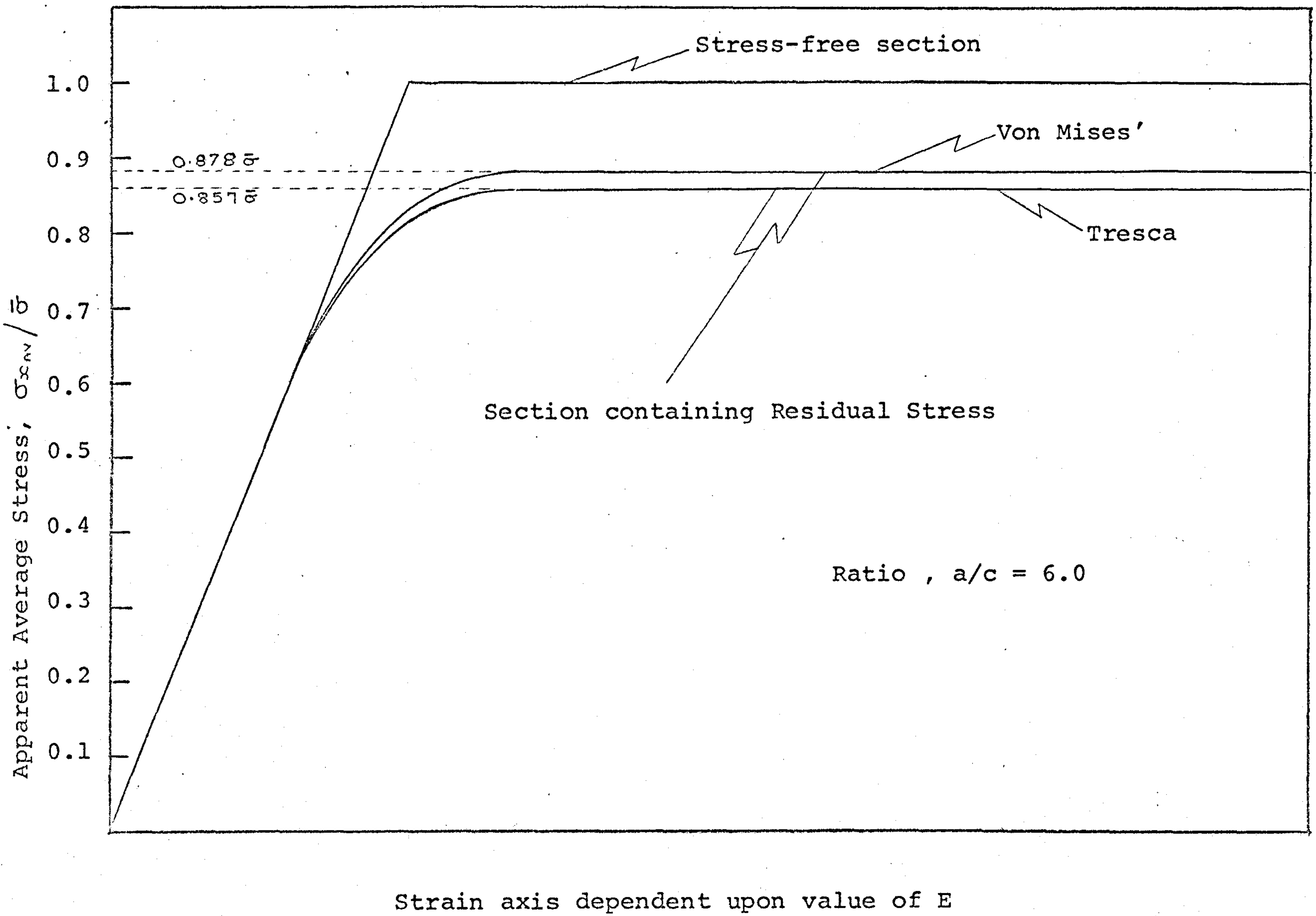

FIG.3.7 THEORETICAL LOAD vs. DISPLACEMENT CHARACTERISTICS FOR TENSILE SPECIMENS.

that specimen. The average applied stress values occurring in a specimen containing residual stress can thus be plotted against the displacement corresponding to the maximum applied axial stress.

A numerical analysis has been carried out for the ratio a/c = 6.0 for both Von Mises' and Tresca's yield criteria, and this method is outlined in the Appendix. The resulting apparent theoretical stress-strain characteristics are illustrated in Fig. 3.7.

3.2 Influence of Residual Stress on the Characteristics of Compression Specimens

3.2.1 Discussion of Buckling Modes

The mode of failure likely to occur when a thin-walled open compression specimen is loaded, depends primarily upon the length/radius of gyration ratio of the specimen under consideration. For a long column the mode of failure is governed by the elastic flexural stiffness, EI; and for a short column by the inelastic strength of the material.

Most columns in use today fall in the intermediate range between these two groups, and it is in this range that secondary factors such as residual stress, accidental crookedness, unintentional end eccentricity, and so forth have the greatest effect on column strength.

Column buckling theory was initiated by Euler who obtained the well-known formula for the "Euler Critical Load" which is 'that load in the elastic range at which a slender axially-loaded column of constant cross section may be in equilibrium in either a straight or a slightly deflected position'. The average stress at the Euler buckling load is obtained by:

$$\sigma_e = \frac{\pi^2 E}{(KL/r)^2} \tag{3.3}$$

This formula was later modified by the development of the Tangent Modulus theory,

$$\sigma_t = \frac{\pi^2 E_T}{(KL/r)^2} \tag{3.4}$$

In this equation the Young's Modulus has been replaced by the Tangent Modulus which takes into account the variation of the stress-strain characteristic brought about by the presence of residual stresses.

Various column strength curves have been proposed describing the behaviour for steel in the inelastic range. A widely-used formula is due to Bleich,[7]

$$\sigma_c = \bar{\sigma} - \frac{\sigma_{x_r}}{\pi^2 E} (\bar{\sigma} - \sigma_{x_R}) \left(\frac{KL}{r}\right)^2 \tag{3.5}$$

This equation is not suitable if $\sigma_{x_r} < 0.5\bar{\sigma}$, in which case erroneous strength values greater than the Euler buckling stress would be predicted for a certain range of KL/r values.

Other modes of failure apart from normal buckling likely to occur in thin-walled open sections are those due to torsional flexural buckling[20] and local buckling. In previous investigations,[10] difficulty has been encountered in separating these two types of failure due to the l/r values employed. In this investigation, it was therefore decided to use only short, stocky sections to prevent the likelihood of failure due to torsional flexural buckling. For this reason only local buckling failure is dealt with in the theory.

3.2.2 Local Buckling Analysis

The plastic buckling strength of cylindrical shells subject to axial compression was first investigated by Timoshenko[13]. His classical solution was based on the inclusion of a reduced modulus term in place of the Young's Modulus term present in the elastic solution.

$$\sigma_c = \frac{2\,E_T\,.\,a}{R\sqrt{3(1-\nu^2)}} \tag{3.6}$$

where a = half-thickness of shell.

R = radius of shell.

E_T = tangent modulus.

A value for the critical buckling load is found by obtaining a pair of values for σ_c and E_T that satisfy both Equation (3.6) and the stress-strain characteristic for the material.

This solution is parallel to that in the reduced modulus column formula, which implies stress reversal or an unloading process during buckling and leads to unconservative results.[14]

The problem was next studied by Bijlaard,[15] whose solution was obtained by the method of solving the characteristic equation derived from a set of equilibrium equations. The stress-strain relationships based on the deformation theory and without stress reversal were used in his solution dealing with both axisymmetric and circumferential buckling modes. It was found that the circumferential buckling mode yields a slightly higher buckling load as compared with that of the axisymmetric mode of buckling.

A more recent analysis has been made by L. H. N. Lee[9] in which Donnell's equations[17] and the principle of virtual work are adapted to determine the critical buckling stresses. A large deflection theory, including the effects of initial imperfections, was used, and stress-strain relationships were considered by both the incremental and deformation theories without the

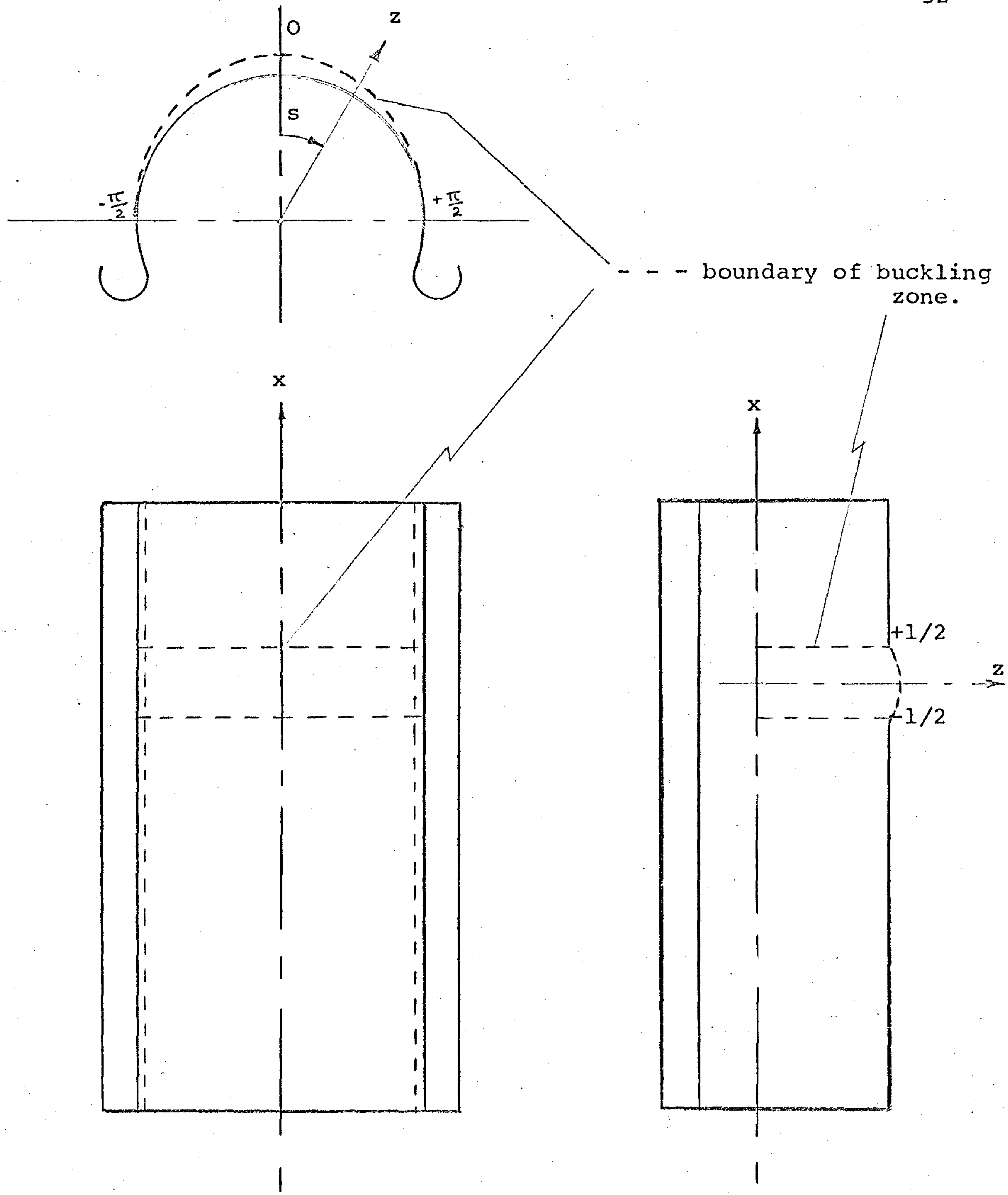

FIG. 3.8 COMPRESSION SPECIMEN SHOWING ASSUMED MODE OF FAILURE.

condition of strain reversal.

In the present analysis, Lee's treatment has been adapted to the type of cross section used in the experimental work. A buckling mode is assumed and stress-strain relationships are considered by the incremental theory, and initial imperfection is neglected.

3.2.2 Analysis of Inelastic Buckling of a Curved Open Section with Stiffeners

The section analyzed is as shown in Fig. 3.8, consisting of a circular curved portion of 220° with circular lips as stiffeners at the ends of the open section. The assumed mode of failure is shown in Fig. 3.8. This type of local buckling occurred in all the experimental tests and was observed to approximate a simple mathematical deflection function,

$$w = At \cos \frac{\pi x}{l} \cdot \cos \frac{s}{r} \tag{3.7}$$

The buckling zone was taken as extending from $-\pi/2$ to $+\pi/2$ in the circumferential direction as was observed in the experimental tests, but the deflection function may easily be modified for buckling through other angles. An exact description of the buckling surface in the axial direction could not be made simply, but the proposed cosine function partially satisfies the boundary conditions and is a close approximation to the buckling surface. Only the conditions regarding continuity of slope at the boundary are not satisfied.

This deflection function is used in the analysis which is based on the principle of virtual work, and the following assumptions usually considered in the theory of thin shells are also made: (a) the displacements are small compared with length or diameter of the specimen, but may be of magnitude comparable with the thickness, and (b) there are no normal stresses in the radial direction, while lines originally normal to the middle surface remain so after loading.

3.2.3 Stress-Strain Relationships

When a body is stressed beyond its elastic limit, the strain ε_{ij} at a point of the body may be considered to consist of two parts, elastic and plastic strains. This may be expressed in tensor notation as

$$\varepsilon_{ij} = \varepsilon^{e}_{ij} + \varepsilon^{p}_{ij}$$

The elastic strain tensor, ε^{e}_{ij}, and the stress tensor, σ_{ij}, have a unique relationship prescribed by the generalized Hooke's Law. There are many theories which may provide a relationship between the plastic strain tensor, ε^{p}_{ij}, and the stress tensor, but only the incremental theory is considered here.

The derivation of the stress-strain relationship by this theory is based on the following assumptions. These are (a) the total work done on the plastic strains must be positive, (b) the increment of the stress tensor and the increment of the strain tensor have a linear relationship, (c) the loading or yield surface is convex and increases in size isotropically during the plastic deformation process, and (d) the loading surface at the loading point has only one normal. As a result, a general plastic stress-strain relation is of the form,

$$d\,\varepsilon^{p}_{ij} = F\left(\frac{\partial f}{\partial \sigma_{ij}}\right)\left(\frac{\partial f}{\partial \sigma_{kl}}\right) d\,\sigma_{kl}, \text{ for } df > 0 \qquad (3.8)$$

The stress-strain relationship will be obtained firstly for Von Mises' yield criterion, and then compared with the relationship for Tresca's yield criterion.

For an isotropic, work-hardening material, assuming a Von Mises' yield surface, the elastic strain increments are given by,[21]

$$d\,\varepsilon^{e}_{ij} = \frac{1+\nu}{E}\,dS_{ij} + \frac{1-2\nu}{E}\,\frac{d\sigma_{KK}}{3}\,\delta_{ij} \qquad (3.9)$$

The loading function is given by $f = \frac{1}{2} S_{ij}S_{ij} = J_2$, the second invariant of the stress deviation tensor. The plastic strain increments are therefore given by

$$d\,\varepsilon^{p}_{ij} = \frac{3}{2}\,\lambda\,S_{ij} \qquad (3.10)$$

where δ_{ij} is the Kroneker delta

λ is a scalar dependent upon both the increment of stress $d\sigma_{ij}$ and the existing state of stress σ_{ij},

$$\lambda = \frac{d\ J_2}{2\ J_2\ E_p^{TAN}} \tag{3.11}$$

and, S_{ij} is the deviator stress

E_p^{TAN} is the plastic tangent modulus

$J_2 = \frac{1}{3}(\sigma_x^{\ 2} - \sigma_x\sigma_s + \sigma_s^{\ 2} + 3\tau_{xs})$

Considering the elastic strain increment, ε^e_{ij}

$$d\ \varepsilon^e_{\ x} = \frac{1+\nu}{E}\ d\ S_x + \frac{1-2\nu}{E}\left[\frac{d\sigma_x + d\sigma_s}{3}\right] \tag{3.12}$$

now, $\quad d\ S_x = \frac{1}{3}\left[2\ d\sigma_x - d\sigma_s\right]$

$$\left.\begin{aligned} \therefore\quad d\ \varepsilon^e_{\ x} &= \frac{d\sigma_x}{E} - \frac{\nu d\sigma_s}{E} \\ \text{Similarly,}\quad d\ \varepsilon^e_{\ s} &= \frac{d\sigma_s}{E} - \frac{\nu d\sigma_x}{E} \end{aligned}\right\} \tag{3.13}$$

The plastic strain increments, ε^p_{ij} in terms of x and s co-ordinates are given by

$$d\ \varepsilon^p_{\ x} = \lambda\left[\sigma_x - \frac{\sigma_s}{2}\right] \tag{3.14}$$

From Equation (3.11)

$$\lambda = \frac{(2\sigma_x-\sigma_s)d\sigma_x+(2\sigma_s-\sigma_x)d\sigma_s + 6\tau_{xs}d\tau_{xs}}{2(\sigma_x{}^2-\sigma_x\sigma_s+\sigma_s{}^2+3\tau_{xs}{}^2)\ E^p{}_{TAN}}$$

$$\therefore\ d\varepsilon^p{}_x = \frac{(2\sigma_x-\sigma_s)d\sigma_x + (2\sigma_s-\sigma_x)d\sigma_s + 6\tau_{xs}d\tau_{xs}}{2(\sigma_x{}^2-\sigma_x\sigma_s-\sigma_s{}^2+3\tau_{xs}{}^2)\ E^p{}_{TAN}}\left[\sigma_x - \frac{\sigma_s}{2}\right]$$

If $\sigma_x >> \sigma_s,\ \tau_{xs}$

$$d\varepsilon_x{}^p = \frac{2\ \sigma_x{}^2\ d\sigma_x - \sigma_x{}^2\ d\sigma_s}{2\sigma_x{}^2\ E^p{}_{TAN}}$$

now,
$$\frac{1}{E^p{}_{TAN}} = \frac{1}{E_T} - \frac{1}{E} \tag{3.15}$$

$$\therefore\ d\varepsilon_x{}^p = \frac{d\sigma_x}{E_T} - \frac{d\sigma_x}{E} - \frac{1}{2}\left[\frac{1}{E_T} - \frac{1}{E}\right]d\sigma_s \tag{3.16}$$

Similarly,

$$d\varepsilon_s{}^p = \frac{(2\sigma_x-\sigma_s)d\sigma_x + (2\sigma_s-\sigma_x)d\sigma_s + 6\tau_{xs}d\tau_{xs}}{2(\sigma_x{}^2-\sigma_x\sigma_s+\sigma_s{}^2+3\tau_{xs}{}^2)\ E^p{}_{TAN}}\left[\sigma_s-\frac{\sigma_x}{2}\right]$$

which for $\sigma_x >> \sigma_s,\ \tau_{xs}$ simplifies to

$$d\varepsilon_s{}^p = -\frac{1}{2}\left[\frac{1}{E_T} - \frac{1}{E}\right]d\sigma_x + \frac{1}{4}\left[\frac{1}{E_T} - \frac{1}{E}\right]d\sigma_s \tag{3.17}$$

Now, the total strain increments are given by

$$d\varepsilon_{ij} = d\varepsilon_{ij}{}^p + d\varepsilon_{ij}{}^e \tag{3.18}$$

from equations (3.13), (3.16-18)

$$\left.\begin{aligned} d\varepsilon_x &= \frac{1}{E_T}\, d\sigma_x - \left[\frac{\nu}{E} + \frac{1}{2}\left(\frac{1}{E_T} - \frac{1}{E}\right)\right] d\sigma_s \\ d\varepsilon_s &= -\left[\frac{\nu}{E} + \frac{1}{2}\left(\frac{1}{E_T} - \frac{1}{E}\right)\right] d\sigma_x + \frac{1}{4}\left(\frac{1}{E_T} + \frac{3}{E}\right) d\sigma_s \end{aligned}\right\} \qquad (3.19)$$

now, $d\gamma xs^p = \frac{3}{2}\,\lambda\,\tau_{xs} \to 0$ as $\tau_{xs} \to 0$

$$\therefore\ d\gamma xs = \left[\frac{2(1+\nu)}{E}\right] d\tau_{xs} \qquad (3.20)$$

Similar relationships may be obtained based upon Tresca's yield criterion. A general two-dimensional form for the yield surface is

$$f = \sigma_x^{\,2} - 2\sigma_x\sigma_s + \sigma_s^{\,2} + 4\tau_{xs} \qquad (3.21)$$

For isotropic strain hardening a tension test will show that,

$$F = \frac{1}{4(\sigma_x^{\,2} - 2\sigma_x\sigma_s + \sigma_s^{\,2} + 4\tau_{xs})}\left(\frac{1}{E_T} - \frac{1}{E}\right) \qquad (3.22)$$

For $\sigma_x >> \sigma_s, \tau_{xs}$, the plastic stress-strain relations in incremental form added to the elastic components become

$$\left.\begin{aligned} d\varepsilon_x &= \frac{1}{E_T}\, d\sigma_x - \left[\frac{\nu}{E} + \left(\frac{1}{E_T} - \frac{1}{E}\right)\right] d\sigma_s \\ d\varepsilon_s &= -\left[\frac{\nu}{E} + \left(\frac{1}{E_T} - \frac{1}{E}\right)\right] d\sigma_x + \frac{1}{E_T}\, d\sigma_s \end{aligned}\right\} \qquad (3.23)$$

$$d\gamma xs = \left[\frac{2(1+\nu)}{E}\right] d\tau_{xs}$$

The stress-strain relationships derived for the criteria of Von Mises and Tresca are different since the normal to the yield surface in each case has a different orientation. The direction of the normal for Tresca's criterion is not unique due to the corner at $\sigma_x = -\bar{\sigma}$, $\sigma_s = 0$. Since subsequent deformation will induce a positive hoop stress, it is reasonable to assume that the normal has a slope of -1 rather than zero. The normal to the yield surface in the case of Von Mises' yield criterion increases as the hoop stress increases, the initial minimum value being -½.

On applying these separate stress-strain relationships to an analysis based on virtual work, different results would be obtained for critical buckling stresses. It must, however, be remembered that these stress-strain relationships only hold true if the stress in the axial direction is much larger than the normal stress in the circumferential direction, and the shear stress in the plane of the shell, i.e., $\sigma_x >> \sigma_s, \tau_{xs}$.

For the deformation configeration assumed, if the stiffened lips on the cross section remain straight, there will be a build up of hoop stress which may well reach values comparable with the axial stress. In this case the stress-strain relationships derived for Von Mises' yield criterion is accurate only at the beginning of buckling since the orientation of the normal to the yield surface changes for all values of the stresses, σ_x and σ_s. Tresca's yield criterion will provide greater accuracy for more significant hoop stresses since its normality is independent of the stresses σ_x and σ_s. (Assuming that σ_x and σ_s are approximately equivalent to principal stresses.) Upper and lower bounds would consequently be anticipated from the application of the two yield criteria.

For either yield criterion the stress-strain relationships may be simplified to

$$\left.\begin{aligned} \varepsilon_x' &= C_{11}\sigma_x' - C_{12}\sigma_s' \\ \varepsilon_s' &= -C_{21}\sigma_x' + C_{22}\sigma_s' \\ \gamma xs &= C_3\ \tau_{xs} \end{aligned}\right\} \qquad (3.24)$$

where the C's indicate the respective coefficients of the stress increments, and the primes indicate differentials.

3.2.4 Membrane Forces and Moments

When a cylindrical-type shell of idealized geometry and material is subjected to axial compression, it may deform with uniform axial shortening and radial expansion prior to the buckling. Let us denote the axial, tangential, and radial components by the displacement increments u, v and w, respectively. The strains or the strain increments may then be determined by the following relationships which include the effects of large deflections.[18]

$$\left.\begin{aligned} \varepsilon_x' &= \left(\frac{\partial u}{\partial x}\right) + \frac{1}{2}\left(\frac{\partial w}{\partial x}\right)^2 && \text{(a)} \\ \varepsilon_s' &= \left(\frac{\partial v}{\partial s}\right) + \frac{1}{2}\left(\frac{\partial w}{\partial s}\right)^2 + \frac{w}{r} && \text{(b)} \\ \gamma xs' &= \frac{\partial u}{\partial s} + \frac{\partial v}{\partial x} + \left(\frac{\partial w}{\partial x}\right)\left(\frac{\partial w}{\partial s}\right) && \text{(c)} \end{aligned}\right\} \quad (3.25)$$

ε_x', ε_s' and $\gamma xs'$ are considered as the middle-surface strain increments.

The membrane forces accompanying the additional displacements are equal to the products of the middle-surface stresses determined by Eqs. (3.24) and the wall thickness, t. This is based on the assumptions that lines originally normal to the middle-surface of the shell remain so after loading, and that no stress reversal occurs anywhere in the shell. These assumptions also provide the basis for the determination of the bending moments; they are

$$
\left.\begin{aligned}
M_x &= -\left[D_{11}\left(\frac{\partial^2 w}{\partial x^2}\right) + D_{12}\left(\frac{\partial^2 w}{\partial s^2}\right)\right] \\
M_s &= -\left[D_{21}\left(\frac{\partial^2 w}{\partial x^2}\right) + D_{22}\left(\frac{\partial^2 w}{\partial s^2}\right)\right] \\
M_{xs} &= D\left(\frac{\partial^2 w}{\partial x \partial s}\right)
\end{aligned}\right] \tag{3.26}
$$

where

$$D_{11} = C_{22}\ t^3/[12(C_{11}C_{22} - C_{21}C_{12})]$$

$$D_{12} = D_{21} = C_{21}t^3/12\,[C_{11}C_{22} - C_{21}C_{12}]$$

$$D_{22} = C_{11}\ t^3/[12(C_{11}C_{22} - C_{21}C_{12})]$$

$$D_3 = t^3/\ 6C_3$$

As a first step towards obtaining a stress function that will be of use in developing equations describing the internal work in the shell, the compatibility equation must be derived by eliminating u and v from Eqs. (3.25). Using the operators $-\frac{\partial}{\partial s}$ on (3.25a); $\frac{\partial}{\partial s}$ on (3.25c)

$$\frac{\partial \varepsilon_{x'}}{\partial s} = \frac{\partial^2 u}{\partial s \partial x} + \left(\frac{\partial^2 w}{\partial x \partial s}\right)\left(\frac{\partial w}{\partial x}\right)$$

$$\frac{\partial \gamma_{xs'}}{\partial x} = \frac{\partial^2 u}{\partial s \partial x} + \frac{\partial^2 v}{\partial x^2} + \left(\frac{\partial^2 w}{\partial x^2}\right)\left(\frac{\partial w}{\partial s}\right) + \left(\frac{\partial w}{\partial x}\right)\left(\frac{\partial^2 w}{\partial x \partial s}\right)$$

subtracting

$$-\frac{\partial \varepsilon_x{}'}{\partial s} + \frac{\partial \gamma_{xs}{}'}{\partial x} = \frac{\partial^2 v}{\partial x^2} + \left(\frac{\partial^2 w}{\partial x^2}\right)\left(\frac{\partial w}{\partial s}\right) \qquad (3.27)$$

Using operators $\frac{\partial^2}{\partial x^2}$ on (3.25b); $\frac{\partial}{\partial s}$ on (3.27)

$$\frac{\partial^2 \varepsilon_s{}'}{\partial x^2} = \frac{\partial^3 v}{\partial s \partial x^2} + \left(\frac{\partial^3 w}{\partial s \partial x^2}\right)\left(\frac{\partial w}{\partial x}\right) + \left(\frac{\partial^2 w}{\partial s \partial x}\right)^2 + \frac{1}{r}\frac{\partial^2 w}{\partial x^2}$$

$$\frac{\partial^2 \gamma xs'}{\partial x \partial s} - \frac{\partial^2 \varepsilon_x{}'}{\partial s^2} = \frac{\partial^3 v}{\partial s \partial x^2} + \left(\frac{\partial^3 w}{\partial s \partial x^2}\right)\left(\frac{\partial w}{\partial s}\right) + \left(\frac{\partial^2 w}{\partial x^2}\right)\left(\frac{\partial^2 w}{\partial s^2}\right)$$

subtracting

$$\frac{\partial^2 \varepsilon_s{}'}{\partial x^2} + \frac{\partial^2 \varepsilon_x{}'}{\partial s^2} - \frac{\partial^2 \gamma xs'}{\partial x \partial s} = \left(\frac{\partial^2 w}{\partial s \partial x}\right) + \frac{1}{r}\left(\frac{\partial^2 w}{\partial x^2}\right) - \left(\frac{\partial^2 w}{\partial x^2}\right)\left(\frac{\partial^2 w}{\partial s^2}\right)$$

(3.28)

thus u and v are eliminated. Now, substituting Eqs.(3.25) into the compatibility equation (3.28)

$$-C_{21}\frac{\partial^2 \sigma_x{}'}{\partial x^2} + C_{22}\frac{\partial^2 \sigma_s{}'}{\partial x^2} + C_{11}\frac{\partial^2 \sigma_x{}'}{\partial s^2} - C_{12}\frac{\partial^2 \sigma_s{}'}{\partial s^2} - C_3\frac{\partial^2 \tau_{xs}}{\partial x \partial s}$$

$$= \left(\frac{\partial^2 w}{\partial s \partial x}\right) + \frac{1}{r}\left(\frac{\partial^2 w}{\partial x^2}\right) - \left(\frac{\partial^2 w}{\partial x^2}\right)\left(\frac{\partial^2 w}{\partial s^2}\right) \qquad (3.29)$$

Let the Airy stress function, $\phi(x,s)$ be defined as follows:

$$\sigma_x{}' = \frac{\partial^2\phi}{\partial s^2}; \quad \sigma_s{}' = \frac{\partial^2\phi}{\partial x^2}; \quad \tau_{xs}{}' = -\frac{\partial^2\phi}{\partial x\partial s} \qquad (3.29a)$$

then the condition of equilibrium for an element in the plane of the shell will be approximately satisfied if no body force is considered. Equation (3.29) then becomes:

$$C_{11}\frac{\partial^4\phi}{\partial s^4} + (C_3-2C_{12})\frac{\partial^4\phi}{\partial x^2\partial s^2} + C_{22}\frac{\partial^4\phi}{\partial x^4} =$$

$$\left(\frac{\partial^2 w}{\partial x\partial s}\right)^2 - \left(\frac{\partial^2 w}{\partial x^2}\right)\left(\frac{\partial^2 w}{\partial s^2}\right) + \frac{1}{r}\left(\frac{\partial^2 w}{\partial x^2}\right) \qquad (3.30)$$

The Airy function ϕ will be the sum of a particular solution of this equation and the general solution of the corresponding homogeneous equation. The particular solution of the stress function ϕ may be obtained if the deflection surface is used as in Equation (3.7)

$$w = At\cos\frac{\pi x}{l} \cdot \cos\frac{s}{r} \qquad (3.7)$$

$$\therefore \frac{\partial^2 w}{\partial x^2} = -\frac{At\pi^2}{l^2}\cos\frac{\pi x}{l} \cdot \cos\frac{s}{r}$$

$$\frac{\partial^2 w}{\partial s^2} = -\frac{At}{r^2}\cos\frac{\pi x}{l} \cdot \cos\frac{s}{r}$$

$$\frac{\partial^2 w}{\partial x\partial s} = \frac{A\pi}{rl}\sin\frac{\pi x}{l} \cdot \sin\frac{s}{r}$$

Equation (3.30) becomes:

$$C_{11}\frac{\partial^4\phi}{\partial x^2} + (C_3 - 2C_{12})\frac{\partial^4\phi}{\partial x^2\partial s^2} + C_{22}\frac{\partial^4\phi}{\partial x^4} =$$

$$\left(\frac{At\pi}{rl}\right)^2 \sin^2\frac{\pi x}{l} \,.\, \sin^2\frac{s}{r} - \left(\frac{At\pi}{rl}\right)^2 \cos^2\frac{\pi x}{l}.\cos^2\frac{s}{r} - \frac{At\pi^2}{rl^2}\cos\frac{\pi x}{l} \,.\, \cos\frac{s}{r}$$

and simplifies to

$$C_{11}\frac{\partial^4\phi}{\partial s^2} + (C_3 - 2C_{12})\frac{\partial^4\phi}{\partial x^2\partial s^2} + C_{22}\frac{\partial^4\phi}{\partial x^4} =$$

$$-\frac{1}{2}\left(\frac{At\pi}{rl}\right)^2\left(\cos\frac{2\pi x}{l} + \cos\frac{2s}{r} + \frac{2r}{At}\cos\frac{\pi x}{l} \,.\, \cos\frac{s}{r}\right) \tag{3.31}$$

Solution of this is

$$\phi = -\frac{1}{2}\left(\frac{At\pi}{rl}\right)^2\left\{\frac{\cos 2\pi x/l}{F} + \frac{\cos 2s/r}{G} + \left(\frac{2r}{At}\right)\frac{\cos \pi x/l.\cos s/r}{H}\right\}$$

where $F = C_{22}\left(\frac{2\pi}{l}\right)^4$; $G = C_{11}\left(\frac{2}{r}\right)^4$

and $H = C_{11}\left(\frac{1}{r}\right)^4 + (C_3 - 2C_{12})\left(\frac{1}{r}\right)^2\left(\frac{\pi}{l}\right)^2 + C_{22}\left(\frac{\pi}{l}\right)^4$

Now certain boundary conditions must be satisfied. When $x = 1/2$, the hoop stress, $\sigma_s = \frac{d^2\phi}{dx^2} = 0$, and when $s = \pi r/2$, then $\sigma_x = \frac{\partial^2\phi}{\partial s^2} = -\sigma$. The total solution incorporating the boundary conditions plus the particular solution is given by

$$\phi = -\frac{1}{2}\left(\frac{At\pi}{rl}\right)^2\left\{\frac{\cos\ 2\pi x/l}{F} + \frac{\cos\ 2s/r}{G} + \frac{2r}{At}\ .\ \cos\frac{\pi x}{l}.\cos\frac{s}{r}\right\}$$

$$+ \frac{1}{16C}\left(\frac{At\pi s}{l}\right)^2 - \frac{\sigma_s{}^2}{2} + \frac{1}{16C}\left(\frac{Atx}{r}\right)^2 \qquad (3.32)$$

3.2.5 Internal and External Work

The work done by the internal stresses in the shell may be considered to be composed of two parts. The first part is due to the average compressive stress, and the second is the work done by the membrane forces and moments caused by buckling. The latter may be expressed as:

$$W_i = \frac{1}{2}\int[t(\sigma_x{}'\varepsilon_x{}'+\sigma_y{}'\varepsilon_y{}'+\tau_{xs}{}'\gamma xs{}')+M_x\frac{\partial^2 w}{\partial x^2}+M_s\frac{\partial^2 w}{\partial s^2}+2M_{xs}\frac{\partial^2 w}{\partial x\partial s}]d_x d_s$$

$$(3.34)$$

Substituting Eqs. (3.24-26) and (3.29a) in (3.34) the internal work due to buckling is obtained:

$$W_i = 2t\int_0^{\frac{1}{2}}\int_0^{\frac{\pi r}{2}}\left[C_{11}\left(\frac{\partial^2\phi}{\partial s^2}\right)^2 - 2C_{12}\left(\frac{\partial^2\phi}{\partial x^2}\right)\left(\frac{\partial^2\phi}{\partial s^2}\right) + C_{22}\left(\frac{\partial^2\phi}{\partial x^2}\right)^2 + C_3\left(\frac{\partial^2\phi}{\partial x\partial s}\right)^2\right]d_s d_x$$

$$+2\int_0^{\frac{1}{2}}\int_0^{\frac{\pi r}{2}} D_{11}\left(\frac{\partial^2 w}{\partial x^2}\right)^2 + 2D_{12}\left(\frac{\partial^2 w}{\partial x^2}\right)\left(\frac{\partial^2 w}{\partial s^2}\right) + D_{22}\left(\frac{\partial^2 w}{\partial s^2}\right)^2 + 2D_3\left(\frac{\partial^2 w}{\partial x\partial s}\right)^2\Bigg]d_s d_x \tag{3.35}$$

In these integrations, it is assumed that no part of the shell is subjected to stress reversal, and E_T is considered to be determined by the average compressive stress only. This is approximately true for small amplitudes, and the peak buckling stress will not be greatly affected by this assumption.

Equation (3.35) may be solved by substitution of the values for ϕ and w using a table of integrals. Solving each part of the integrand separately, and substituting in the limits for x and s yields the solutions:

$$\int_0^{\frac{1}{2}}\int_0^{\frac{\pi r}{2}}\left(\frac{\partial^2\phi}{\partial s^2}\right)^2 d_s d_x = \frac{3\ A^4t^4\ \pi^5}{2\ r^7 1^3\ G^2} + \frac{16\pi^3A^3t^3}{3r^6 1^3\ GH} + \frac{\pi^5A^2t^2}{16r^5 1^3\ H}$$

$$-\frac{2A\pi t\sigma}{r^2 1\ H} - \frac{A^2t^2\pi^3\sigma}{r^3 1\ G} + \frac{\pi r 1\sigma^2}{4}$$

$$\int_0^{\frac{1}{2}}\int_0^{\frac{\pi r}{2}}\left(\frac{\partial^2\phi}{\partial x^2}\right)^2 d_s d_x = \frac{3A^4t^4\pi^4}{2r^3 l^7F^2} + \frac{16A^3t^3\pi^7}{3\ l^7r^2HF} + \frac{A^2t^2\pi^9}{16\ rl^7H^2}$$

$$\int_0^{\frac{1}{2}}\int_0^{\frac{\pi r}{2}}\left(\frac{\partial^2\phi}{\partial x^2}\right)\left(\frac{\partial^2\phi}{\partial s^2}\right) d_s d_x = \frac{A^4\pi^7t^4}{r^5l^5FG} + \frac{8A^3\pi^5t^3}{3r^4l^5FH} - \frac{A^2t^2\pi^5\sigma}{2\ r\ l^3\ F} +$$

$$\frac{8A^3\pi^5t^3}{3r^4l^5GH} + \frac{A^2\pi^7t^2}{16r^3l^5H^2} - \frac{A\pi^3t\sigma}{l^3H}$$

$$\int_0^{\frac{1}{2}}\int_0^{\frac{\pi r}{2}}\left(\frac{\partial^2\phi}{\partial x\partial s}\right)^2 d_s d_x = \frac{A^2t^2\pi^7}{16r^3l^5H^2}$$

$$\int_0^{\frac{1}{2}}\int_0^{\frac{\pi r}{2}}\left(\frac{\partial^2 w}{\partial x^2}\right) d_s d_x = \frac{A^2\pi^5t^2r}{16\ l^3}$$

$$\int_0^{\frac{1}{2}}\int_0^{\frac{\pi r}{2}}\left(\frac{\partial^2 w}{\partial x^2}\right)\left(\frac{\partial^2 w}{\partial x^2}\right) d_s d_x = \frac{A^2\pi^3t^2}{16rl}$$

$$\int_0^{\frac{1}{2}}\int_0^{\frac{\pi r}{2}}\left(\frac{\partial^2 w}{\partial s^2}\right) d_s d_x = \frac{A^2\pi t^2 l}{16r^3}$$

$$\int_0^{\frac{1}{2}}\int_0^{\frac{\pi r}{2}}\left(\frac{\partial^2 w}{\partial x\partial s}\right)^2 d_s d_x = \frac{A^2\pi^3t^2}{16rl}$$

The expression for the internal work therefore becomes,

$$W_i = 2t\{C_{11}[\frac{3\ A^4t^4\pi^5}{2\ r^7\ l^3\ G^2} + \frac{16\pi^3A^3t^3}{3r^6\ l^3\ GH} + \frac{\pi^5\ A^2\ \ t^2}{16r^5\ l^3\ H^2} - \frac{2\ A\pi t\sigma}{r^2\ lH}$$

$$- \frac{A^2t^2\pi^3\sigma}{r^3\ l\ G} + \frac{\pi r\ l\ \sigma^2}{4}]$$

$$-2C_{12}[\frac{A^4\ \pi^7\ t^4}{r^5\ l^5\ FG}\ \frac{8A^3\ \pi^5\ \ {}^3}{3r^4\ l^5\ FH} - \frac{A^2t^2\pi^5\sigma}{2\ r\ l^3\ F}$$

$$+ \frac{8\ A^3\ \pi^5\ t^3}{3\ r^4\ l^5\ GH} + \frac{A^2\ \pi^7t^2}{16r^3\ l^5\ H^2} - \frac{A\pi^3\ \ t\sigma}{l^3H}]$$

$$+ C_{22}[\frac{3A^4\ t^4\ \pi^4}{2r^3\ l^7\ F^2} + \frac{16A^3\ t^3\ \pi^7}{3\ l^7\ r^2\ HF} + \frac{A^2\ t^2\ \pi^9}{16r\ l^7\ H^2}]$$

$$+ C_3\ [\frac{A^2\ t^2\ \pi^7}{16r^3\ l^5\ H^2}]\}$$

$$+ 2\{\frac{D_{11}\ A^2\ \pi^5\ t^2r}{16\ l} + \frac{2\ D_{12}\ A^2\ \pi^3\ t^2}{16\ r\ l} + \frac{D_{22}\ A^2\pi t^2 l}{16\ r} + \frac{2D_3A^2\pi^3t^2}{16\ r\ l}\} \tag{3.36}$$

Similarly, the work done by the external axial force, the product of the cross-sectional area and the compressive stress, σ_{x_A}, may also be considered to consist of two parts. The first part is the work done on the axial shortening of the cylinder consisting of the length L-l, in which no buckling occurs. This part of the external work is essentially independent of the amplitude parameter, A, consequently these parts of the work need not be considered in the variational procedure.

The second part of the work done by the external force is on the shortening of the buckling length, 1. This shortening may be determined by the following steps: The strain-displacement relations may be formulated by use of Eqs. (3.24) and (3.29a). From the relations the expression

$$\frac{\partial u}{\partial x} = \left[C_{11} \frac{\partial^2 \phi}{\partial s^2} - C_{12} \frac{\partial^2 \phi}{\partial x^2}\right] - \frac{1}{2}\left(\frac{\partial w}{\partial x}\right)^2 \tag{3.37}$$

is readily obtained. If the assumption is made that the axial stress, σ_x is the same over the whole of the cross section, the external work expression is given by

$$W_e = 4t \int_0^{\frac{\pi r}{2}} \sigma \int_0^{\frac{l}{2}} \frac{\partial u}{\partial x}\, dx ds \tag{3.38}$$

If, however, the variation of σ_x is taken into account, the external work expression is

$$W_e = 4t \int_0^{\frac{\pi r}{2}} \left(\sigma_x \Big|_{x=\frac{l}{2}} \left[\int_0^{\frac{l}{2}} \frac{\partial u}{\partial x}\, dx \right] \right) ds \tag{3.39}$$

The effects of these different assumptions on the theoretical buckling load will be seen subsequently.

These work expressions on substitution of Equ. (3.37) become:

<u>For σ_x assumed constant:</u>

$$W_e = 4t\{-\frac{A^2t^2\pi^3C_{11}\sigma}{2r^3\ 1\ G} - \frac{At\pi\sigma C_{11}}{r^2\ 1\ H} + \frac{\pi r l\sigma^2 C_{11}}{4}$$

$$+\frac{A^2t^2\pi^5\sigma C_{12}}{2\ r\ 1^3\ F} - \frac{At\pi^3C_{12}\sigma}{1^3\ H} + \frac{A^2t^2\pi^3 r\sigma}{32\ 1}\} \tag{3.40}$$

<u>For σ_x variable:</u>

$$W_e = 4t\{\frac{3A^4t^4\pi^5C_{11}}{2r^7\ 1^3\ G^2} + \frac{8A^3t^3\pi^3C_{11}}{3r^6\ 1^3\ GH} - \frac{A^2t^2\pi^3\sigma C_{11}}{2r^3\ 1\ G}$$

$$-\frac{8A^3t^3\pi^5C_{12}}{3r^4\ 1^5\ GH} - \frac{3A^4t^4\pi^5}{32r^3 1^3 G} - \frac{A^2t^2\pi^3\ \sigma\ C_{11}}{2\ r^3\ 1\ G}$$

$$-\frac{A\ t\ \pi\ \sigma\ C_{11}}{r^2\ 1\ H} + \frac{C_{11}\ \sigma^2\pi r l}{4} - \frac{A^2t^2\pi^5\ \sigma\ C_{12}}{2\ r\ 1^3\ F}$$

$$-\frac{At\pi^2C_{12}\sigma}{1^3\ H} + \frac{A^2t^2\pi^3 r\sigma}{32\ 1}\} \tag{3.41}$$

Now, for equilibrium to be established,

$$\delta(W_i - W_e) = 0$$

Since the work expression is comprised of parameters A and 1, equilibrium is represented by

$$\frac{\partial (W_i - W_e)}{\partial A} = 0 \tag{3.42a}$$

and,
$$\frac{\partial (W_i - W_e)}{\partial l} = 0 \tag{3.42b}$$

For simplicity only Equation (3.42a) will be explicitly satisfied while a spectrum of values of l to minimize the work term will essentially satisfy (3.42b). Equation (3.42a) takes the form of

$$A\ [A^2P + AQ + (R\sigma + S)] = 0 \tag{3.43}$$

As required the trivial solution occurs while the non-trivial solution is given by

$$A^2\left[\frac{12t^5\pi^5C_{11}}{r^7\ l^3\ G} - \frac{16t^5\pi^7C_{12}}{r^5\ l^5\ FG} - \frac{12t^5\pi^7C_{12}}{r^3\ l^7\ F^2}\right]$$

$$+ A\left[\frac{32t^4\pi^3C_{11}}{r^6\ l^3\ GH} - \frac{32t^4\pi^5C_{12}}{r^4\ l^5\ FH} - \frac{32t^4\pi^5C_{12}}{r^4\ l^5\ GH} - \frac{32t^4\pi^7C_{22}}{l^7\ r^2\ HF}\right]$$

$$+\left[-\frac{t^3\pi^5C_{11}}{4r^5l^3H^2} - \frac{t^2\pi^7C_{12}}{2r^3l^5H^2} + \frac{t^2\pi^9C_{22}}{4rl^7H^2} + \frac{t^2\pi^7C_3}{4r^3l^5H^2} - \frac{t^3\pi^3r\sigma}{4\ l}\right.$$

$$\left. + \frac{D_{11}t^2\pi^5r}{4\ l} + \frac{D_{12}t^2\pi^3}{2rl} + \frac{D_{22}t^2\pi l}{4r}\quad \frac{D_3t^2\pi^3}{2rl}\right] = 0 \tag{3.44}$$

for the case of σ_x assumed constant, and,

$$A^2\left[\frac{12t^5\pi^3C_{22}}{r^3\ l^7\ F^2} + \frac{3t^5\pi^5}{2r^3l^3G}\right]$$

$$+ A\left[- \frac{32t^4\pi^5C_{12}}{r^4\ l^5\ FH} + \frac{32t^4\pi^7C_{22}}{l^7\ r^2\ HF}\right]$$

$$+\left[- \frac{t^3\pi^3r\sigma}{4\ l} + \frac{t^3\pi^5C_{11}}{4r^5l^3H^2} - \frac{t^3\pi^7C_{12}}{2r^3l^5H^2} - \frac{t^3\pi^9C_{22}}{4rl^7H^2}\right.$$

$$\left. + \frac{t^3\pi^7C_3}{4r^3l^5H^2} + \frac{D_{11}t^2\pi^5r}{4\ l^3} + \frac{D_{12}t^2\pi^3}{2rl} + \frac{D_{22}t^2\pi l}{4r^3} + \frac{D_3t^2\pi^3}{2rl}\right] = 0 \tag{3.45}$$

for the case σ_x variable.

For any given value of σ_x, the parameter A may be obtained in the form

$$A = \frac{-Q \pm \sqrt{Q^2 - 4P(R\sigma_x + S)}}{2P}$$

Prior to buckling, A would be expected to be complex and hence real values would be anticipated only for the sought-after post-buckling state. A solution for σ_x, just at incipient buckling, may be found from

$$\sigma_x = \left(\frac{Q^2}{4P} - S\right)/R \tag{3.46}$$

The values for P, Q, R and S are taken from Equations (3.44) and (3.45) for the cases of σ_x assumed constant and σ_x variable respectively.

Computer programs have been compiled for the solution of Equation (3.46) to obtain the post-buckling equilibrium paths for the various cases of σ_x assumed constant and σ_x-variable; Von Mises' and Tresca's yield criteria; and various values of the ratio R/t.

Figure 3.9 illustrates the post-buckling equilibrium path obtained from the virtual work and incremental theories for σ_x variable, and Von Mises' yield criterion, superimposed on the apparent theoretical stress-strain characteristic obtained earlier in this chapter. The equilibrium path is drawn by plotting the computed values of σ_x against values of E_T occurring for various strains on the apparent theoretical stress-strain characteristic. For the case illustrated, R = 1.35 in., and R/t ≃ 28.

The post-buckling equilibrium paths may be drawn for various buckling wavelengths. The path which gives the lowest buckling stress coincident with the apparent theoretical stress-strain characteristic will indicate the critical buckling wavelength. The post-buckling equilibrium paths for various wavelengths, however, are almost identical, so for this reason only one path is shown on the small scale of Fig. 3.9. It may be seen from this figure that the predicted buckling stress is very close to the yield strength, $\bar{\sigma}$ of the material.

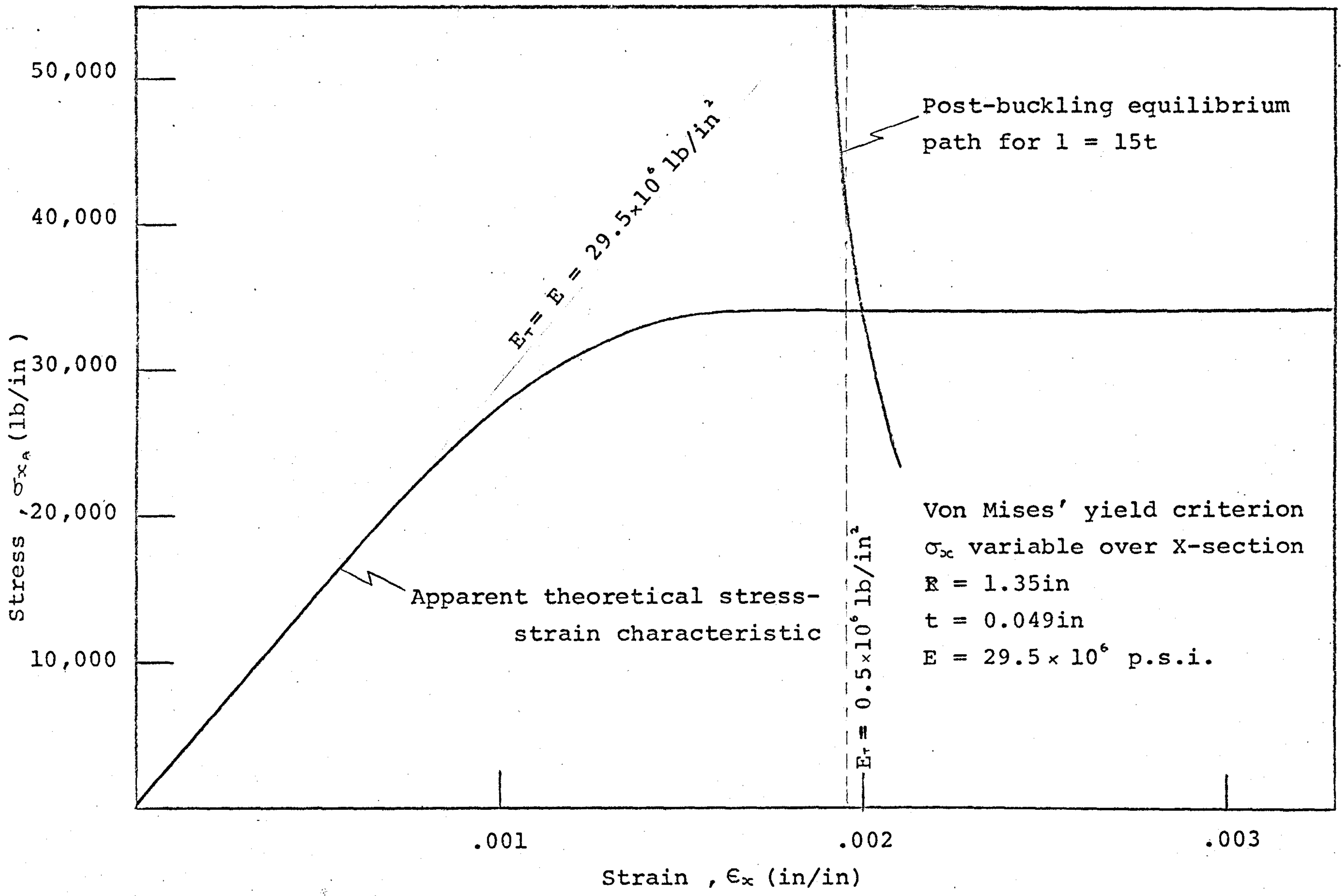

FIG.3.9 INTERSECTION OF POST BUCKLING EQUILIBRIUM PATHS AND APPARENT THEORETICAL STRESS-STRAIN CURVE.

Similar constructions may be performed for the prediction of the critical buckling stress based on the assumption that σ_x is constant over the cross section. The post-buckling paths obtained are almost identical to the case assuming σ_x is variable over the cross section. It seems reasonable to infer that the approximation made by assuming σ_x is constant over the cross section does not appreciably alter the virtual work equations, or introduce a significant error in the predicted critical stress value.

The critical buckling stress predicted from the apparent theoretical stress-strain characteristic, however, does not take into account the effects of work hardening or the Bauschinger effect during the bending operation. For this reason, the predicted critical buckling stress is considerably lower than would be expected in experimental tests. A more realistic analysis may be performed by making use of an experimental stress-strain curve obtained from tests on tensile specimens curved to the required radius.

Fig. 3.10 makes use of the stress-strain curve obtained from a tensile test performed on a specimen curved to a radius of 1 5/32". The post-buckling equilibrium path for the critical wavelength, $l = 15t$, is plotted onto the stress-strain curve and gives a predicted critical

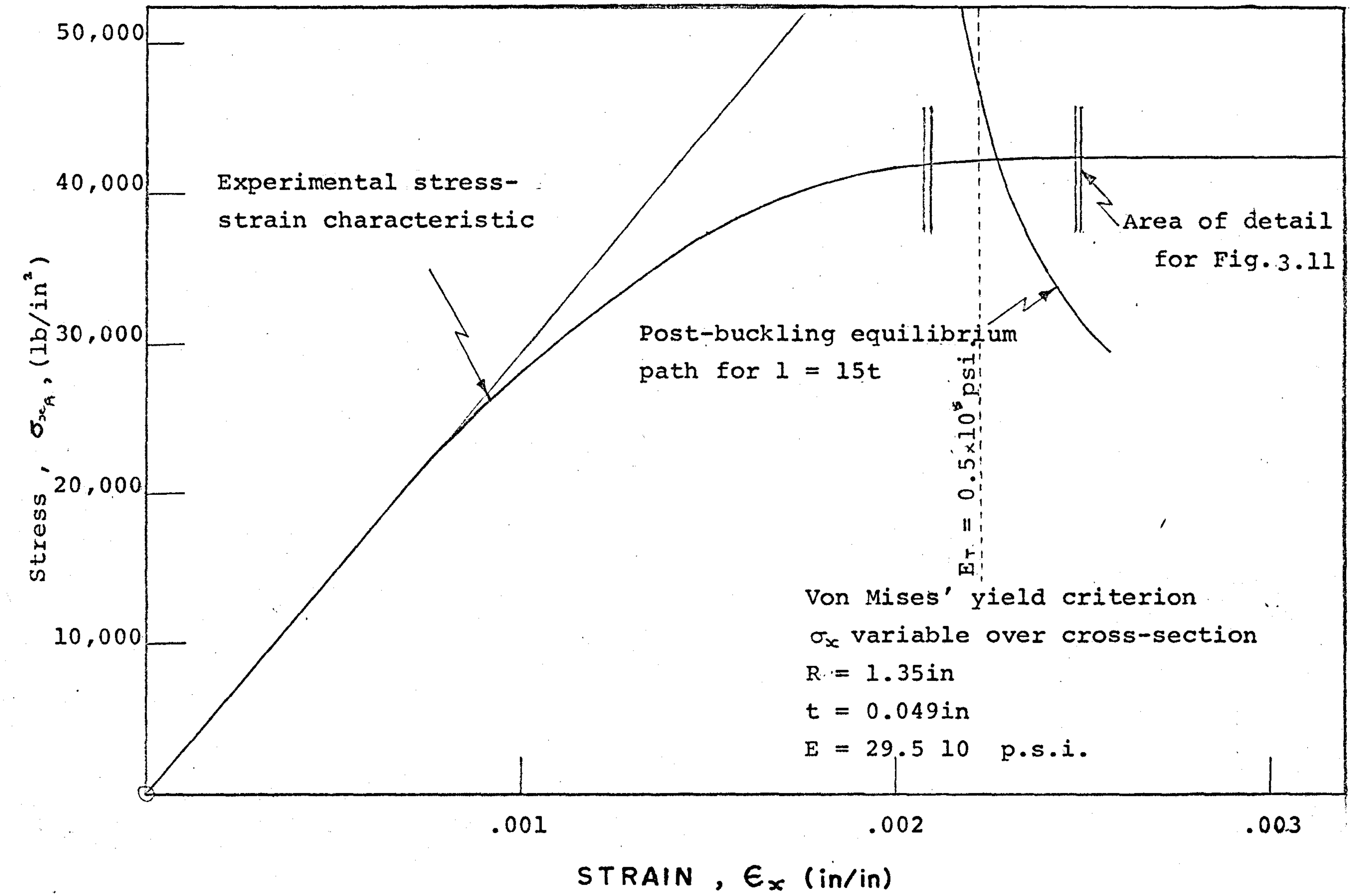

FIG.3.10 INTERSECTION OF POST-BUCKLING EQUILIBRIUM PATHS AND EXPERIMENTAL STRESS-STRAIN CURVE.

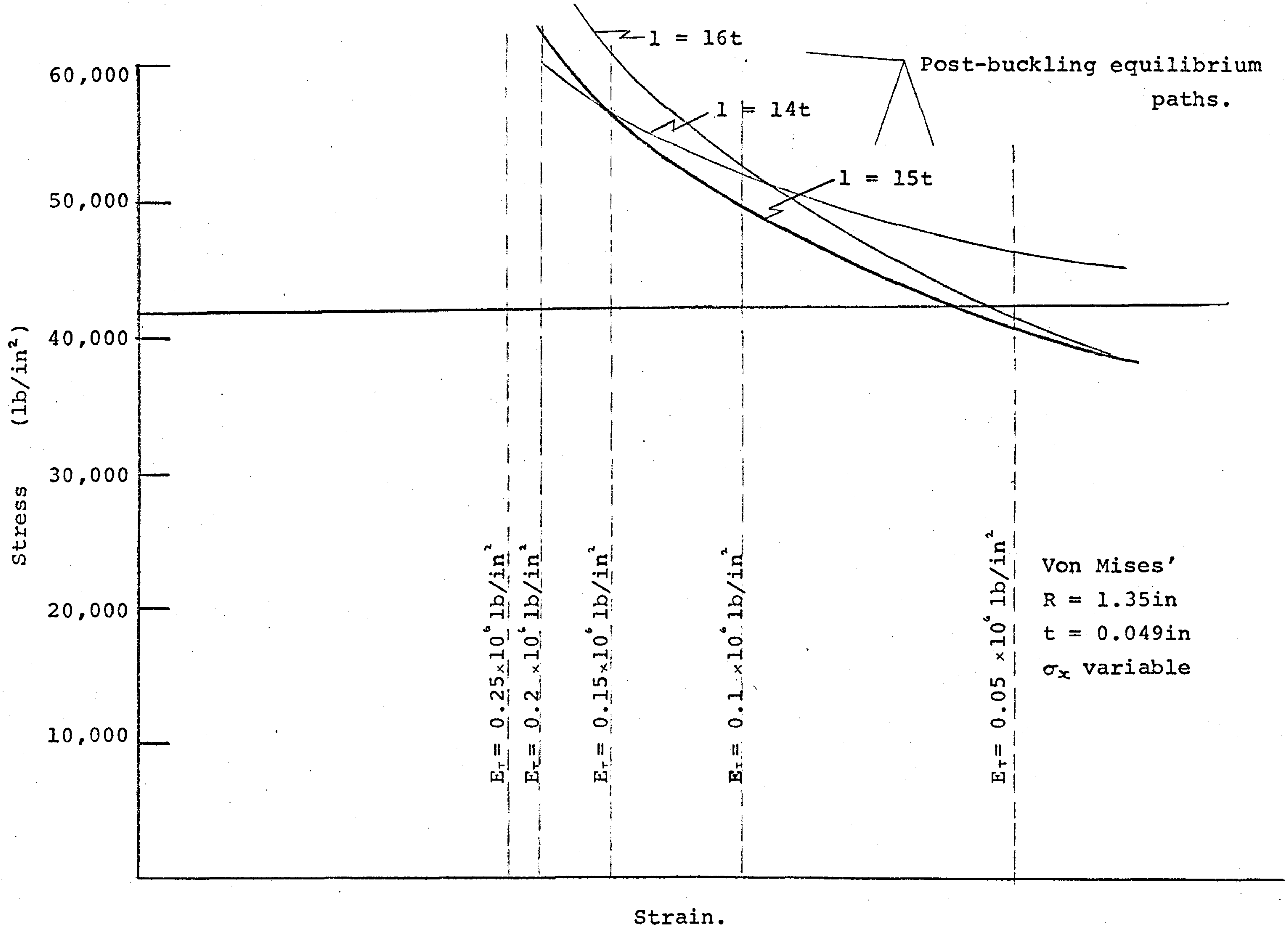

FIG. 3.11 DETAIL OF INTERSECTION OF POST BUCKLING PATHS AND EXPERIMENTAL STRESS-STRAIN CURVE.

stress value of just less than 42,000 lb/in^2. This value is considerably higher than that obtained from the theoretical stress-strain characteristic, and represents a much more satisfactory result.

To illustrate the influence of variation of the assumed buckling length on the post-buckling paths, the intersection of the experimental stress-strain curve and various post-buckling equilibrium paths will be studied more closely.

Fig. 3.11 shows this intersection with the strain axis exaggerated. It may be seen that it is impossible to pinpoint the positions on the stress-strain characteristic where specific values of E_T occur. It has been assumed, however, for illustration purposes, that the stress-strain curve is exponentially asymptotic to a value of σ_x = 42,000 lb/in^2, and so various values of E_T have been marked out logarithmically on the stress-strain curve. The post-buckling equilibrium paths are plotted using these values, so that the difference between the paths for various values of buckling wavelength, l is clearly illustrated. The diagram indicates that for the particular values of R and t considered, the critical buckling wavelength is 15t. This corresponds to a wavelength of 0.75 in.; a value which is compared with the experimental values obtained in Chapter IV.

3.2.6 Variation of Ratio R/t

The constructions performed for the prediction of the critical buckling stress were for the particular value of the ratio, $R/t = 28$. Different critical buckling stresses will occur for different values of the ratio R/t and clearly a construction of this type may be carried out for each case.

A program, shown in the Appendix, has been compiled to obtain the post-buckling equilibrium paths for various R/t to enable calculation of the critical buckling stress in each case. To facilitate the plotting of the critical stress vs. R/t curve, the values of stress corresponding to various values of E_T on the experimental stress-strain characteristic are obtained as in Fig. 3.12. These values are then plotted in Fig. 3.13.

The critical post-buckling equilibrium paths for various values of the ratio, R/t, are then plotted across the curve of σ_x vs. E_T to give the critical buckling stress in each case. Thus the characteristic of critical buckling stress vs. R/t is obtained as shown in Fig. 3.13.

It is significant to notice the variation of critical wavelength for various values of the ratio, R/t. It has been shown earlier that for a value of $R/t \simeq 28$ the critical wavelength is 15t, whereas for a value of,

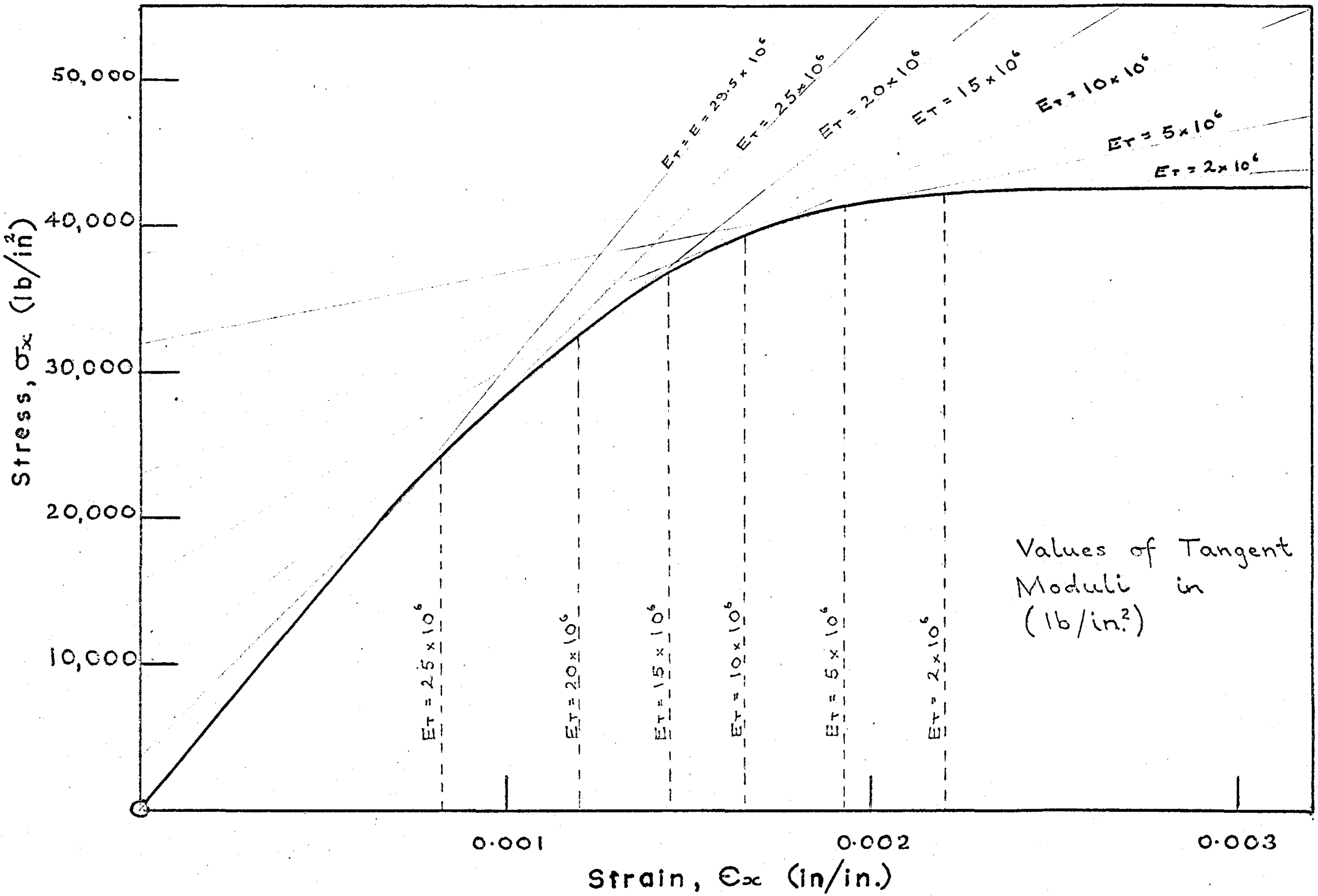

FIG 3.12 VARIATION OF TANGENT MODULUS FOR EXPERIMENTAL STRESS - STRAIN CURVE.

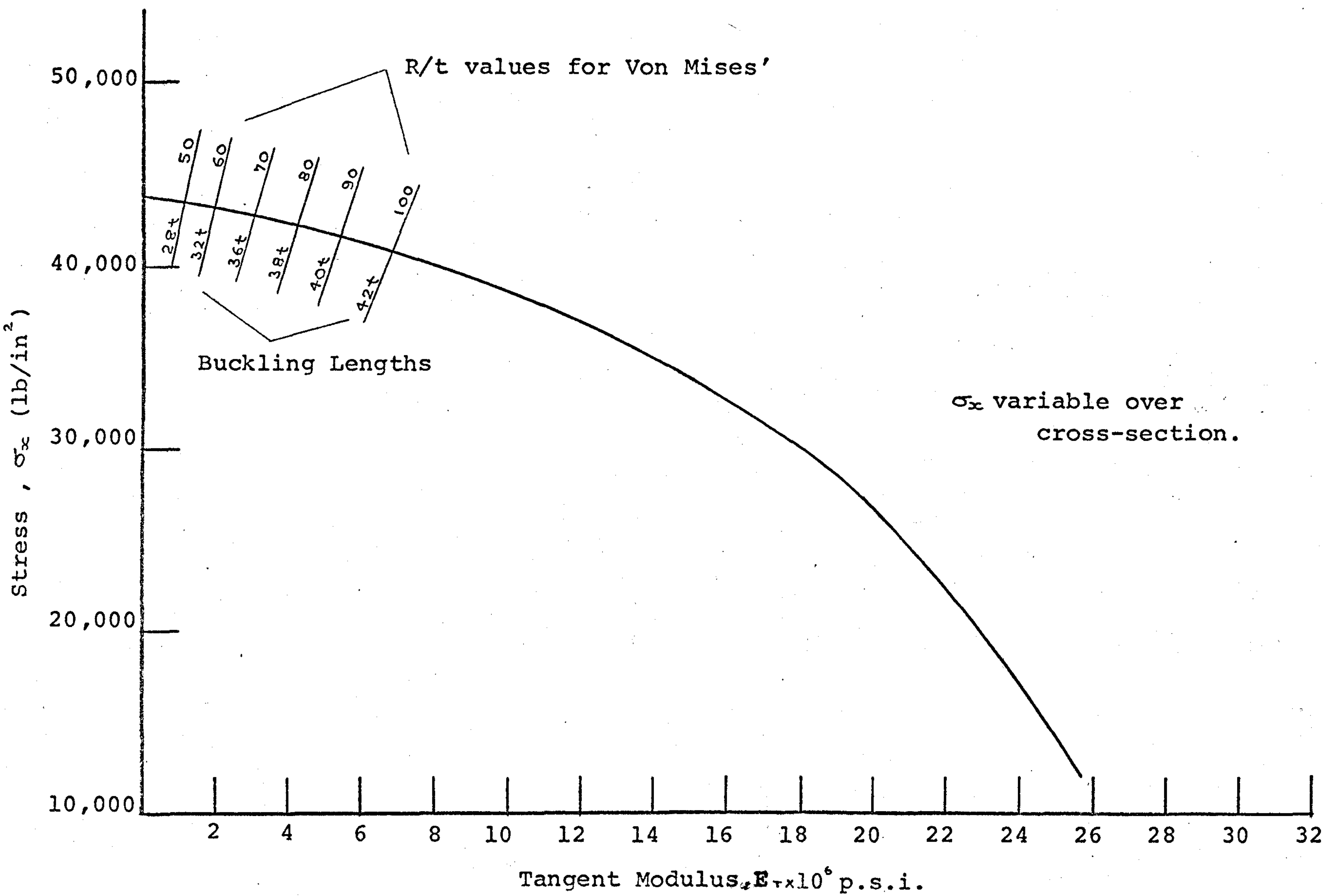

FIG. 3.13 TANGENT MODULUS vs. STRESS FOR EXPERIMENTAL CURVE SHOWING POST BUCKLING EQUILIBRIUM PATHS FOR VARIOUS R/T VALUES.

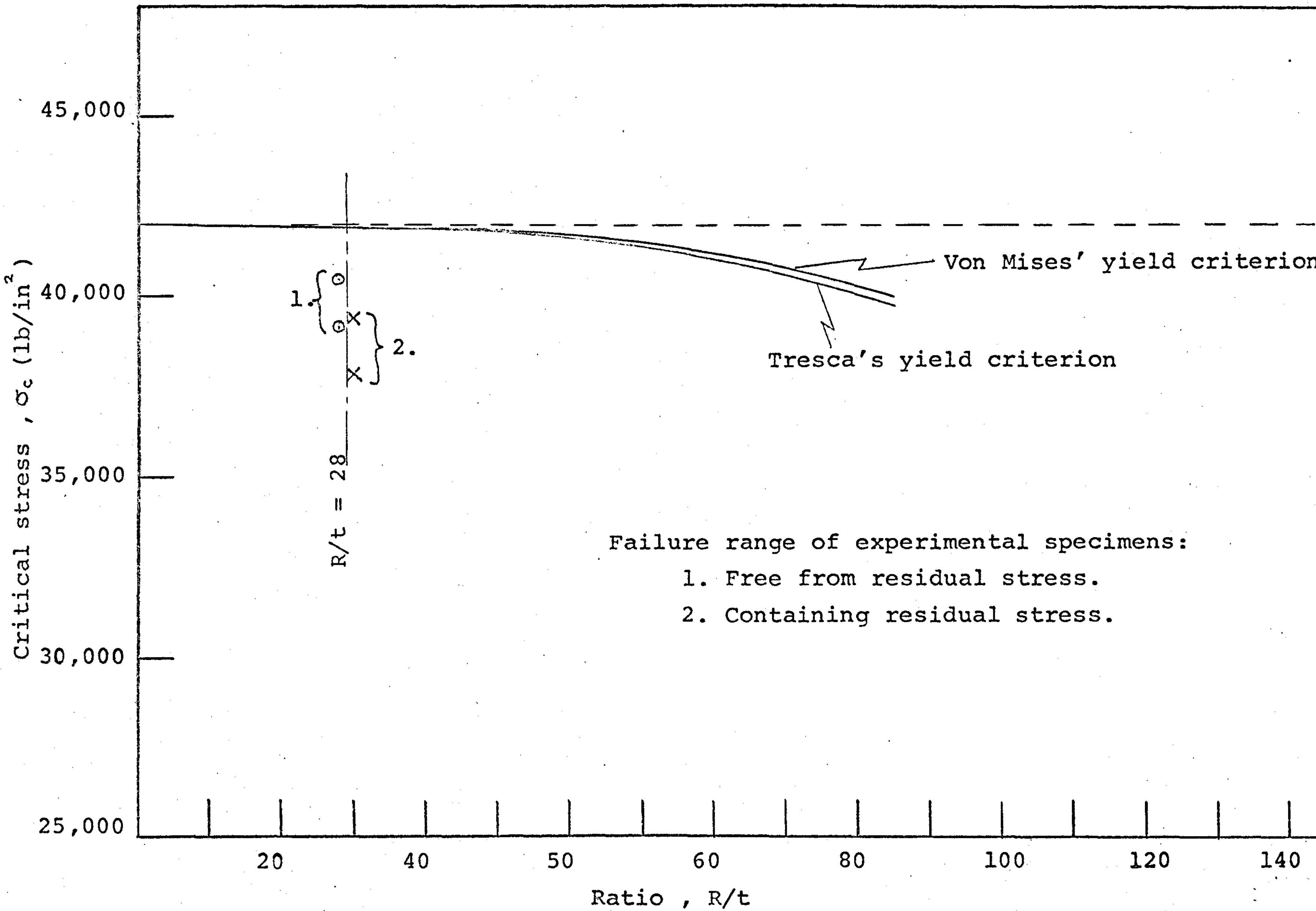

FIG. 3.14 CRITICAL BUCKLING STRESS FOR LOCAL BUCKLING FAILURE.

say, R/t = 90, the critical wavelength is 40t. These values appear reasonable inasmuch as the buckling length increases as R/t increases, so that with R constant, the result is a smaller wavelength as thickness decreases.

It has been assumed in the above procedure that the experimental stress-strain characteristic is the same for all values of R/t. This clearly is not true, and for an exact analysis for any particular ratio R/t a tensile test should be performed to obtain the correct stress-strain characteristic for a specimen with that value of R/t.

However, it was noticed in the experimental work that a great deal of change in the stress-strain curve did not occur for different values of R/t. It is, therefore, tacitly assumed that employing only the stress-strain characteristic for R/t = 28 in all cases does not introduce a serious error in the predicted critical stress values obtained.

Buckling was assumed to be of a local nature with effectively only 180° of the specimen subjected to it. Since the stiffeners and their neighbourhood fibres are presumed to remain straight throughout the loading history, post-buckling behaviour would be expected to be capable of supporting a higher stress than the buckled region would support alone. When buckling stresses approach the yield stress, $\bar{\sigma}$, however, there is very little difference between the incipient buckling stress and the maximum average compressive stress.

The curve shown in Fig. 3.14 indicates the critical buckling stress is only slightly less than the squashing strength of the material for all values of the ratio, R/t below 50. For larger values of R/t, the critical buckling stress is smaller as would be expected. For large values of the ratio, R/t, however, multimodal buckling will probably occur and the effect of initial imperfections may become prohibitively large. These predictions must, therefore, be treated with caution when applied to specimens with large values of the ratio, R/t.

For small values of R/t, the curve shown in Fig. 3.14 should give a fairly accurate prediction of the critical buckling stress likely to occur in specimens of the type used in the experimental tests. The effects of both residual stress and work hardening have been taken into account in this theoretical prediction, although the important consideration of initial imperfections, for simplicity, had to be omitted.

Comparison between these theoretical predictions and the experimental results will be discussed fully in Chapter V.

CHAPTER IV

EXPERIMENTAL WORK AND RELATED DISCUSSIONS

The practical tests carried out to verify theoretical predictions were in three major sections:

(a) Investigation of the strains occurring in the outer fibres of a thin metal sheet during a bending operation, including the measurement of elastic springback.

(b) Investigation into the influence of residual stress due to cold bending on sections loaded in tension.

(c) Investigation into the influence of residual stress due to cold bending on sections loaded in compression.

The material used throughout these experiments was 18 gauge (0.049 in. thick) galvanized sheet steel. This gauge of sheeting was found to be most suitable because of the ease with which it could be rolled and fabricated into the various shapes required. Using a thicker size of sheeting would have led to fabrication difficulties, especially during the bending of lips on the compression specimens.

Galvanized steel sheeting was used to ensure that before fabrication of the specimens commenced the material was completely free from residual stress. The galvanizing process took place during manufacture after the cold rolling operations had been completed, and consisted of passing the sheeting through a bath of molten zinc at a temperature of 1700°F. This temperature was sufficient to remove all the residual stresses due to the cold rolling process, and as the sheeting was subsequently allowed to cool slowly, no significant residual stresses were set up due to differential cooling. Initial tensile tests on this steel sheeting showed an almost perfectly linear elastic-plastic stress-strain characteristic, indicating that the steel was in fact free from residual stresses of any kind.

Primary tests were carried out on the galvanized sheeting to determine its basic material properties. The static and ultimate yield points, and a value for Young's modulus were determined by A.S.T.M. standard tension tests. An A.S.T.M. standard test was also included to verify the assumed value of Poisson's Ratio and the various results obtained are shown in the Tables 4.2 and 4.3.

4.1 Investigation of the Strains Occurring in the Outside Fibres of a Thin Metal Sheet During a Bending Operation

The initial aim of this section of the experimental work was to verify the theoretical predictions of strains likely to occur in two perpendicular directions during the bending of a thin sheet in one direction. The strains

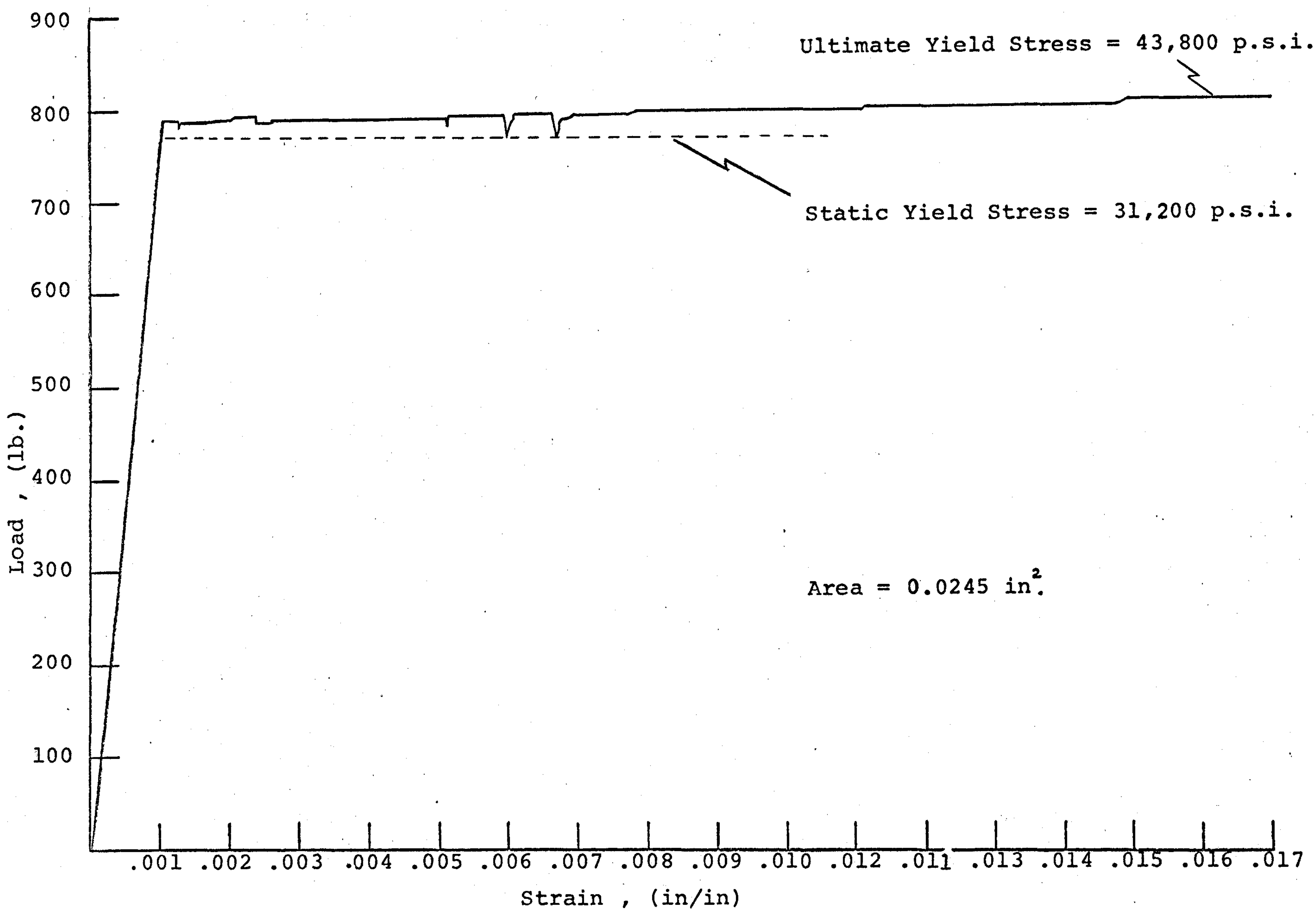

FIG. 4.1 TENSILE TEST No.3.

Table 4.2

Tensile Test Results

Dimensions of Specimens: ½" wide, 2" gauge length to A.S.T.M. standards.

Test No.	Static Yield Load (lb.)	Ult. Yield Load (lb.)	Static Yield Stress (lb./in.^{2})	Ult. Yield Stress (lb./in.^{2})
1	770	1078	30,800	43,100
2	775	1083	31,000	43,400
3	780	1094	31,200	43,800

Average Static Yield Stress = 31,000 lb/in^2

Average Ultimate Yield Stress = 43,400 lb/in^2

Young's Modulus of Elasticity, $E = 29.5 \times 10^6$ lb/in^2

Table 4.3

Poisson's Ratio Test Results

Dimensions of Specimens: 1½" wide to A.S.T.M. standards

Test No.	Poisson's Ratio
1	0.31
2	0.32
3	0.32

Average Poisson's Ratio, $\nu = 0.316$

measured were those along the x and s axes as shown in Fig. 2.5. The pyramid rolling press used is shown in Photograph 4.1, and consisted of 3 No. 2 5/16" diameter rollers. One of these rollers could be screwed down vertically alongside the other two rollers. These two rollers could be rotated by means of a gearing system, thus enabling the sheeting to be rolled through the press to the radius of bend required.

The roller over which the sheet steel was bent had two ¼" deep grooves turned out of it as illustrated in Photograph 4.2. This made room for strain gauges to be mounted on the inside circumferential fibres, enabling strains to be measured on both the inside and outside of the bend. The strain gauges used throughout all the experimental work were various types of Budd Foil Resistance Gauges having a resistance of 120 ohms. A multiple switching and bridge unit with a galvanometer indicator was used for balancing the gauges, and both two and three lead balancing systems were used.

Strain gauges were mounted on the steel sheet as shown in Fig. 4.4, so that the strains could be measured in the longitudinal and circumferential directions on both the inside and outside of the bend. Two additional gauges were employed on the outside of the bend, positioned over the grooves, to check against any distortion of the

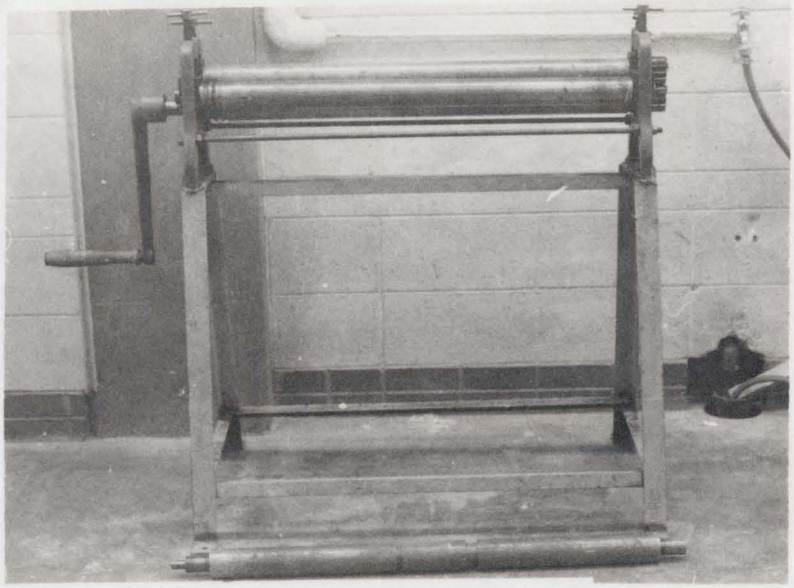

PHOTOGRAPH 4.1 PYRAMID ROLLER USED IN FABRICATION.

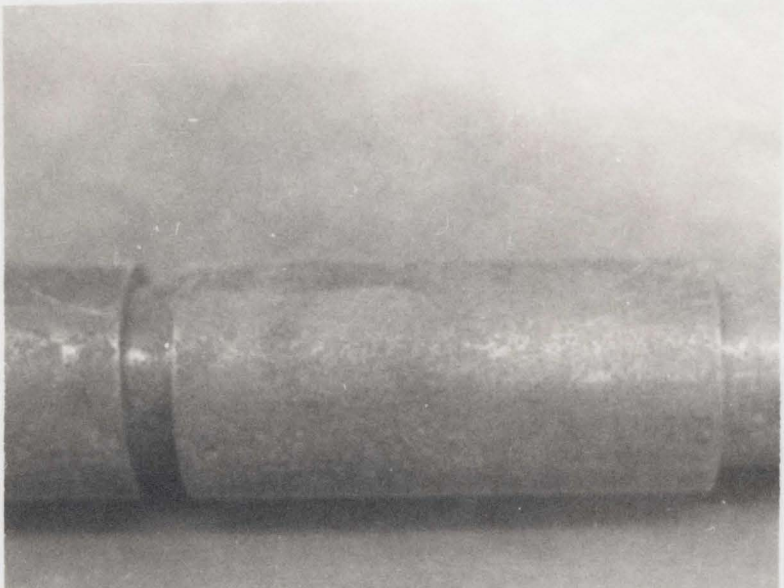

PHOTOGRAPH 4.2 GROOVES IN ROLLER FOR STRAIN GAUGE CLEARANCE.

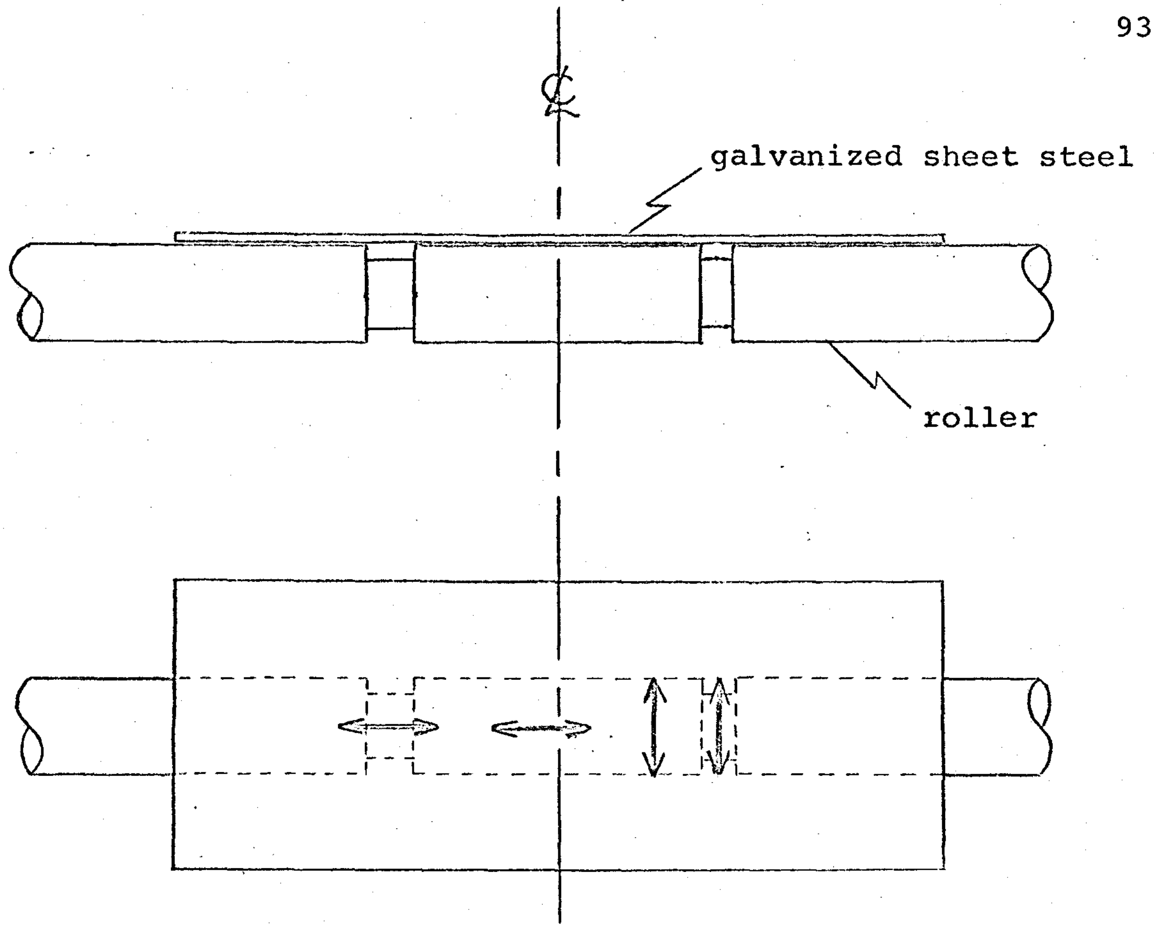

Strain Gauges mounted on Outside of Bend .

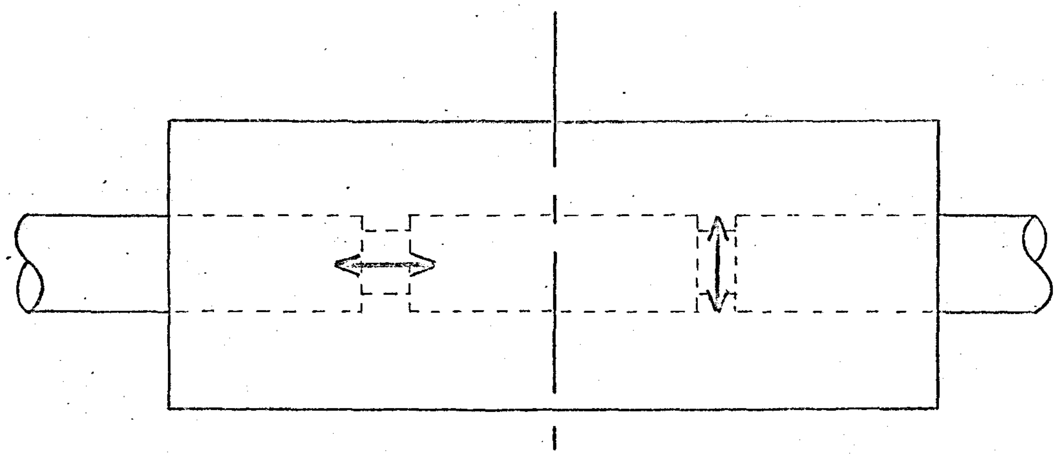

Strain Gauges mounted on Inside of Bend.

FIG. 4.4 SHEET BENDING OPERATION SHOWING POSITIONS AND ORIENTATION OF STRAIN GAUGES.

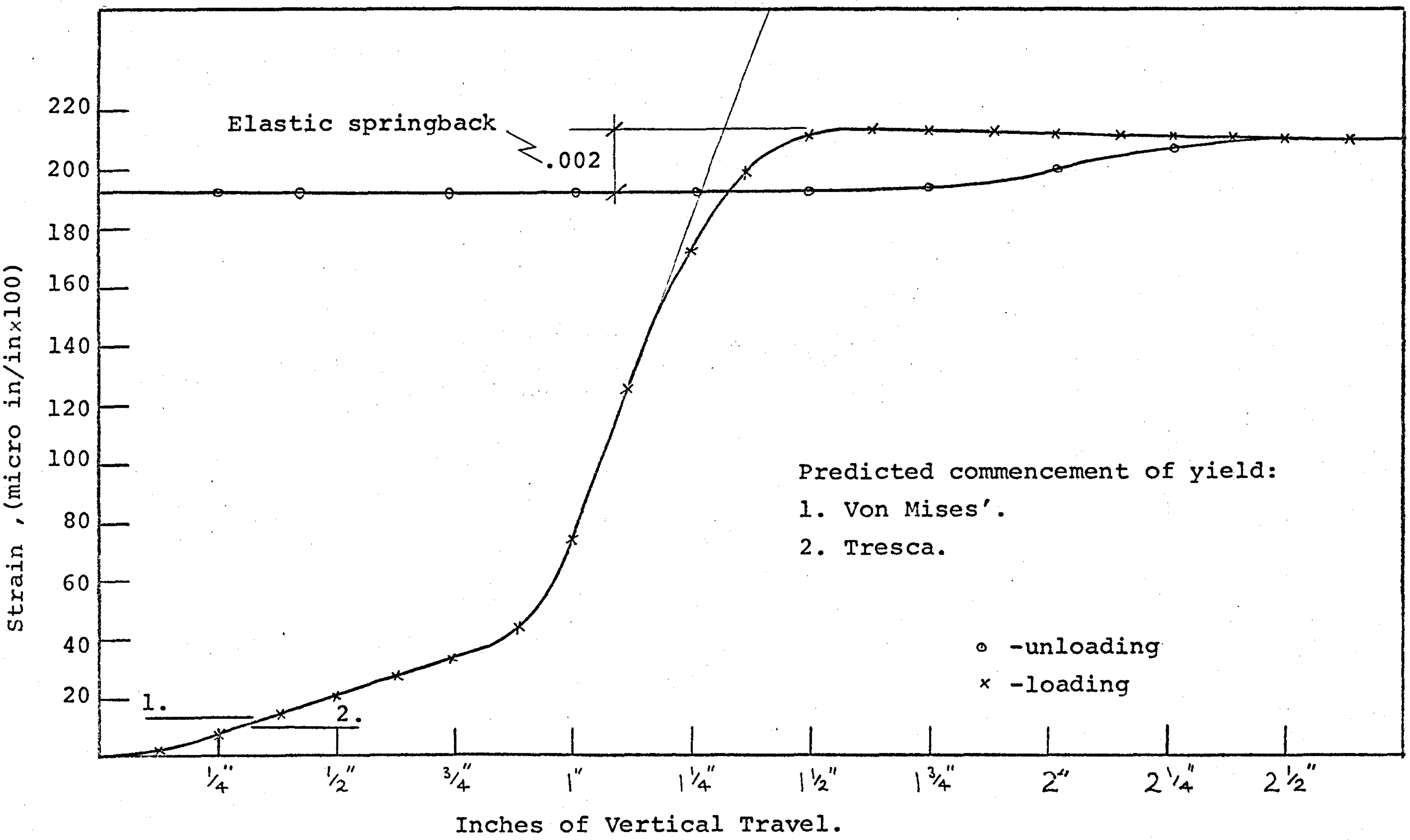

FIG 4.5 CIRCUMFERENTIAL STRAIN OF OUTER FIBRES DURING BENDING.

sheet over these grooves.

The sheet was slowly bent by manually screwing down the roller, A, and strain readings were taken at every ¼ turn of the screw thread which corresponded to 0.025 in. of travel. Strain readings were taken until the screws reached the end of their travel, and then the screws were loosened to allow elastic springback to occur, and readings were once again taken every ¼ turn until elastic springback was complete.

The circumferential strain gauges all gave almost identical readings throughout the bending process, and they are plotted against the travel of the screws in Fig. 4.5. No distortion of the sheet occurred over the grooves, and from the strain readings it can be seen that the tensile strain of the outside circumferential fibres was the same as the compressive strain of the inside circumferential fibres. The experimental value for the outside fibre strain at initial yielding of the outside fibres could not be determined from the graph in Fig. 4.5. The value of elastic springback occurring experimentally was 0.002 in/in. which is similar to the predicted values based on Von Mises' and Tresca's yield criteria, and will be discussed further in the concluding chapter.

The gauges mounted in the longitudinal direction gave strain readings that were very small, but also very erratic. As the object of measuring the strain in this direction was to verify the predicted value of zero strain, it is clear that the gauges used were distorted during the bending operation and so no conclusions could be drawn from these readings. Wire gauges of lengths of around 6 in. should have been used to measure any small strain in this direction, but they were not available at the time of testing.

4.2 Investigation into the Influence of Residual Stress Due to Cold Bending on Sections Loaded in Tension

Tensile tests were carried out on specimens that were cut from 18 gauge sheet steel that had been previously bent in a rolling press to various radii. Special rollers were installed in the pyramid rolling press to fabricate sections by bending the sheet steel over rollers of different diameters. The diameters of the rollers used were 1 3/8", 2 5/16" and 3 3/8"; the exact dimension of the tensile specimens are shown in Fig. 4.6.

The widths of the cross sections of the various specimens were made as large as possible to increase the effect of the residual stress in each section, and the designs were limited only by the capacity of the jaws in the testing machine.

Pilot tests were initially performed to develop

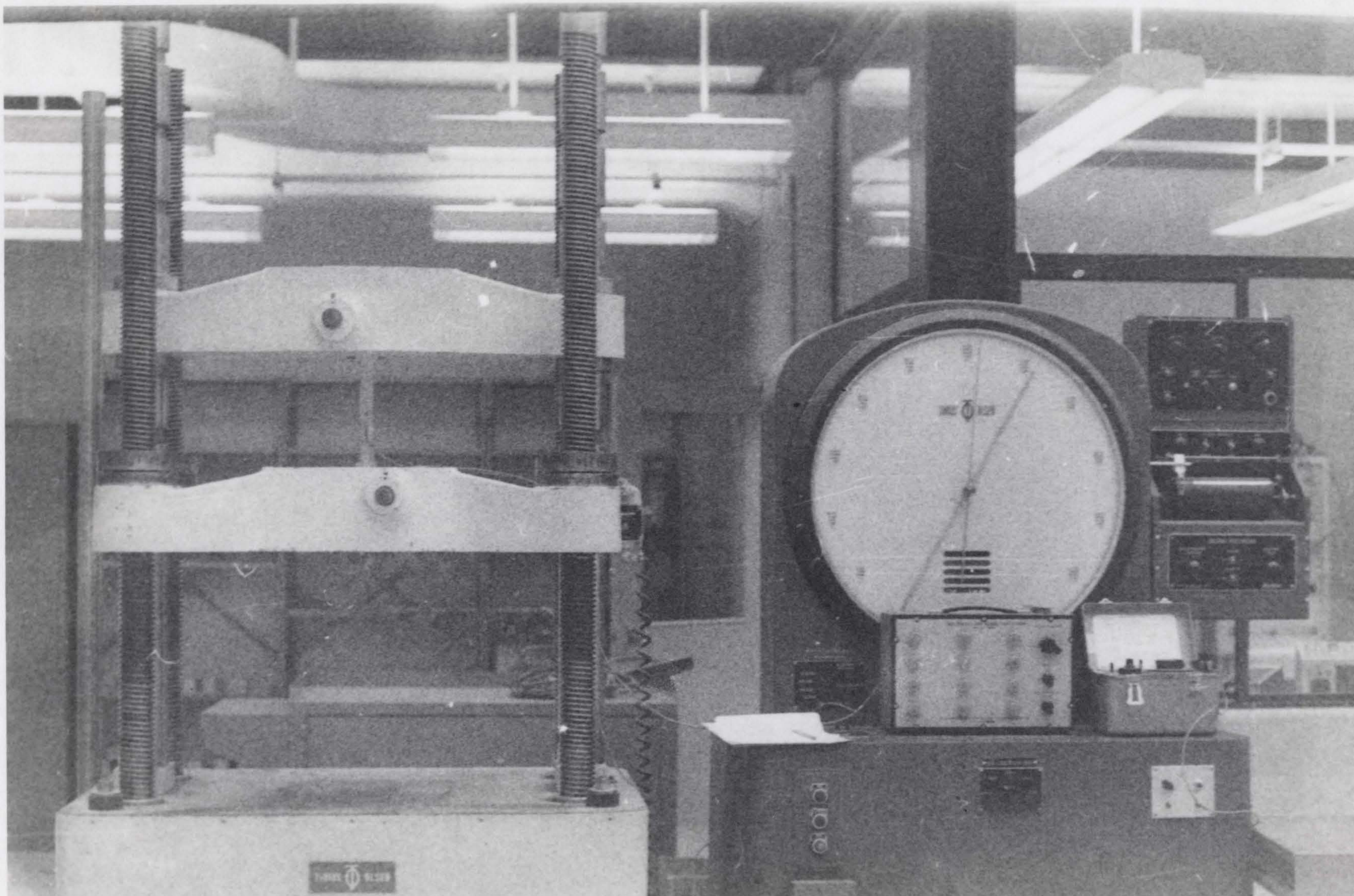

PHOTOGRAPH 4.3 LAYOUT OF TESTING APPARATUS.

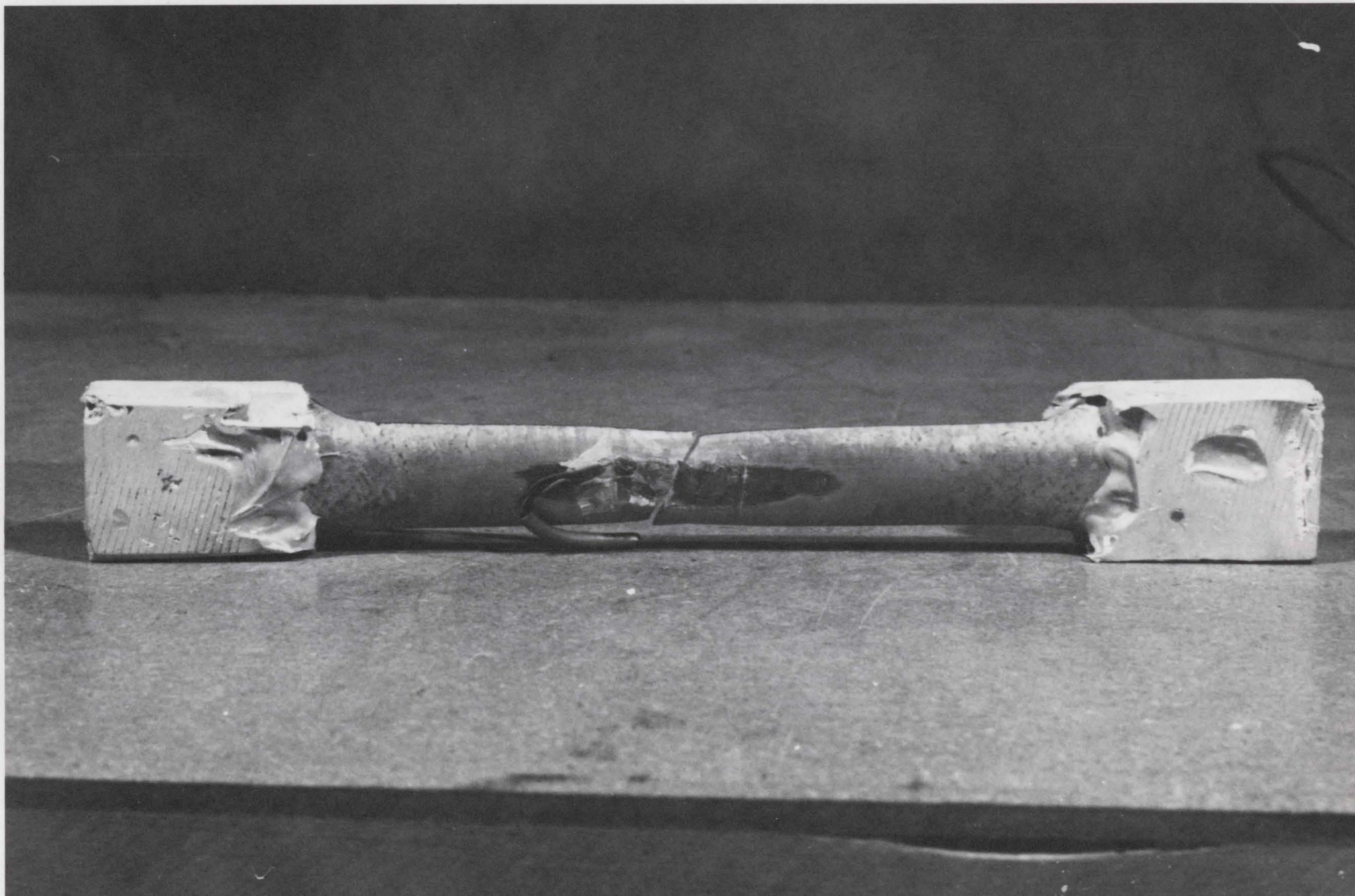

PHOTOGRAPH 4.4 TENSILE SPECIMEN.

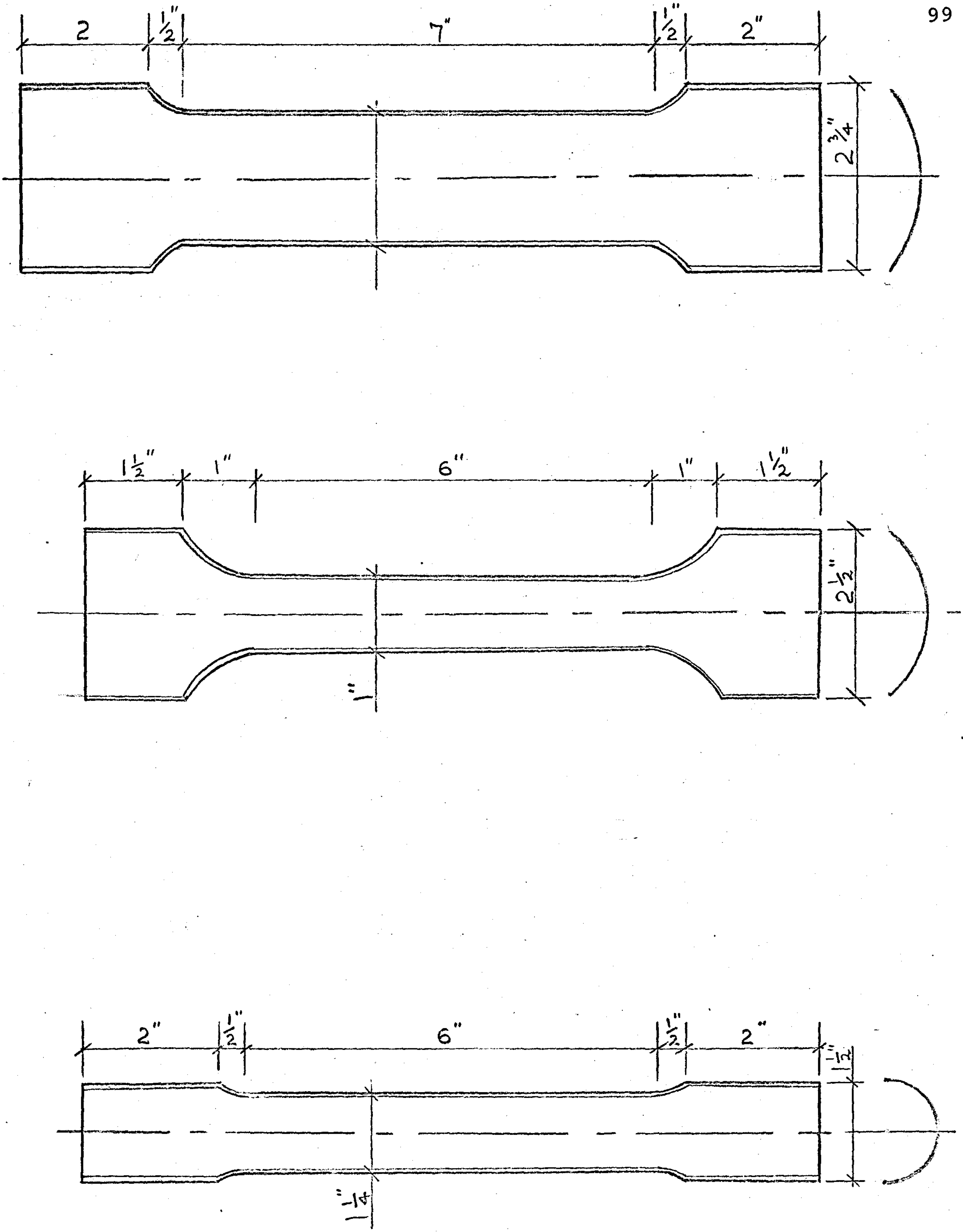

FIG.4.6 DIMENSIONS OF TENSILE SPECIMENS.

an effective method of gripping the ends of these curved tensile specimens during testing. It was considered to be unnecessarily expensive to make special curved jaws to fit in the testing machine to grip each size of specimen used, so some form of end block was considered. Eventually it was decided to use end blocks formed from "Colma-dur gel", a two-part chemical adhesive which possesses a very high compressive strength as well as excellent adhesive properties. Several holes were drilled in the ends of each specimen, and metal pins passed through them before the "Colma-dur" was formed around them. This considerably improved the bond between the specimens and the "Colma-dur", and prevented any slip between the two materials during testing. It was found to be necessary to cool the specimens with ice as the "Colma-dur" hardened around the ends, since the exothermic nature of the adhesive may otherwise have led to the introduction of residual stress due to differential temperature change.

The only difficulty resulting from this technique of gripping the tensile specimens was that the "Colma-dur" did tend to slip slowly in the jaws during testing, making it difficult to determine accurately the rate of straining of the specimens.

Before the construction of these end blocks, one half of the total number of specimens to be tested were stress-relieved by heating in an oven to 800°F, and maintaining them at this temperature for 24 hours. These specimens were then cooled inside the oven as slowly as possible to ensure that residual stresses due to differential cooling were not introduced. The temperature chosen was found to be just sufficient to release any residual stress present in the specimens without changing the crystalline formation of the steel and hence its basic material properties.

Budd Foil Strain gauges, type C6-1418, with 120 ohm resistance were used to measure the strains of the specimens under tension. Two strain gauges were mounted on each specimen, one being on each face at the centre of the narrow section. The tests were carried out on a "Tinius Olsen" screw type testing machine, and the specimens were all strained at a constant rate of 0.005 in/in., although as previously mentioned, this was difficult to maintain at higher loads because of the slipping of the "Colma-dur" block in the jaws.

The stress-strain relationships obtained are as shown in Figs. 4.7, 4.8 and 4.9, and the effect of the residual stress in the specimens is immediately apparent. The specimens that had been stress relieved tended to give a purely elastic-perfectly plastic characteristic, whereas those containing residual stress gave a markedly curved

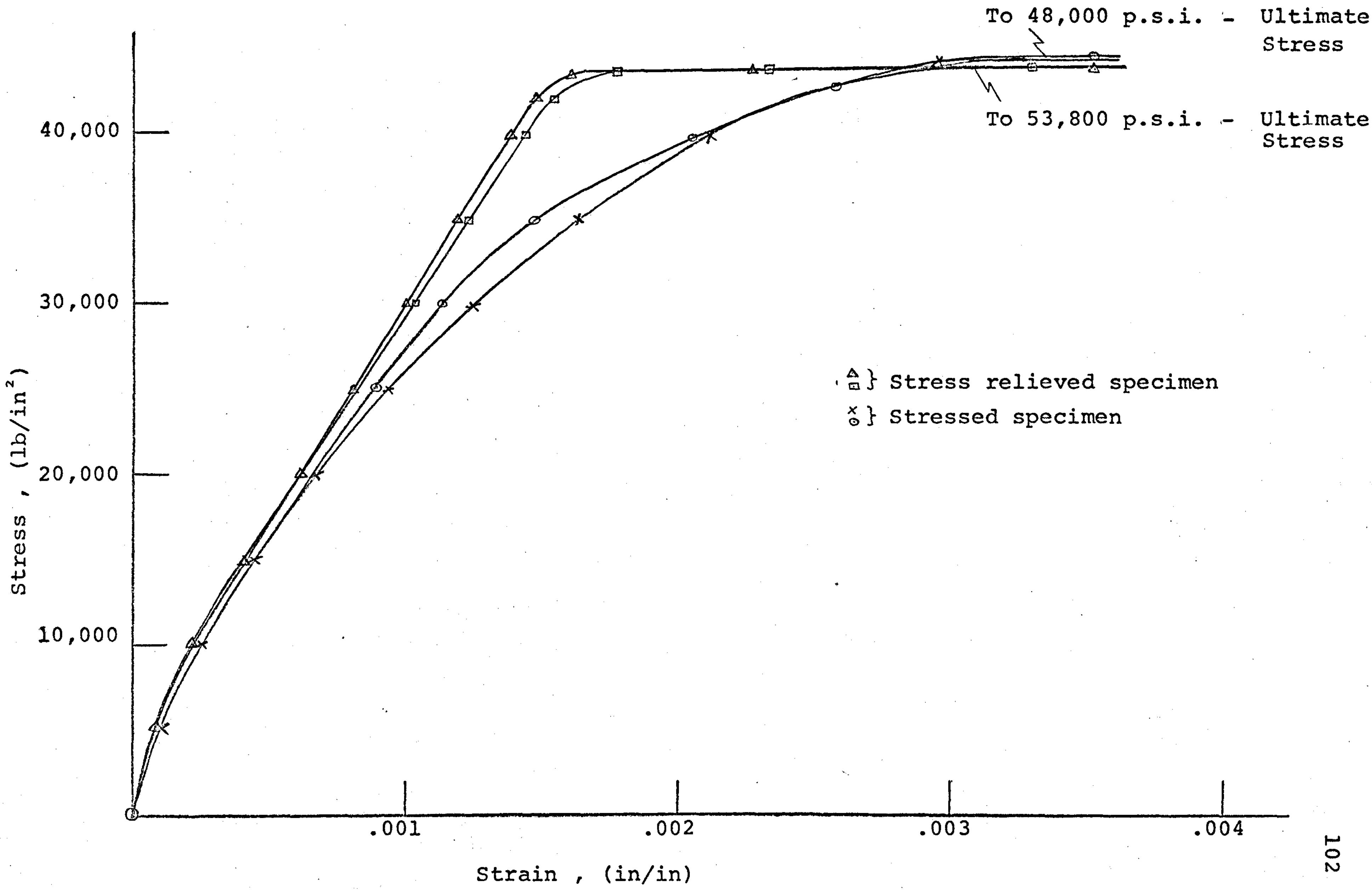

FIG. 4.7 TENSILE TESTS - 1" Ø BEND.

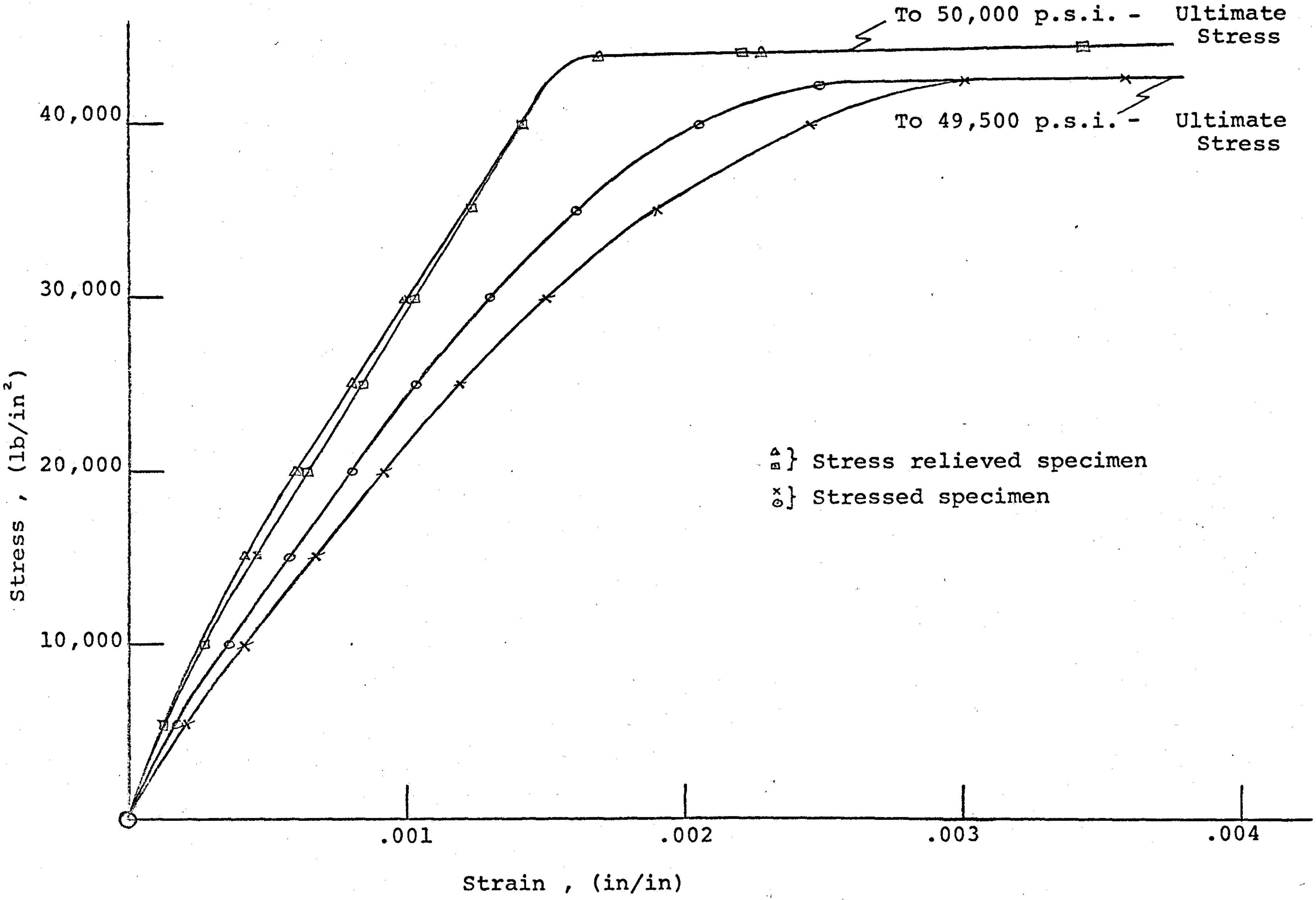

FIG. 4.8 TENSILE TESTS - 2 5/16" Ø BEND.

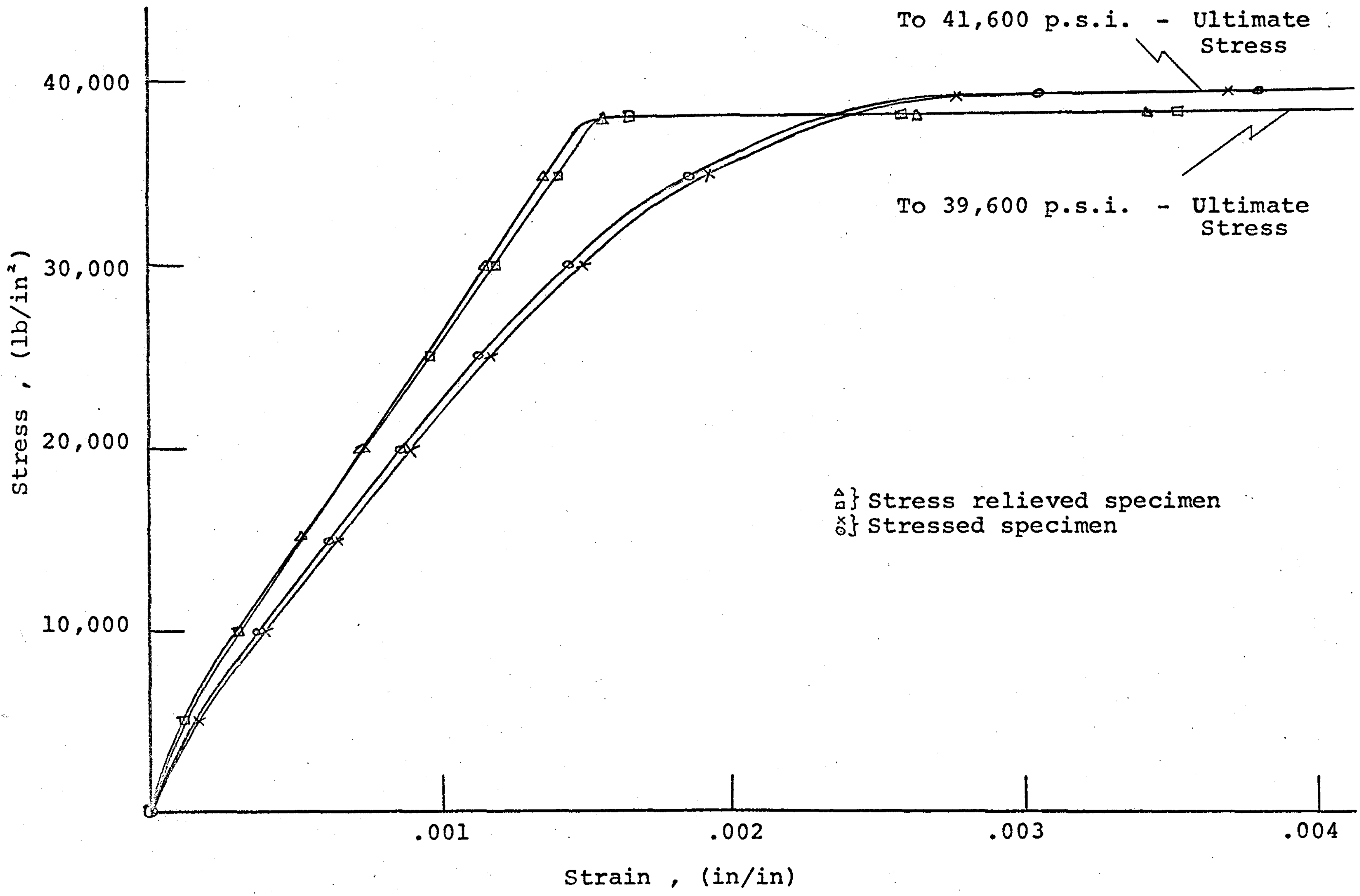

FIG. 4.9 TENSILE TESTS - 3"Ø BEND.

stress-strain characteristic. It can be seen that for all the specimens tested, the stress-strain characteristic is initially non-linear. This is almost certainly because of a twisting effect of the specimens resulting from misalignment in the testing machine, although initial imperfections may also be a factor.

No noticeably significant differences in the ultimate stress capacity of the sections could be seen with the small number of tests performed. The significance of these characteristics in relation to theoretical predictions is discussed in the concluding chapter.

4.3 Investigation Into the Influence of Residual Stress Due to Cold Bending on Sections Loaded in Compression

The purpose of this section of the testing procedure was to obtain the average stress-strain characteristics for various sizes of thin-walled open sections which contained residual stresses formed during fabrication, and compare them with the stress-strain characteristics of similar sections which had undergone a stress-relieving process.

The type of section required was to be fabricated from 18-gauge galvanized steel sheet, and had to satisfy three basic conditions:

(a) Must be fabricated easily.

(b) Must have a symmetrical residual stress distribution that is simple to predict from the theory.

(c) Must have a consistent, single mode of failure, free from torsional buckling.

Various cross-sectional shapes were tested before a cross section was obtained that consistently failed in local buckling in the same part of the cross section. The type of cross section used is illustrated in Photograph 4.7. It consisted of a constant diameter curved portion forming an arc of 240°, with lips at each end. These lips were included to strengthen the specimens against torsional buckling, and prevent distortion of the free ends of the cross section. The lips were formed as circular arcs, so that the residual stress distribution throughout the complete cross section could be predicted theoretically. The complete operation of fabrication of the three sizes of specimens having this type of cross section was carried out as follows:

The required length of galvanized steel sheeting to form one particular specimen was bent in the pyramid rolling press thorugh an angle of 180° to produce the shape shown in Fig. 4.10(a). Lips were then formed on the section by bending the sheet around steel rods welded to a steel bar of the appropriate diameter as shown in Photograph 4.5. This produced the shape shown in Fig. 4.10(b).

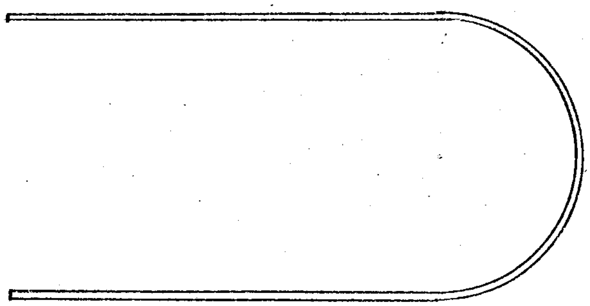

(a) Initial Bending Process.

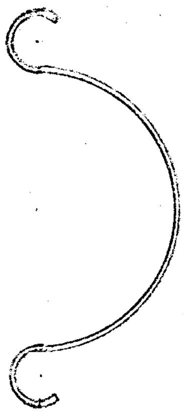

(b) Lip Forming.

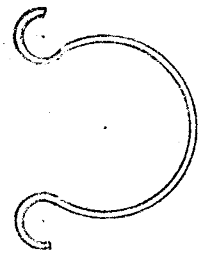

(c) Final Bending Process.

FIG. 4.10 STAGES DURING FABRICATION OF COMPRESSION SPECIMENS.

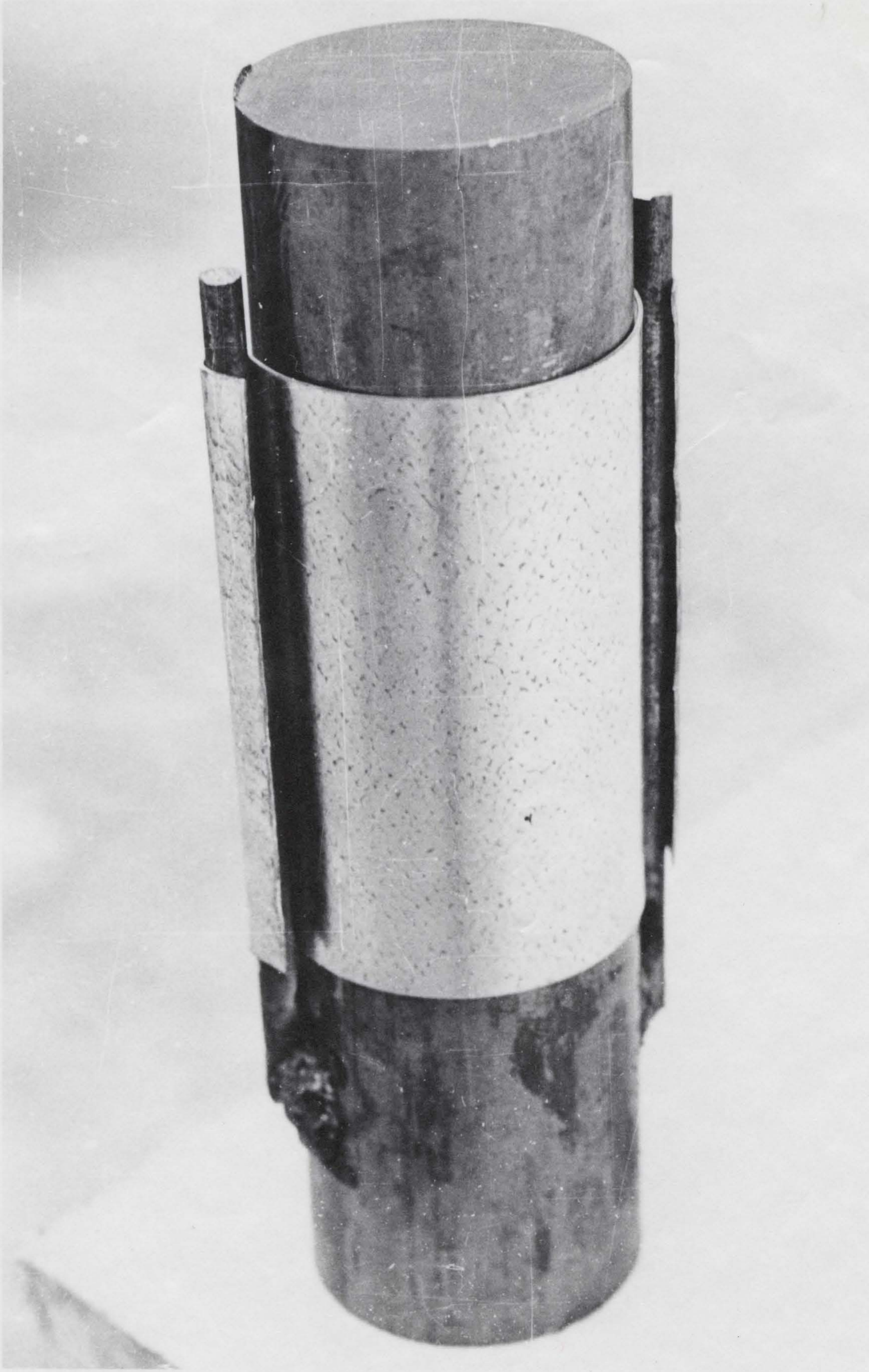

PHOTOGRAPH 4.5 FORMATION OF LIPS ON COMPRESSION SPECIMEN.

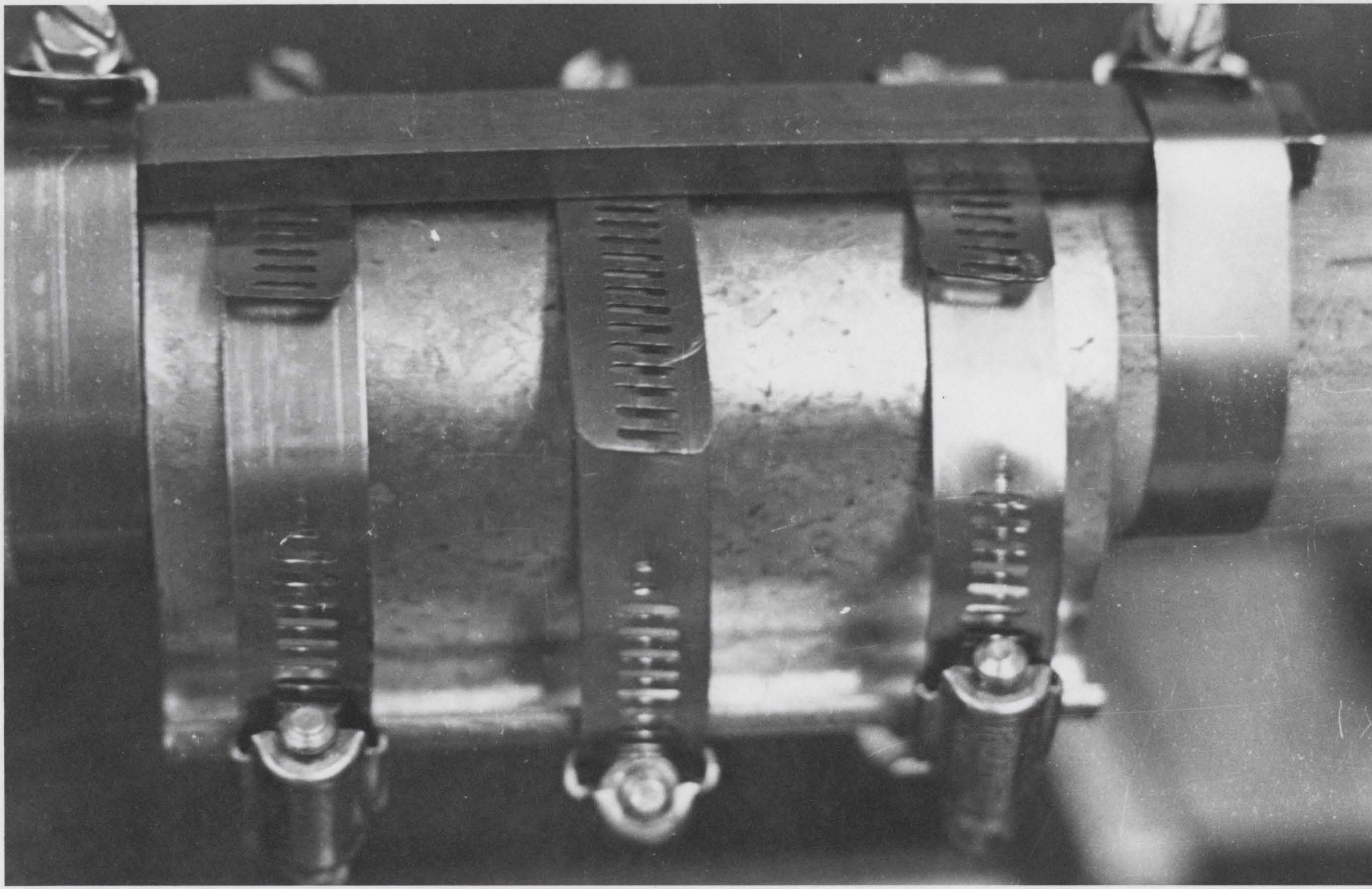

PHOTOGRAPH 4.6 FINAL BENDING OF COMPRESSION SPECIMEN.

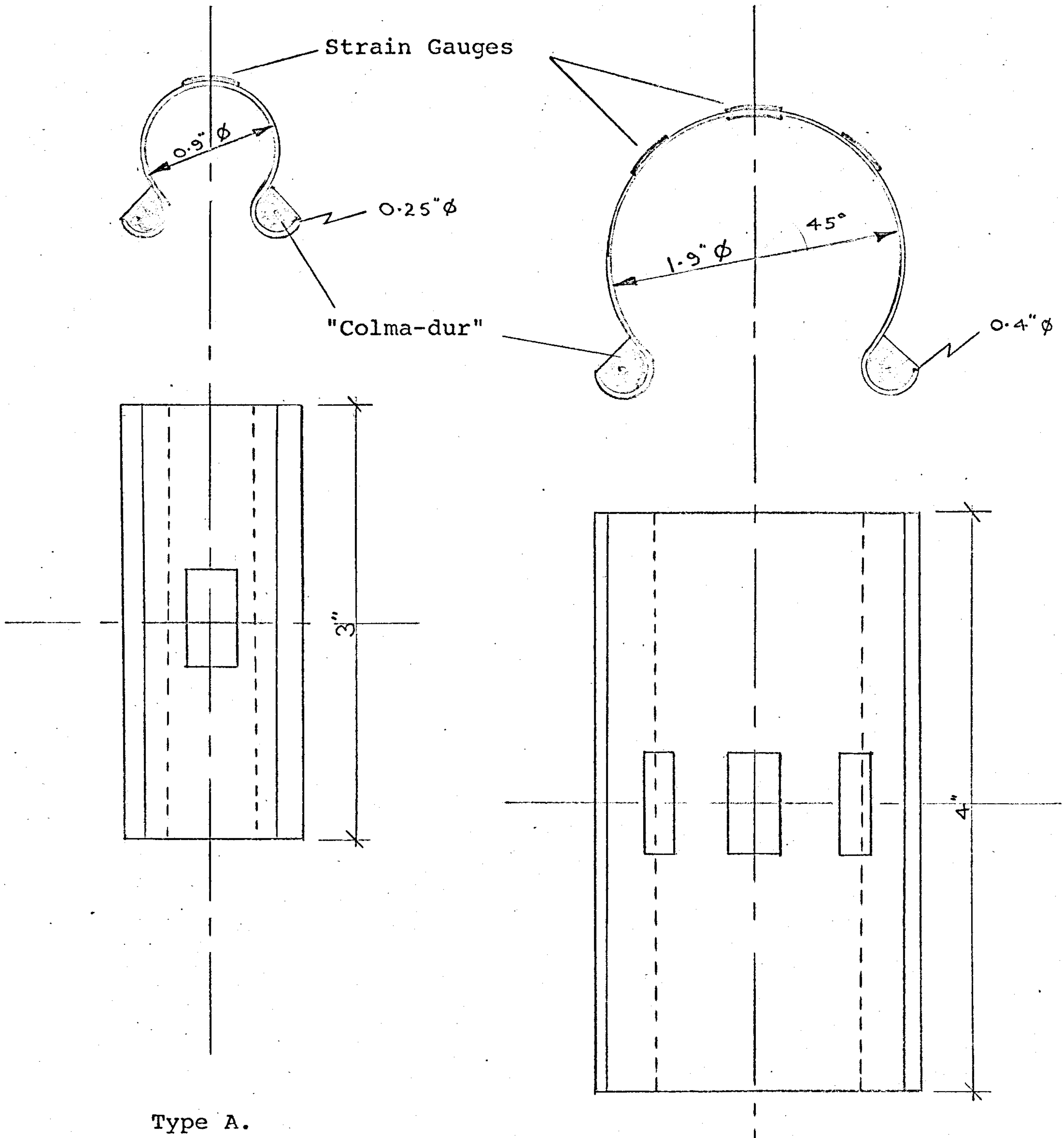

Scale: Full Size.

FIG. 4.12 COMPRESSION SPECIMENS SHOWING STRAIN GAUGES.

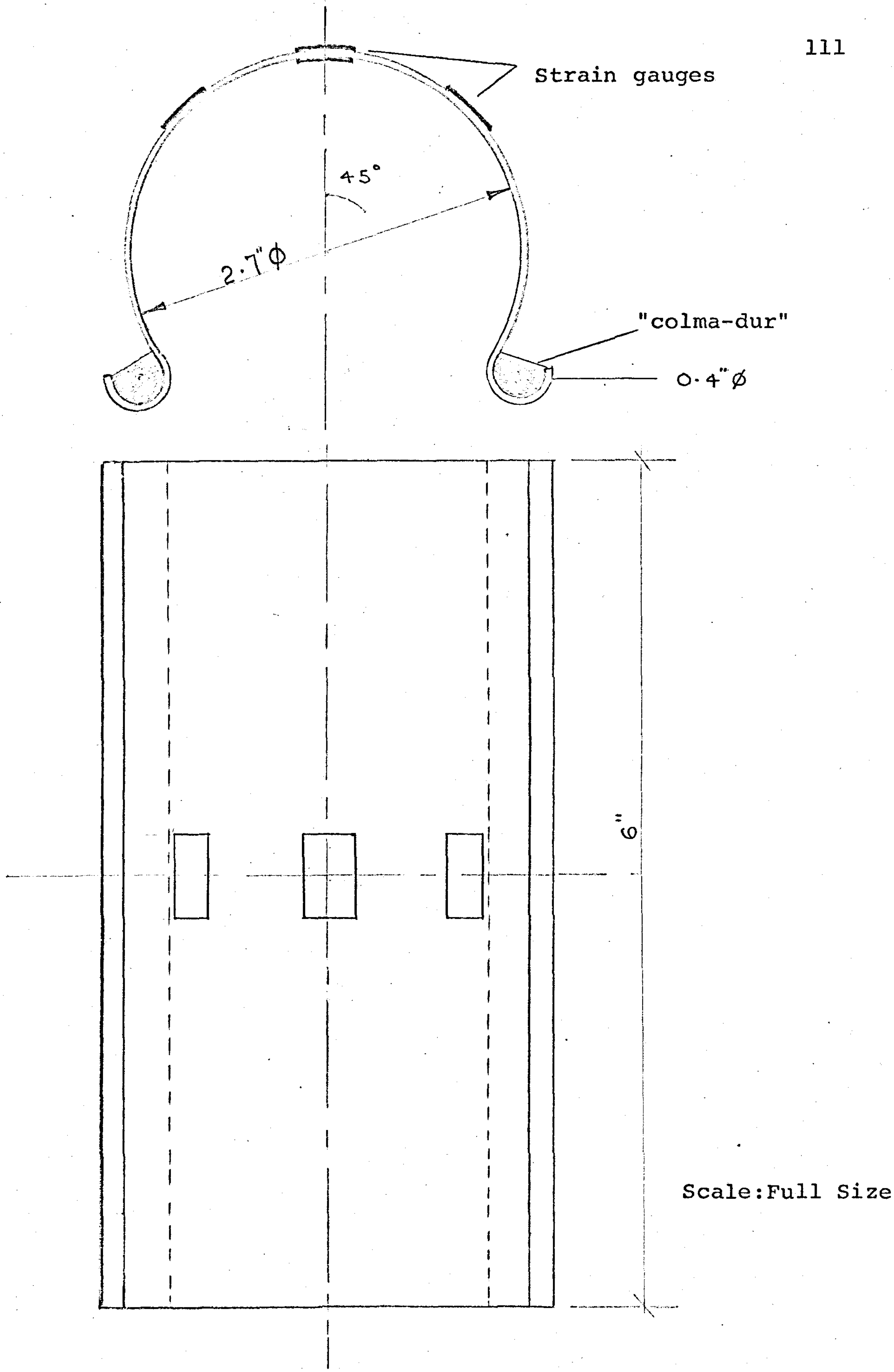

FIG.4.13 COMPRESSION SPECIMEN TYPE C SHOWING STRAIN GAUGES.

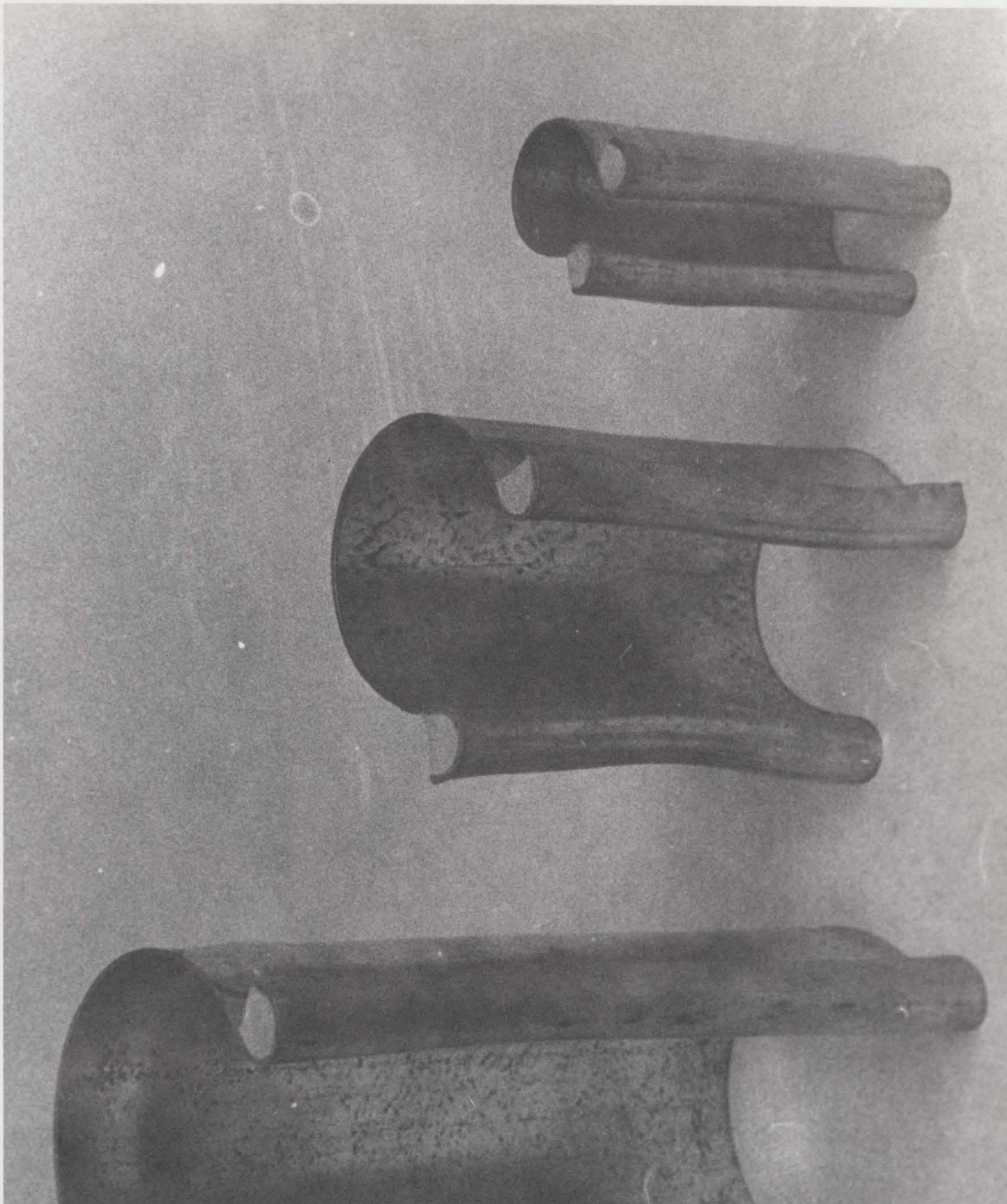

PHOTOGRAPH 4.7 COMPRESSION SPECIMENS.

To obtain a more balanced cross section, this shape was bent once more by wrapping it around a wooden dowel of reduced diameter by means of hose clamps as shown in Photograph 4.6. Thus, the final cross section shown in Fig. 4.10(c) was obtained.

Three different sizes of specimens were formed in this manner and the dimensions of these specimens are given in Table 4.11. Theoretical values for the finished diameters of the various specimens are shown in the table, and the calculations for these values are given in the Appendix.

Table 4.11

Dimensions of Compression Specimens

Type of Specimen	Type A	Type B	Type C
Dia. of doweling used in fabrication	0.8"	1.7"	2.35"
Theoretical finished dia. after spring-back	0.88"	1.89"	2.67"
Experimental finished dia. after spring-back	0.9"	1.9"	2.7"
Area of Specimen (in^2)	0.176	0.306	0.370
Length of Specimen	3.0"	4.0"	6.0"

Four specimens were fabricated to each of the three different sizes, and two of each size were stress relieved in an oven at 800°F for 24 hours and then cooled slowly in the same manner as were the tensile specimens. The ends of all the specimens were then squared on a lathe and checked visually for imperfections.

It was found to be advantageous to add to the stiffness of the lips formed on each specimen by filling them with "Colma-dur" gel. This helped to prevent premature normal buckling of the lips, which were difficult to form free from imperfections and ensured a local buckling failure in the curved portion of the cross section. Tests were carried out on various specimens to find out if this stiffening of the lips increased the load carrying capacity of the sections by forming a composite type of member. No significant difference in buckling load between the stiffened and unstiffened lips was found, so it was taken that the inclusion of the adhesive did not appreciably increase the carrying capacity of the specimens.

The twelve specimens to be tested were mounted with Budd Foil Resistance gauges, type C6-141B, 120 ohms positioned as shown in Figs. 4.12 and 4.13. These gauges were used to measure the strains occurring throughout the cross section during compressive loading. Three gauges were mounted on the convex side of the larger size specimens (Types B and C) the outer two being used to check that the specimen was being loaded axially, and no bending was occurring. One other strain gauge was mounted on the concave face of the specimens to ensure that there was no bending occurring in the other perpendicular direction. The specimens Type A had only space for one strain gauge which was positioned as illustrated in Fig. 4.12.

The tests were carried out in a Tinius Olsen screw type testing machine, and the ends of the specimens were placed against fixed plates so that no rotation of the ends could occur. The ends of the specimens bore directly onto 1/10 in. lead plates which in turn bore onto aluminium sheets. This allowed for any small imperfections in the squaring-off of the specimens, and allowed the load to be carried throughout the complete cross section permitting uniform application of stress on the ends.

The load on the cross section was initially increased to about one-quarter of the expected yield value of the specimen, and held at this value for several minutes whilst the specimen settled into the load plates and bore evenly onto the flat aluminium sheets. When the strain gauges gave identical readings for load values between zero and the value of one quarter of the expected yield load, the specimen was considered to be exactly square on the plates and carrying load evenly on the whole cross section.

The specimen was then loaded from zero load at a slow strain rate of 0.0025 in/min., and strain gauge readings were taken at increments of 100 lb. Straining was continued until the specimen failed and the collapse load was recorded. As the cross-sectional areas of the specimens were known, the average stress throughout the cross sections could be evaluated for incremental value of loading.

The average stress-strain characteristics obtained for the various sizes of specimens tested are shown in Figs. 4.14, 4.15, 4.16, 4.17 and 4.18.

Fig. 4.14 shows a typical characteristic for the behaviour of specimens type A, before and after stress relieving. All the type A specimens failed in local buckling, and it is clear from Fig. 4.14 that the residual stresses present considerably influenced the behaviour of the specimens. The limit of proportionality was considerably lower for the specimens containing residual stress than for the stress-relieved specimens, and the presence of residual stresses clearly rendered the behaviour of the specimen non-linear.

The typical average stress-strain relationships for specimens, type B are shown in Figs. 4.15 and 4.16. It can be seen that the strains were not the same for

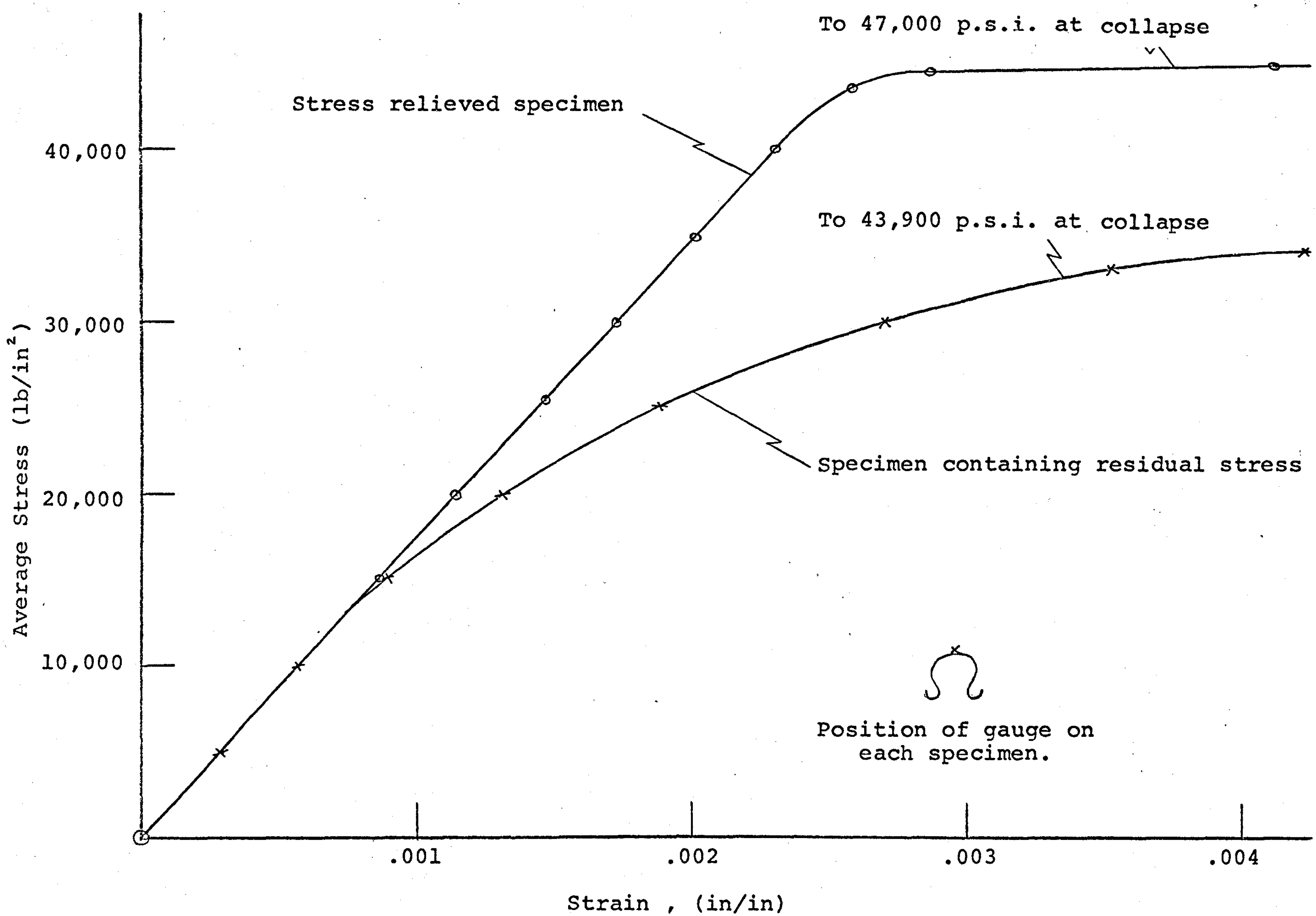

FIG. 4.14 TYPICAL CHARACTERISTICS FOR COMPRESSION SPECIMENS - TYPE A.

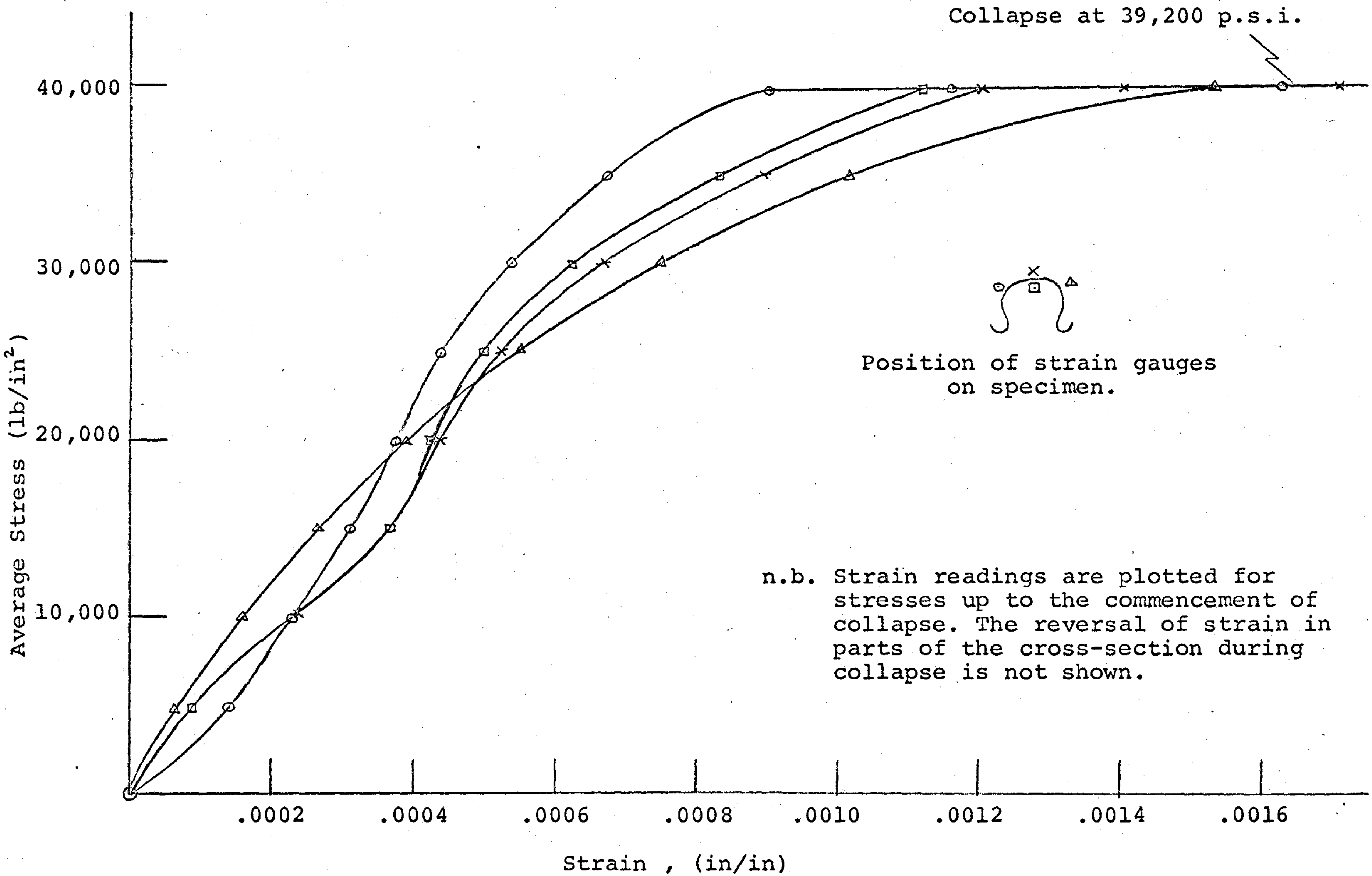

FIG. 4.15 COMPRESSION SPECIMEN TYPE B - CONTAINING RESIDUAL STRESS.

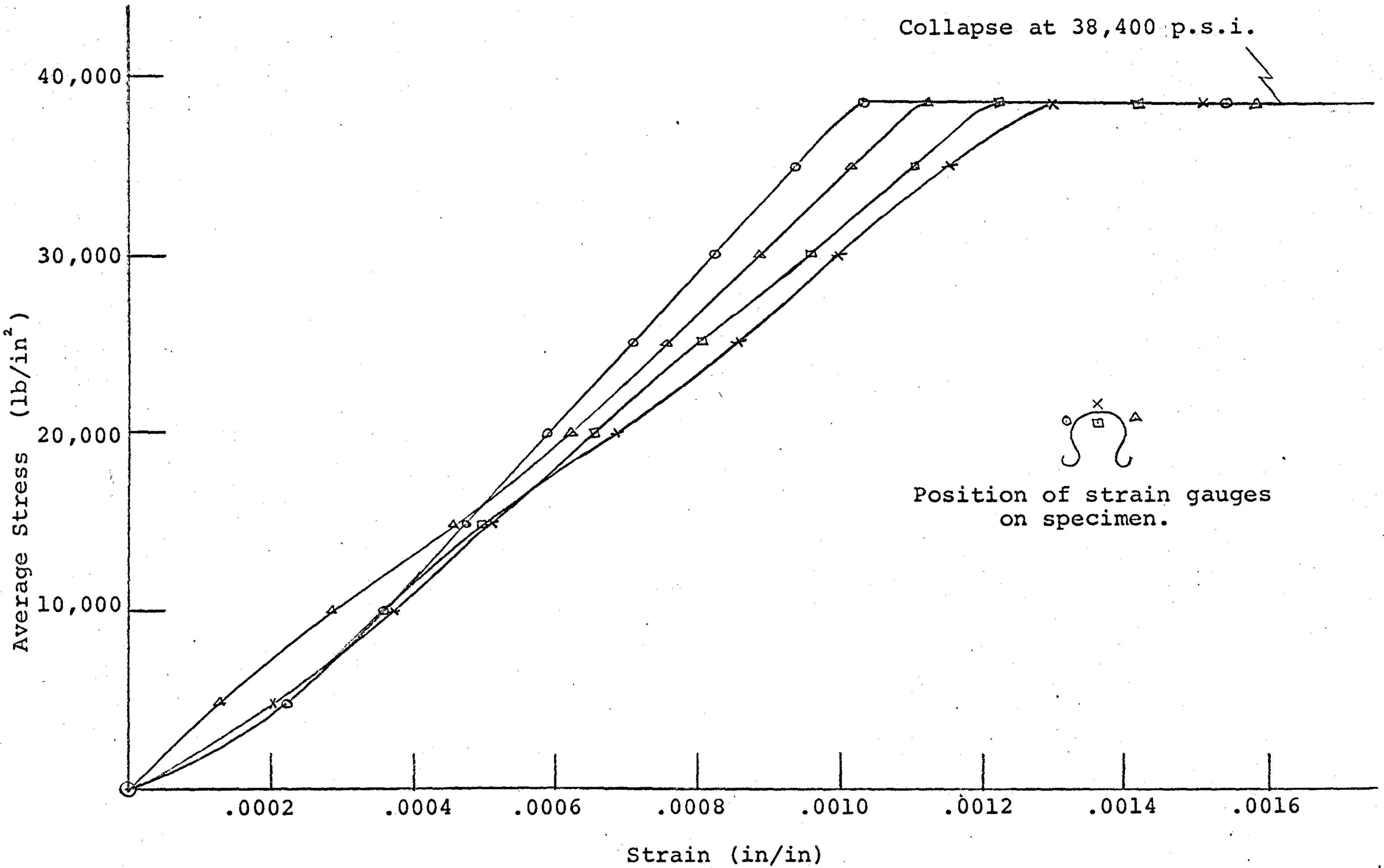

FIG. 4.16 COMPRESSION SPECIMEN TYPE B - STRESS RELIEVED.

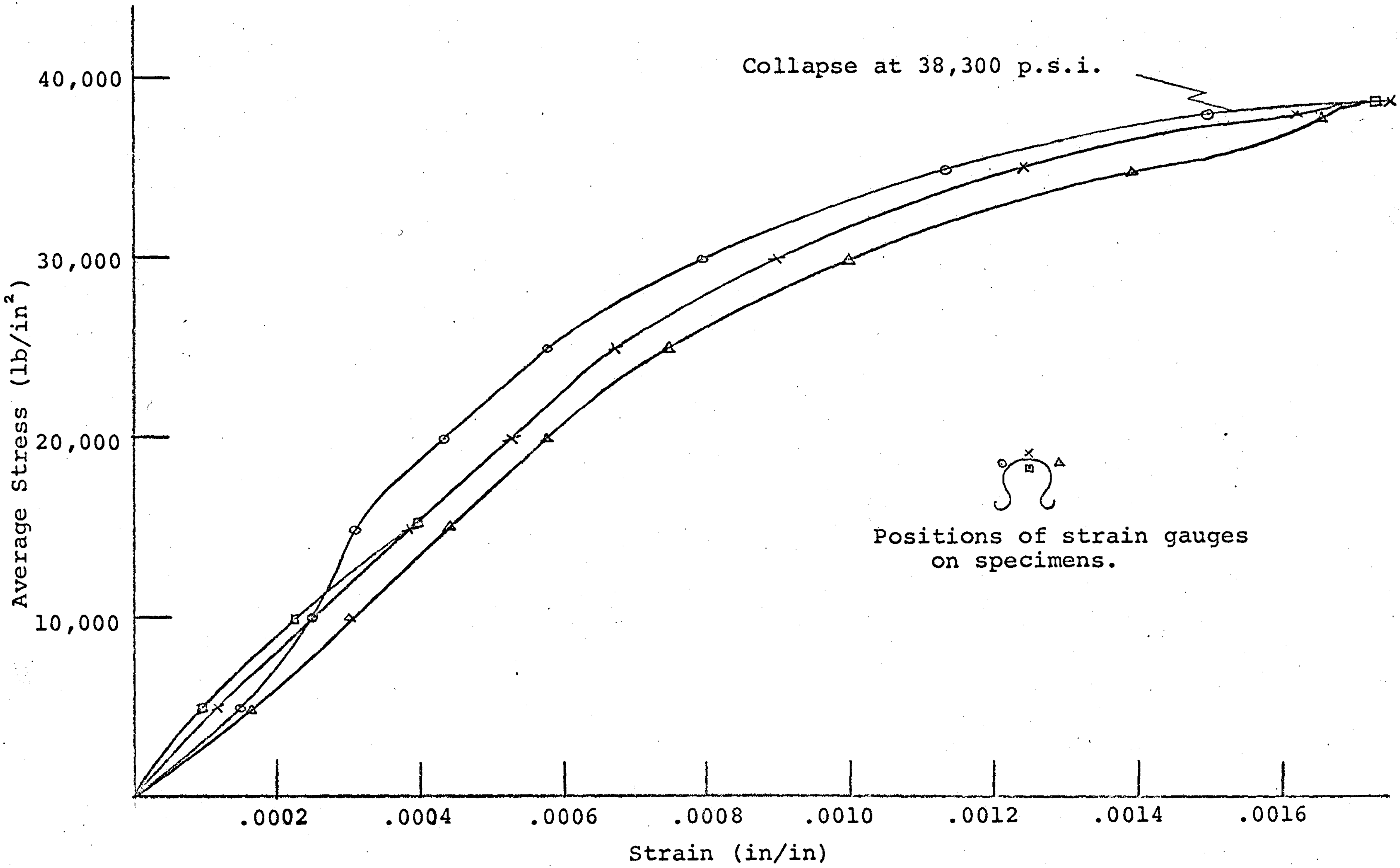

FIG. 4.17 COMPRESSION SPECIMEN TYPE C - CONTAINING RESIDUAL STRESS.

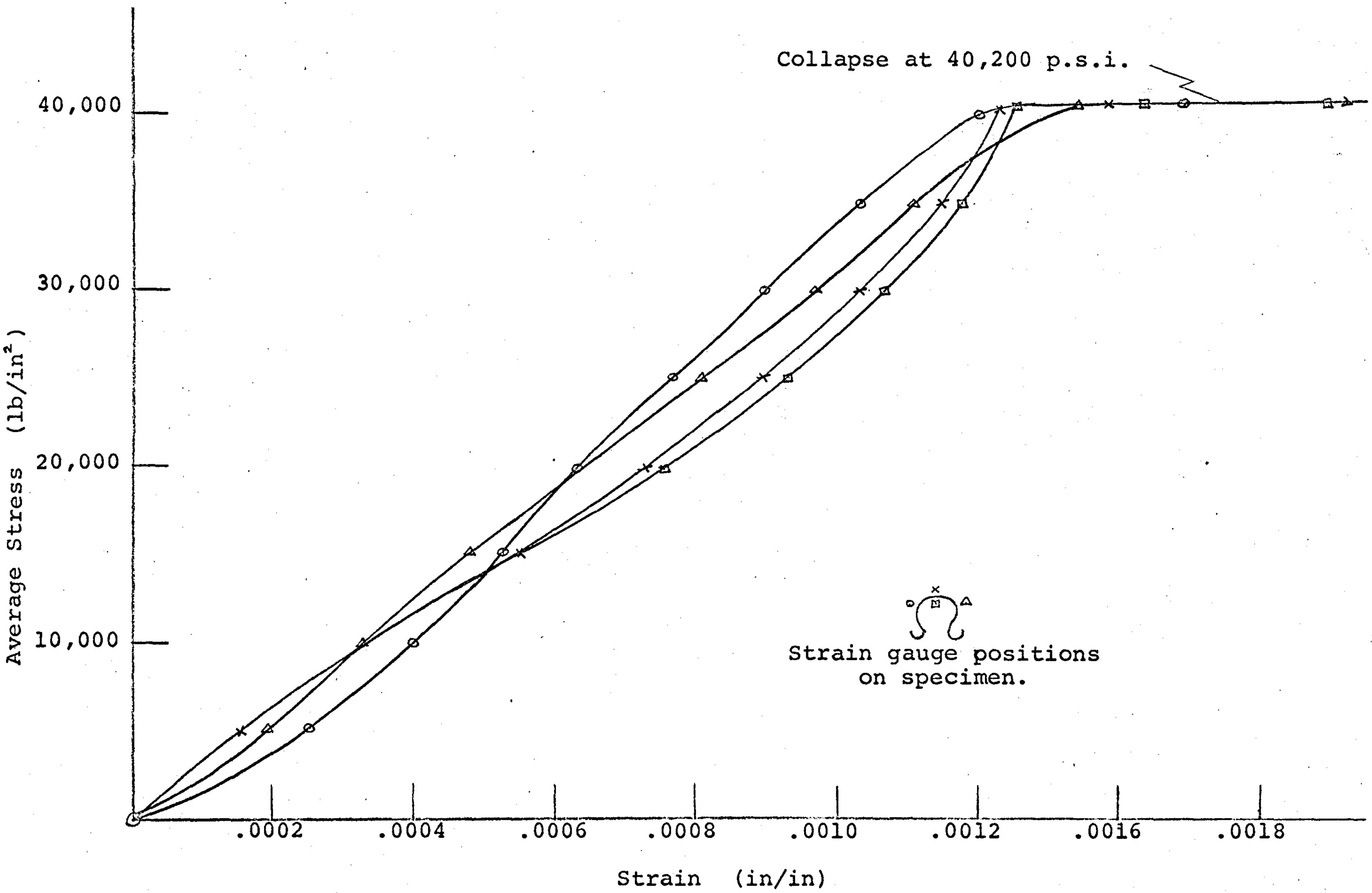

FIG. 4.18 COMPRESSION SPECIMEN TYPE C - STRESS RELIEVED.

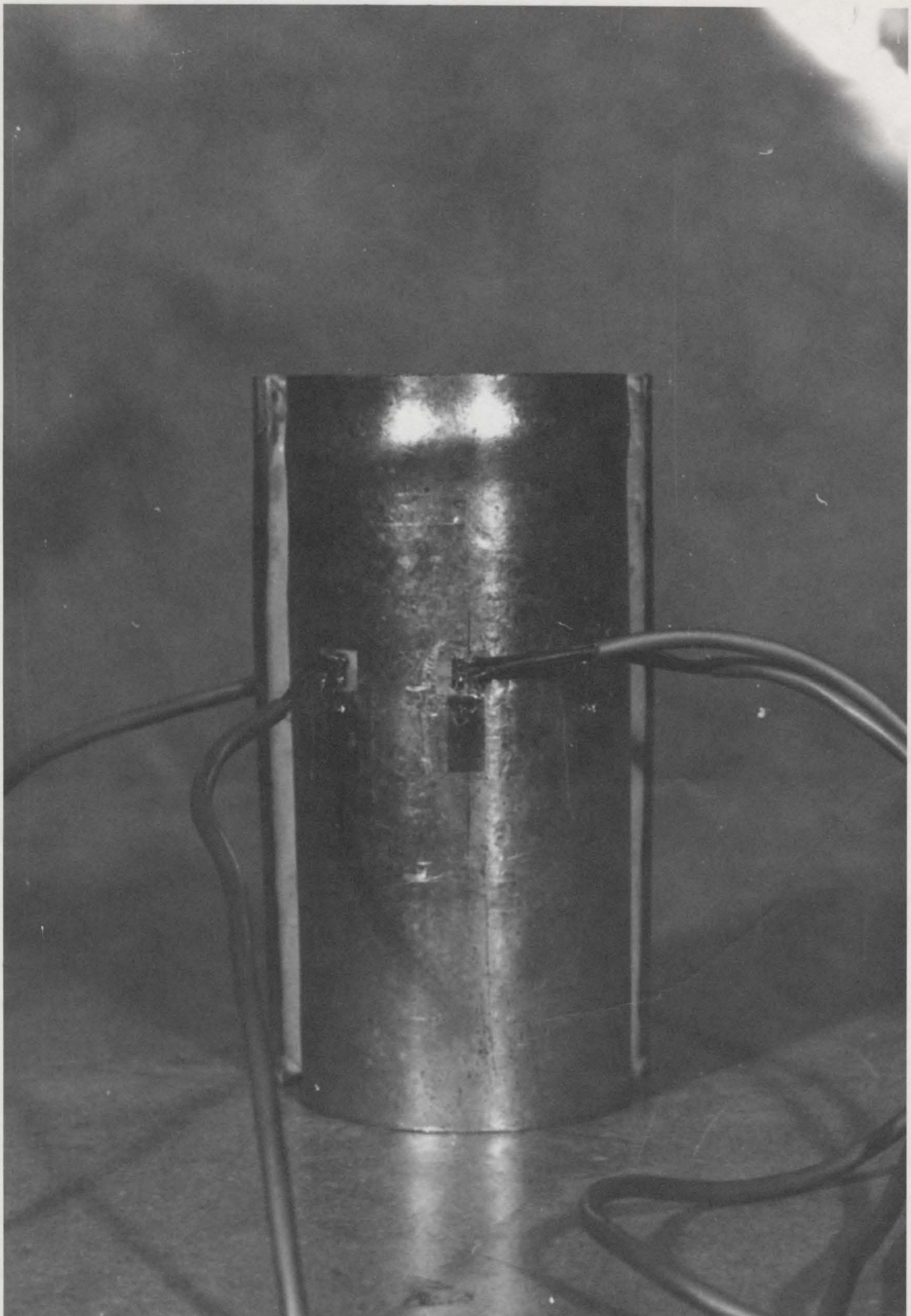

PHOTOGRAPH 4.8 LOCAL BUCKLING FAILURE OF COMPRESSION SPECIMEN TYPE C .

each part of the cross section, indicating that the stress was not uniform throughout the cross section. This occurred because the ends of the specimen were probably not perfectly square, and initial imprefections in the specimens caused bending to take place within the specimen as loading proceeded. There is a clear difference, however, between the characteristics of the specimen containing residual stress and the stress-relieved specimen. The stress-relieved specimen exhibits an almost purely elastic-perfectly plastic behaviour, whereas the behaviour of the specimen containing residual stress shows a non-linear characteristic in the region of higher average stress.

The characteristics shown for specimens type C are similar to type B with the behaviour of the stress-relieved specimens being almost purely elastic-perfectly plastic, and the behaviour of the specimens containing residual stress being partially non-linear.

A noticeable difference between the collapse load of the stress-relieved specimens and those containing residual stress was not observed, and no conclusions could be made regarding the collapse load in view of the small number of tests performed.

The lengths of the local buckling waves that occurred for the three sizes of specimens tested increased as the R/t ratio of the specimens increased.

It was not possible to accurately isolate the boundaries of the buckling waves, but reasonable estimates for the wave lengths were made. These approximate lengths are shown in Table 4.19, and may be compared with the values obtained from the theoretical analysis.

Table 4.19

Buckling Wave Lengths for Compression Specimens

Specimen	R/t ratio	Approx. Buckling Wave Length	
		xt	ins.
Type A	9	7t	0.35
Type B	20	10t	0.5
Type C	28	15t	0.75

4.4 Results of Compression Tests on Type C Specimens

To determine the influence of residual stresses due to cold forming on the compressive capacity of Type C sections, a series of tests was conducted to provide a reasonable statistical average. Sixteen of this size specimen were fabricated in the same manner as before, and eight of these were stress relieved, and the other eight left containing the residual stresses set up in the bending process. The circular lips were filled with "Colma-dur" gel, and tested in a "Tinius Olsen" screw-press to destruction and the collapse loads recorded.

Table 4.20

Results of Compressive Tests for Specimens Containing Residual Stress

Data

Area of Specimens = 0.37 in.^{2}

Rate of Straining = 0.01 in./min.

Specimen	Collapse Load	Average Stress
1	14,080 lb.	38,000 lb/in^2
2	14,100 lb.	38,100 lb/in^2
3	14,020 lb.	37,900 lb/in^2
4	14,600 lb.	39,400 lb/in^2
5	14,430 lb.	39,000 lb/in^2
6	14,000 lb.	37,900 lb/in^2
8	14,010 lb.	37,900 lb/in^2

Average Stress at Collapse = 38,360 lb/in^2

Distribution of stresses. 37,900 to 39,400 lb/in^2

Table 4.21

Results of Compressive Tests for
Stress-Relieved Specimens

Specimen	Collapse Load	Average Stress
1	14,050 lb.	37,900 lb/in^2
2	14,700 lb.	39,800 lb/in^2
3	15,020 lb.	40,600 lb/in^2
4	14,500 lb.	39,200 lb/in^2
5	14,920 lb.	40,300 lb/in^2
6	15,000 lb.	40,600 lb/in^2
7	14,650 lb.	39,600 lb/in^2

Average Stress at Collapse = 40,020 lb/in^2
(omitting erroneous no. 1)

Distribution of stresses 39,200 to 40,600 lb/in^2
(omitting erroneous no. 1)

The results tabulated in Tables 4.20 and 4.21 indicate a marginally higher collapse load in the case of the stress-relieved specimens. The range of values for both the stress-relieved specimens and those containing residual stress is shown on the theoretical curve in Fig. 3.14.

The significance of these results in ascertaining the influence of residual stress due to cold bending on the collapse load of compression specimens, and a correlation with the theoretical results follows in Chapter V.

CHAPTER V

COMPARISON OF EXPERIMENTAL RESULTS WITH THEORY

5.1 Influence of Cold Bending on Elastic Springback

The theoretical values for elastic springback strain calculated from Von Mises' and Tresca's yield criteria may be compared with the experimental value as shown in Table 5.1.

Table 5.1

Elastic Springback Strains, σ_{s_r} in Outside Fibres

Von Mises' yield criterion	0.0017 in./in.
Tresca's yield criterion	0.0015 in./in.
Experimental value	0.002 ± .0001 in./in.

The theoretical criteria used have both predicted values of elastic springback smaller than the value measured experimentally. Von Mises' criterion has yielded the more satisfactory prediction of elastic springback strain, being within 15% of the experimental value. It is more simple to compare these outside fibre strains than to relate the change in radii for a particular bent specimen, although this may be calculated from Equation (2.21).

The discrepancy between the experimental result and the theory is to be expected in view of the approximation made in the assumed distribution of stress through the cross section of the sheet before elastic springback. By far the most significant reason for the underestimation of the value of elastic springback appears to be the omission of the consideration of work hardening of the material during cold bending. Work hardening considerably affects the stress distribution through the cross section of the sheet during the bending process, causing higher values of outside fibre stress than those predicted. Inspection of Figs. 2.10 and 2.11 indicates that this higher value of outside fibre stress results in an increased value of elastic springback. Clearly, for valid predictions to be made for the amount of elastic springback likely to occur after a cold bending process, tests must first be performed to evaluate the work hardening properties of the material to be used. Once these properties have been established, the values for elastic springback for various fabrication operations involving various thicknesses of sheeting may be theoretically predicted for this material.

Furthermore, the stress-strain relations in uniaxial tension were used to specify the value $\bar{\sigma}$. As Fig. 4.1 indicates, the value of the static yield stress is somewhat lower than the upper yield stress, so applying the value of $\bar{\sigma}$ = 31,000 p.s.i. would yield conservative results. However, in the bending test, the static yield stress is not strictly applicable, and hence its application may account for 3 to 4% of the error relating to spring-back calculations.

5.2 Tensile Stress-Strain Characteristics

The theoretical stress-strain characteristic obtained for curved tension specimens containing residual stress is of a similar shape to the experimental characteristics. In both cases nonlinearity commences at a value of about half the yield stress obtained from the primary tensile tests. (e.g., Figs. 3.7 and 4.7.)

The theoretical characteristics, however, indicate a perfectly plastic behaviour at a stress of $0.878\bar{\sigma}$ for Von Mises', and $0.857\bar{\sigma}$ for Tresca's yield criterion. On the other hand, the experimental results do not show a perfectly plastic behaviour until a stress of approximately $1.35\bar{\sigma}$ is reached. The discrepancy between theoretical and experimental results is certainly substantial. As described in the previous section, up to 15% of the spring-back error could be attributed to strain hardening. A difference of 40% cannot be solely due to this cause, and therefore must be due in large measure to the Bauschinger effect. Mathematically the Bauschinger effect can be described as a translation of the yield surface in stress space in the direction of the plastic strain increment. The prescription of yielding then is a function not only of the stresses, but also of the plastic strain history apart from isotropic strain hardening. Whether this phenomenon can account for a 25% discrepancy is not known and should be the basis of a further study.

Both the specimens that contained residual stress, and those which had undergone a stress-relieving operation, became perfectly plastic at higher values than would be expected from primary tensile test results. This indicated that the stress-relieving process tended to remove the residual stresses from the curved specimens, but not the influence of work hardening and the Bauschinger effect.

The theoretical stress-strain characteristic indicated an initial non-linearity at a value of about half the nominal yield stress. This was verified by the experimental tests which indicated initial non-linearity of the stress-strain characteristic at a value of about half the modified value of yield stress increased by work hardening.

No significant difference in the ultimate yield of the curved tensile specimens was observed in the experimental tests for the specimens containing residual stress and those which had been stress relieved.

5.3 Local Buckling of Compression Specimens

The experimental tests performed on the three sizes of compression specimens clearly indicated the influence of residual stress due to cold bending on the stress-strain characteristics. The specimens containing residual stress all showed a non-linearity in the stress-strain characteristic, whereas those which had undergone a stress-relieving operation showed a fairly linear characteristic.

The compression tests performed on the specimens type C to obtain values of the collapse load all failed in local buckling. The average stress at collapse for the specimens containing residual stress was found to be approximately 4% lower than the average value obtained for the stress-relieved specimens. These experimental results are shown on the theoretical graph in Fig. 3.14. The theoretical predictions based on the virtual work and incremental theories have overestimated the collapse stress for both Von Mises' and Tresca's yield criteria. There are several possible reasons for this overestimation:

By assuming a deflection function with a finite number of parameters, an upper bound on the actual state of behaviour will result. The constraint imposed on the mode of deformation will require a higher load than would otherwise be the case. While the general shape of the buckle observed is similar to that prescribed mathematically, a somewhat larger region in the circumferential direction was distorted than was assumed. Furthermore, the assumption of straight stiffeners during post-buckling was not completely satisfactory as shown in Photograph 4.7. Although considerable care was taken to avoid geometric imperfections, these could not be eliminated entirely. Consequently, some influence from initial distortion would be anticipated.

Von Mises' yield criterion would be expected to yield buckling loads higher than those predicted by Tresca's yield criterion due to the form of the yield surfaces. Since the investigation is centred about the neighbourhood of the compressive axial stress component, however, little difference would be anticipated.

There has been a general tendency for incremental theories of plasticity to overestimate the buckling load, and subsequent post-buckling behaviour.[9] Some opinion[16] does attribute this discrepancy to imperfections, which if correct would confirm the comments already made.

Good correlation was evident between the theoretical buckling wavelength and values determined from experimental tests. Although experimental values were difficult to ascertain with any degree of accuracy the values may be seen to be of the same order as those obtained theoretically.

Considering the number of approximations made in the theoretical analysis, it may be concluded that the methods employed based on virtual work and plastic incremental theories, and the application of experimental stress-strain curves, yield results of a reasonably high degree of accuracy.

CHAPTER VI

CONCLUSIONS

The elastic springback likely to occur after a cold forming process can be reliably predicted for metal sheets. The analysis given herein is simplified to include materials which exhibit elastic-perfectly plastic characteristics. The observed error between theoretical predictions and observation is about 15% and is accounted for by work hardening in the material. The resulting residual stress distribution is expected to be within 15% of the computed values. A theory taking into account isotropic strain hardening would reduce the springback error considerably.

The essential form of the apparent stress-strain relation in the direction perpendicular to that of rolling, but in the plane of the sheet, agrees with that predicted. Ultimate values differ considerably by up to 40% and must be dependent on strain hardening and the Bauschinger effect to a large extent. This is confirmed by the good agreement of results derived from Tresca's and Von Mises' yield criteria. The influence of anisotropic behaviour of the material prior to cold forming is unknown, but mechanical properties in the thickness direction would be expected to be considerably different from in-plane properties. Since stress components are essentially confined to the plane of the sheet, the assumption of an isotropic material is probably reasonable.

The theoretical maximum compressive stress of the shape considered is dependent on the tangent modulus. For the range of radius to thickness ratios considered plausible for the buckling mode assumed, the corresponding value of the ratio of Young's modulus to the tangent modulus is certainly greater than 10. This result suggests that for elastic-plastic or strain hardening materials the maximum load carried by such a section of intermediate length tends to the squash load equivalent. This result is confirmed by Batterman[23] who performed tests on cylinders with similar R/t. He has also shown that for E/E_T greater than 9.5 no unloading would occur during buckling which verified that this assumption was reasonable for our case.

Based on the experimental stress-strain curve, the incremental theories for local buckling failures yield slightly unconservative results. The influence of imperfections for the tests conducted is clearly small but for fabricated sections to be used in practice, these are likely to be of greater significance.

The experimental results for heat-treated and non-heat-treated sections indicates a slight benefit of heat treatment on compressive carrying capacity. Although these particular tests do not substantiate the sensitivity of premature buckling to residual stresses, only one section was studied in detail because the effect of imperfections was significant for a wide range of others. It follows that for sections which are sensitive to residual stresses they are probably also sensitive to geometric imperfections.

The major difficulty in the study of the influence of residual stress on the behaviour of cold formed sections is that the isolation of this effect from other associated effects is almost impossible. It is possible, however, to obtain an understanding of the combined influence of these effects, which, in the final evaluation, is more useful in the practical application to engineering problems.

SUGGESTIONS FOR FURTHER RESEARCH

1. The constructions performed in Chapter II may be modified to take into account the influence of work hardening on the amount of elastic springback, by using a revised estimation of the stress-strain distribution across the sheet before elastic springback.
2. The theoretical predictions for the behaviour of thin-walled sections under tensile and compressive load may also be modified to take into account the influence of work hardening. The Bauschinger effect

also required further study as this appears to be the principle source of error in quantitative predictions of axial stress-strain behaviour.

3. To confirm the applicability of the local buckling analysis based on the virtual work and incremental theories, other parameters should be introduced to account for more extensive buckling. To complement this theoretical work, compression tests may be performed on open sections having various values of R/t.

4. The theoretical analysis performed for local buckling may be repeated using deformation theory instead of incremental theory, and with the variational procedure for both theories treating the buckling wavelength, l, as a time parameter.

5. The effect of geometric imperfections on sections sensitive to them requires study, before a rational approach to the effect of residual stress in combination with imperfections may be made.

APPENDIX 1

Calculation of dimensions of Compression Specimens after elastic springback

Type A

Diameter of doweling	= 0.8 in.
Diameter of bent sheet to N.A.	= 0.8 + 0.049
	= 0.849 in.
Outside fibre strain	$= \frac{a}{r} = \frac{2a}{d} = \frac{0.049}{0.849}$
	= 0.0577 in./in.
Theoretical springback strain	= 0.002 in./in.
∴ Outside fibre strain after spring-back	= 0.0577-0.002 = 0.0557 in/in.
∴ Diameter of finished specimen to N.A.	$= \frac{0.049}{0.0557}$
	= 0.88 in.

Type B

Diameter of doweling	= 1.7 in.
Diameter of bent sheet to N.A.	= 1.7 + 0.049
	= 1.749 in.
Outside fibre strain	$= \frac{0.049}{1.749}$ = 0.0280 in/in.
Theoretical springback strain	= 0.002 in./in.
∴ Outside fibre strain after spring-back	= 0.0280-0.002 = 0.026 in./in.
∴ Diameter of finished specimen to N.A.	$= \frac{0.049}{0.0260}$
	= 1.89 in.

Type C

Diameter of doweling = 2.35 in.

Diameter to N.A. of sheeting = 2.35 + .049 = 2.399

Outside fibre strain $= \frac{.049}{2.399} = .0204$ in./in.

Theoretical springback strain = 0.002 in./in.

∴ Outside fibre strain after springback = 0.0204 - 0.001

= 0.0184 in./in.

∴ Diameter of finished specimen to ℄ of sheet $= \frac{0.049}{0.0184}$

= <u>2.67 in.</u>

APPENDIX 2

Numerical Prediction of Load vs. Displacement Characteristic for Specimens containing residual stress

The required applied stresses to bring each fibre to the yield point when loaded axially are shown in the figure. The distribution may be approximated by a numerical method to facilitate solution by computer.

The applied axial stress distribution is approximated by a stepped curve, with step intervals of $0.01\bar{\sigma}$ max. applied stress. The average applied stress for each step is approximated by the formula:

$$\sum_{n=1}\left[\sigma_{x_n}\left(\frac{D_n - D_{n-1}}{2a}\right)\right] + \sigma_{x_{n+1}}\left(\frac{2a - D_N}{2a}\right) = \sigma_{x_{A\ AV.}}$$

where n = the number of the step considered.

$2a$ = the thickness of the sheet.

D = the fraction of the sheet that has become plastic.

Incremental values of σ and D" from diagram -

$\sigma_1 = 0.5\bar{\sigma}$ | $D_1 = 0.3"$ | $D_6 = 6.6"$

$\sigma_2 = 0.6\bar{\sigma}$ | $D_2 = 1.0"$ | $D_7 = 7.1"$

$\sigma_3 = 0.7\bar{\sigma}$ | $D_3 = 2.9"$ | $D_8 = 8.1"$

σ_4 = etc. | $D_4 = 4.8"$ | $D_9 = 9.0"$

$\sigma_8 = 1.2\bar{\sigma}$ | $D_5 = 5.7"$

$\sigma_9 = 1.25\bar{\sigma}$

<u>Point 1</u> $\sigma_{max} = 0.5\bar{\sigma}$

$\therefore \sigma_{AV} = 0.5\bar{\sigma}$

<u>Point 2</u> $\sigma_{max} = 0.6\bar{\sigma}$

$\therefore \sigma_{AV} = (0.5)\ .3/9 + (0.6)\ 8.7/9 = 0.597\bar{\sigma}$

<u>Point 3</u> $\sigma_{MAX} = 0.7\bar{\sigma}$

$\therefore \sigma_{AV} = 0.017 + (0.6)\ .7/9 + (0.7)\ 8/9 = 0.688\bar{\sigma}$

<u>Point 4</u> $\sigma_{MAX} = 0.8\bar{\sigma}$

$\therefore \sigma_{AV} = 0.063 + (0.7)\ 1.9/9 + (0.8)\ 6.1/9 = 0.743\bar{\sigma}$

<u>Point 5</u> $\sigma_{MAX} = 0.9\bar{\sigma}$

$\therefore \sigma_{AV} = 0.200 + (0.8)\ 1.9/9 + (0.9)\ 4.2/9 = 0.789\bar{\sigma}$

<u>Point 6</u> $\sigma_{MAX} = 1.0\bar{\sigma}$

$\therefore \sigma_{AV} = 0.369 + (0.9)\ .9/9 + (1.0)\ 3.3/9 = 0.825\bar{\sigma}$

<u>Point 7</u> $\sigma_{MAX} = 1.1\bar{\sigma}$

$\therefore \sigma_{AV} = 0.459 + (1.0)\ .9/9 + (1.1)\ 2.4/9 = 0.852\bar{\sigma}$

<u>Point 8</u> $\sigma_{MAX} = 1.2\bar{\sigma}$

$\therefore \sigma_{AV} = .559 + (1.1)\ .5/9 + (1.2)\ 1.9/9 = 0.873\bar{\sigma}$

<u>Point 9</u> $\sigma_{MAX} = 1.25\bar{\sigma}$

$\therefore \sigma_{AV} = .620 + (1.2)\ 1/9 + (1.25)\ .9/9 = 0.878\bar{\sigma}$

Tresca

$\sigma_1 = 0.5\bar{\sigma}$	$d_1 = 0.5"$	$d_6 = 6.7"$
$\sigma_2 = 0.6\bar{\sigma}$	$d_2 = 1.3"$	$d_7 = 7.7"$
$\sigma_3 =$ etc.	$d_3 = 3.4"$	$d_8 = 9.0"$
$\sigma_8 = 1.2\bar{\sigma}$	$d_4 = 5.4"$	
	$d_5 = 6.1"$	

Point 1 $\quad \sigma_{AV} = 0.5\bar{\sigma}$

Point 2 $\quad \sigma_{AV} = (0.5)\ .5/9 + (0.6)\ 8.5/9 = 0.594\bar{\sigma}$

Point 3 $\quad \sigma_{AV} = .028 + (0.6)\ .8/9 + (0.7)\ 7.7/9 = 0.681\bar{\sigma}$

Point 4 $\quad \sigma_{AV} = .081 + (0.7)\ 2.1/9 + (0.8)\ 5.6/9 = 0.743\bar{\sigma}$

Point 5 $\quad \sigma_{AV} = .245 + (0.8)\ 2.0/9 + (0.9)\ 3.6/9 = 0.783\bar{\sigma}$

Point 6 $\quad \sigma_{AV} = .423 + (0.9)\ .7/9 + (1.0)\ 2.9/9 = 0.815\bar{\sigma}$

Point 7 $\quad \sigma_{AV} = .493 + (1.0)\ .6/9 + (1.1)\ 2.3/9 = 0.842\bar{\sigma}$

Point 8 $\quad \sigma_{AV} = .560 + (1.1)\ 1/9 + (1.2)\ 1.3/9 = 0.857\bar{\sigma}$

These values obtained for σ_{AV} are plotted against the displacements for σ_{MAX}, and are illustrated in Fig. 3.7.

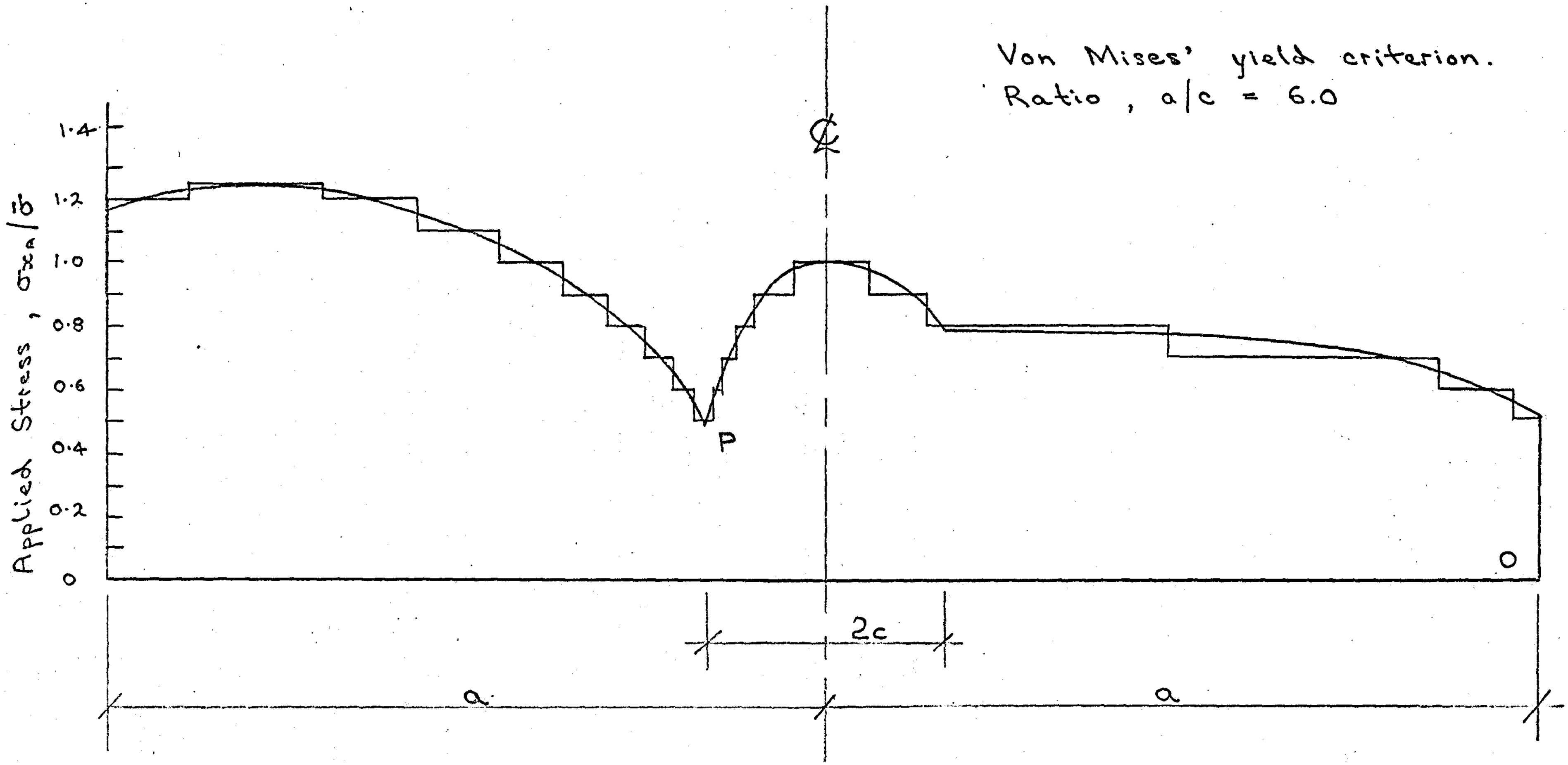

Numerical Approximation for Yield Stresses of fibres in X-section.

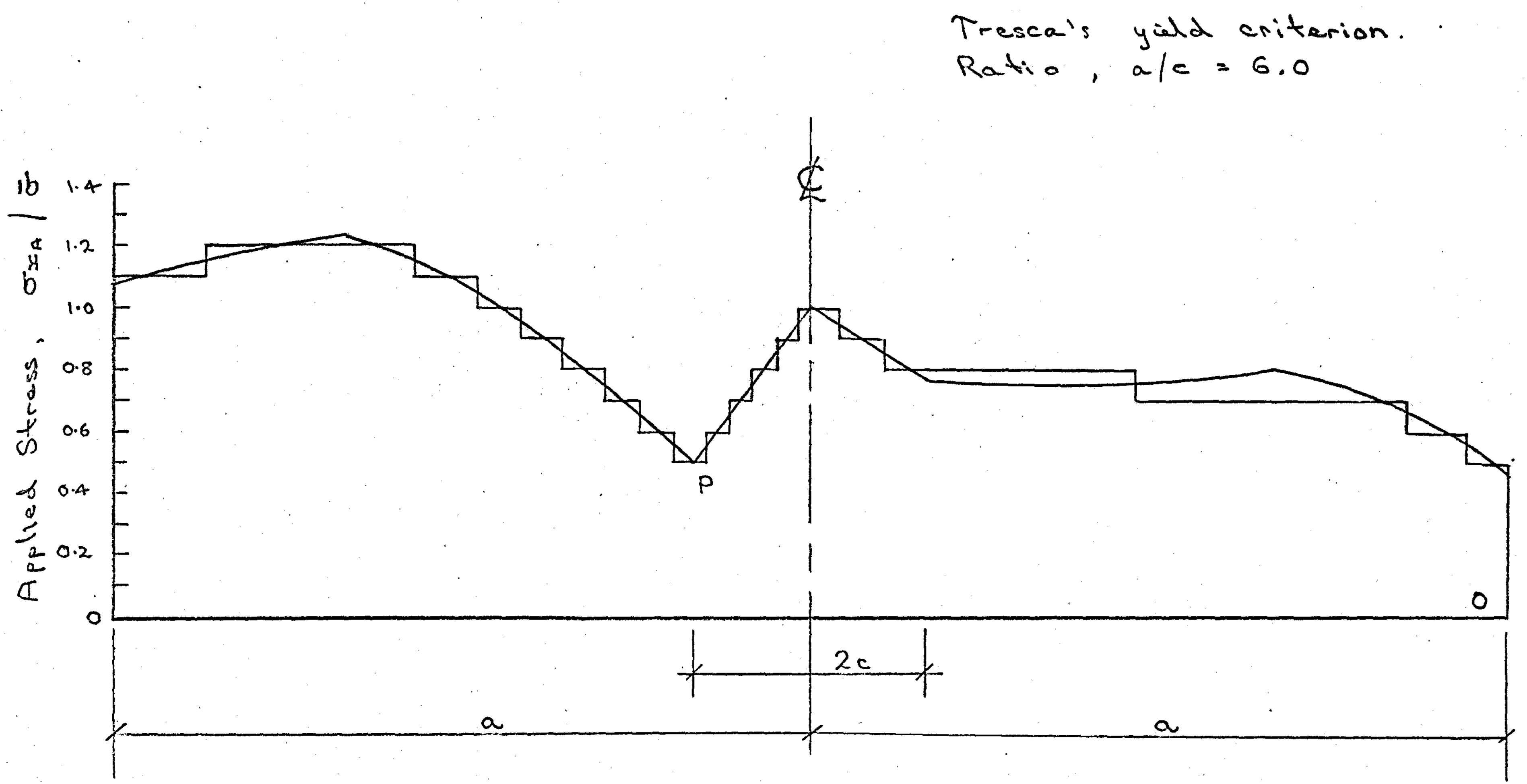

Numerical Approximation for Yield Stresses of fibres in X-section.

Appendix 3.


```
$JOB     WATFOR   003334 DANIELS L          100     010     030
$IBJOB
$IBFTC
C        CALCULATION OF STRESSES IN SHEET BENDING.
C       VON MISES.
        Y= 31000.0
        V=0.3
        E= 22000000.0
        C=Y*(SQRT(3.0)/4.0)*ALOG(ABS((2.0*SQRT(1.0-V+V**2)-SQRT(3.0))/
       1 (2.0*SQRT(1.0-V+V**2)+SQRT(3.0))))-(1.0-2.0*V)*V*Y/SQRT
       2  (1.0-V+V**2)
        WRITE (6,6)
      6 FORMAT (6X,8HCONSTANT/)
        WRITE (6,7) C
      7 FORMAT (4X,F15.5/)
        WRITE (6,3)
      3 FORMAT (8X,5HSIGMX,15X,5HSIGMZ,12X,6HSTRAIN/)
        SIGMZ=0.34
      8 SIGMX=(SQRT(SIGMZ**2-4.0*(SIGMZ**2-1.0))+SIGMZ)/2.0
        A=(1.0-2.0*V)*SIGMZ*Y-((SQRT(3.0)*Y)/4.0)*ALOG(ABS((2.0-SQRT(3.0)
       1 *SIGMX)/(2.0+SQRT(3.0)*SIGMX)))+C
        STRAIN = (A+Y*(1.0-V**2)/SQRT(1.0-V+V**2))/E
        WRITE (6,2) SIGMX,SIGMZ,STRAIN
      2 FORMAT (4X,F10.5,10X,F10.5,10X,E12.6//)
        IF (SIGMZ-0.60) 5,9,9
      5 SIGMZ=SIGMZ+0.01
        GO TO 8
      9 STOP
        END
$ENTRY
$IBSYS
$JOB     WATFOR   003334 DANIELS L          100     010     030
$IBJOB            NODECK
$IBFTC
C        CALCULATION OF STRESSES IN SHEET BENDING.
C        TRESCA
        WRITE (6,3)
      3 FORMAT (4X,5HSIGMZ,4X,6HSTRAIN/)
        V=0.3
        Y=31000.0
        E=22000000.0
        P=0.91*Y/E
        SIGMZ=0.3
      7 A=P+((0.5-V)*(SIGMZ*Y-V*Y)+0.75*Y*ALOG(ABS((1.0-2.0*V)/
       1 (1.0-2.0*SIGMZ*Y/Y))))/E
        WRITE (6,4) SIGMZ , A
      4 FORMAT (2F10.5//)
        IF (SIGMZ-1.0) 5,6,6
      5 SIGMZ=SIGMZ+0.025
        GO TO 7
      6 STOP
        END
$ENTRY
$IBSYS

                        CD TOT    0054
```

```
$JOB           003334 DANIELS L          100     010     030
$IBJOB         NOMAP,NODECK
$IBFTC
C CRITICAL STRENGTH OF COMPRESSION SPECIMENS  BY LEE,S METHOD.
C STRESS SIGMA Z VARIABLE OVER X-SECTION.
C TRESCA,S YIELD CRITERION.
C VARIABLE RATIO R/T.
      Z=3.142
      V=0.3
      T=0.049
      RAD= 10.0*T
      E= 29500000.0
   10 RATIO=RAD/T
      WRITE (6,11)
   11 FORMAT (4X,9HRATIO R/T)
      WRITE (6,12) RATIO
   12 FORMAT  (F10.2)
      W=40.0*T
    9 ET=500000.0
      WRITE (6,1)
    1 FORMAT  (5X,1HQ,12X,1HP,12X,1HS,12X,1HR,7X,6HSTRESS,12X,2HET)
    3 C11=(1.0/ET)
      C12=(V/E+(1.0/ET-1.0/E))
      C22=(1.0/ET)
      C3=2.0*(1.0+V)/E
      D11=C22*T**3.0/(12.0*(C11*C22-C12**2.0))
      D12=C12*T**3.0/(12.0*(C11*C22-C12**2.0))
      D22=C11*T**3.0/(12.0*(C11*C22-C12**2.0))
      D3=T**3.0/(6.0*C3)
      F=C22*(2.0*Z/W)**4.0
      G=C11*(2.0/RAD)**4.0
      Q1=C11*(1.0/RAD)**4.0+(C3-2.0*C12)*(1.0/RAD)**2.0
     1 *(Z/W)**2.0+C22*(Z/W)**4.0
      P=+(12.0*T**5*Z**9*C22)/(RAD**3*W**7*F**2)
     1+(3.0*T**5*Z**5)/(2.0*RAD**3*W**3*G)
      Q=-(32.0*T**4*Z**5*C12)/(RAD**4*W**5*F*Q1)
     2+(32.0*T**4*Z**7*C22)/(RAD**2*W**7*F*Q1)
      S=+(T**3*Z**5*C11)/(4.0*RAD**5*W**3*Q1**2)
     1-(T**3*Z**7*C12)/(2.0*RAD**3*W**5*Q1**2)
     2+(T**3*Z**9*C22)/(4.0*RAD*W**7*Q1**2)
     3+(T**3*Z**7*C3)/(4.0*RAD**3*W**5*Q1**2)
     4+(D11*T**2*Z**5*RAD)/(4.0*W**3)
     5+(D12*T**2*Z**3)/(2.0*RAD*W)
     6+(D22*T**2*Z*W)/(4.0*RAD**3)
     7+(D3*T**2*Z**3)/(2.0*RAD*W)
      R=-(T**3*Z**3*RAD)/(4.0*W)
      STRESS= ((Q**2)/(4.0*P)-S)/R
      WRITE (6,2)  Q,P,S,R,STRESS,ET
    2 FORMAT  (6E12.5)
      ET=ET+500000.0
      IF (ET-10000000.0) 3,4,4
    4 W=W-(4.0*T)
      WRITE (6,5)
    5 FORMAT( 5X,1HW)
      WRITE (6,6) W
    6 FORMAT (F10.5)
      IF (W-6.0*T) 8,7,7
    7 GO TO 9
```

```
    8 RAD=RAD+10.0*T
      IF (RAD-100.0*T) 10,10,13
   13 STOP
      END
$ENTRY
$IBSYS
$JOB           003334 DANIELS L        100     010     030
$IBJOB         NOMAP,NODECK
$IBFTC
C CRITICAL STRENGTH OF COMPRESSION SPECIMENS  BY LEE,S METHOD.
C STRESS,SIGMAZ VARIABLE OVER CROSS-SECTION.
C VON MISES, YIELD CRITERION.
C VARIABLE RATIO R/T.
      Z=3.142
      V=0.3
      T=0.049
      RAD= 10.0*T
      E= 29500000.0
   10 RATIO=RAD/T
      WRITE (6,11)
   11 FORMAT (4X,9HRATIO R/T)
      WRITE (6,12) RATIO
   12 FORMAT  (F10.2)
      W=40.0*T
    9 ET=500000.0
      WRITE (6,1)
    1 FORMAT  (5X,1HQ,12X,1HP,12X,1HS,12X,1HR,7X,6HSTRESS,12X,2HET)
    3 C11=(1.0/ET)
      C12=(V/E+(1.0/ET-1.0/E)/2.0)
      C22=(1.0/ET+3.0/E)/4.0
      C3=2.0*(1.0+V)/E
      D11=C22*T**3.0/(12.0*(C11*C22-C12**2.0))
      D12=C12*T**3.0/(12.0*(C11*C22-C12**2.0))
      D22=C11*T**3.0/(12.0*(C11*C22-C12**2.0))
      D3=T**3.0/(6.0*C3)
      F=C22*(2.0*Z/W)**4.0
      G=C11*(2.0/RAD)**4.0
      Q1=C11*(1.0/RAD)**4.0+(C3-2.0*C12)*(1.0/RAD)**2.0
     1 *(Z/W)**2.0+C22*(Z/W)**4.0
      P=+(12.0*T**5*Z**9*C22)/(RAD**3*W**7*F**2)
     1+(3.0*T**5*Z**5)/(2.0*RAD**3*W**3*G)
      Q=-(32.0*T**4*Z**5*C12)/(RAD**4*W**5*F*Q1)
     2+(32.0*T**4*Z**7*C22)/(RAD**2*W**7*F*Q1)
      S=+(T**3*Z**5*C11)/(4.0*RAD**5*W**3*Q1**2)
     1-(T**3*Z**7*C12)/(2.0*RAD**3*W**5*Q1**2)
     2+(T**3*Z**9*C22)/(4.0*RAD*W**7*Q1**2)
     3+(T**3*Z**7*C3)/(4.0*RAD**3*W**5*Q1**2)
     4+(D11*T**2*Z**5*RAD)/(4.0*W**3)
     5+(D12*T**2*Z**3)/(2.0*RAD*W)
     6+(D22*T**2*Z*W)/(4.0*RAD**3)
     7+(D3*T**2*Z**3)/(2.0*RAD*W)
      R=-(T**3*Z**3*RAD)/(4.0*W)
      STRESS= ((Q**2)/(4.0*P)-S)/R
      WRITE (6,2)  Q,P,S,R,STRESS,ET
    2 FORMAT  (6E12.5)
      ET=ET+500000.0
      IF (ET-10000000.0) 3,4,4
    4 W=W-(4.0*T)
```

```
      WRITE (6,5)
    5 FORMAT( 5X,1HW)
      WRITE (6,6) W
    6 FORMAT (F10.5)
      IF (W-6.0*T) 8,7,7
    7 GO TO 9
    8 RAD=RAD+10.0*T
      IF (RAD-100.0*T) 10,10,13
   13 STOP
      END
$ENTRY
$IBSYS
```

REFERENCES

1. Beedle, L. S., Huber, A. W., "Residual Stress and the Compressive Strength of Steel", Welding Journal, Vol. 33, No. 12, December 1954, p. 589-s.
2. Beedle, L. S., Tall, L. A., "Basic Column Strength", Journal of Struct. Div. A.S.C.E. July 1960.
3. Nagaraja Rao, N. R., Estuar, F. R., Tall, L., "Residual Stresses in Welded Shapes", Welding Research Supplement, Vol. 43, p. 295-s, July 1964.
4. Hill, R., "The Mathematical Theory of Plasticity", Oxford, 1950.
5. Schroeder, W. "Mechanics of Sheet Metal Bending", Transactions of the A.S.M.E., November 1943, p. 817-827.
6. Alexander, J. M., "An Analysis of the Plastic Bending of Wide Plate, and the Effect of Stretching in Transverse Residual Stresses", Proc. Instn. Mech. Engrs., Vol. 173, No. 1, 1959, p. 73-85.
7. Bleich, F., "Buckling Strength of Metal Structures", McGraw-Hill, 1962.
8. Johnston, B.G., "Guide to Design Criteria for Metal Compression Members", Column Research Council, John Wiley & Son, 1960.

9. Lee , H. N. L., "Inelastic Buckling of Initially Imperfect Cylindrical Shells Subject to Axial Compression", Journal of the Aerospace Science, Jan. 1962.

10. Divakaran, S., "The Influence of Shape on the Strength of Thin-Walled Open Columns", M. Eng. Thesis, McMaster University, 1964.

11. Karren, K. W., Winter, G., "Effects of Cold-Forming on Light-Gage Steel Members", Journal of Struct. Div. A.S.C.E., Feb. 1967.

12. Lay, M. G., "Flange Local Buckling in Wide-Flange Shapes", Journal of Struct. Div. A.S.C.E., Dec. 1965.

13. Timoshenko, S., "Theory of Elastic Stability", McGraw-Hill Book Co., Inc., New York, 1936.

14. Shanley, F. R., "Inelastic Column Theory", Journal of the Aeronautical Sciences, Vol. 14, No. 5, May, 1949.

15. Bijlaard, P. P., "On the Plastic Stability of Thin Plates and Shells", Proc. Koninklijke Nederlandsche Akademie von Wetenschappen, Vol. L, No. 7, Sept. 1947.

16. Onat, E. T., Drucker, D. C., "Inelastic Instability and Incremental Theories of Plasticity", Journal of the Aeronautical Sciences, Vol. 20, No. 3, pp. 181-186, March 1953.

17. Donnell, L. H., "Stability of Thin-Walled Tubes Under Torsion", N.A.C.A. Rep. 479, 1933.

18. Loo, T. T., "Effects of Large Deflections and Imperfections on the Elastic Buckling of Cylinders Under Torsion and Axial Compression", Proceedings of the Second U.S. National Congress of Applied Mechanics, A.S.M.E., 1954.

19. Fung, Y. C., Wittrich, W. H., "A Boundary Layer' Phenomenon in the Large Deflexion of Thin Plates", Quart. Journal Mech. and App. Math., Vol.VIII, Pt.2. 1955.

20. Winter, G., Chajes, A., "Torsional-Flexural Buckling of Thin-Walled Members", Journal of the Struct. Div. Proceedings of the A.S.C.E., August 1965.

21. Drucker, D. C., "Introduction to Mechanics of Deformable Solids", McGraw-Hill, 1967.

22. Timoshenko, S., Gere, "Theory of Elastic Stability", McGraw-Hill Book Co., Inc., New York.

23. Batterman, S. C. "Plastic Buckling of Axially Compressed Cylindrical Shells", N.S.F. Research Grant G.P. 1115, Brown University, March 1964.